CHARACTERISATION OF ULTRASONIC TRANSDUCERS USED IN MEDICAL APPLICATIONS AND INVESTIGATION OF THEIR EFFECTS IN PHANTOM TISSUE

by

Baki Karaböce

Submitted to the Institute of Graduate Studies in
Science and Engineering in partial fulfillment of
the requirements for the degree of
Doctor of Philosophy
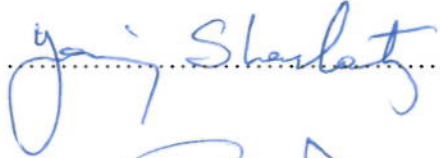in
Physics Department

Yeditepe University
2014

CHARACTERISATION OF ULTRASONIC TRANSDUCERS USED IN MEDICAL
APPLICATIONS AND INVESTIGATION OF THEIR EFFECTS IN PHANTOM TISSUE

APPROVED BY:

Prof. Dr. Ahmet T. İnce
(Supervisor)

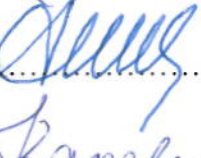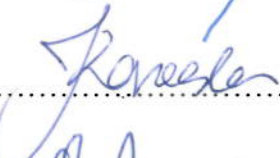Prof. Dr. Yani Skarlatos
(Co-advisor)

Prof. Dr. Şahin Aktaş

Assoc. Prof. Dr. Ertan Akşahin

Prof. Dr. Ali Şahin

Assoc. Prof. Dr. İpek Karaaslan

Assist. Prof. Dr. Vildan Üstoğlu Ünal

DATE OF APPROVAL: …... / …... / …...….

ACKNOWLEDGEMENTS

I would like to thank Prof.Dr. Ahmet T. İnce from Yeditepe University for being an advisor and for his great support of my research.

I would also like to thank Prof.Dr. Yani Skarlatos from Boğaziçi University for always encouraging me for every stage of the thesis.

I thank Prof. Dr. Şahin Aktaş from Marmara University and Associate Prof. Dr. Ertan Akşahin from Yeditepe University who act in my dissertation committee for their thoughtful insights and guidance throughout my graduate studies.

Most importantly, none of these studies would have been possible without the endless support of my wife, Nuray Karaböce.

My thesis has been dedicated to my grandfather who has showed me my direction and always made things in the right way.

ABSTRACT

CHARACTERISATION OF ULTRASONIC TRANSDUCERS USED IN MEDICAL APPLICATIONS AND INVESTIGATION OF THEIR EFFECTS IN PHANTOM TISSUE

The overall goal of this thesis is to characterize the high intensity focused ultrasound (HIFU) transducers used in medical applications and to investigate the effect in phantom tissue. Two types of HIFU transducers have been characterized by electrical, acoustical and thermal methods. A new method has been presented for measurement of instantaneous input electrical power of HIFU transducers. The aim is to establish a relationship between ultrasonic powers produced due to applied electrical power and measure the effectiveness of HIFU transducers. New ultrasound pressure measurement system has been designed and constructed at TUBİTAK UME Ultrasound Laboratory. System consists of a water tank, positioning system, measurement devices and a controlling program. The ultrasound field radiated by HIFU has been investigated by measuring its pressure field and mapping in 2-D and 3-D. A temperature measurement set up in a phantom tissue has been constructed. Two temperature sensors that were produced at TÜBİTAK UME Temperature laboratories were used. Platinum resistance (Pt100) temperature sensors and thin wire thermocouples are embedded into a phantom tissue. Temperature change and temperature distribution have been investigated. Correlations between ultrasonic power, electrical power, ultrasonic pressure and temperature rise have been presented. Theoretical model found in literature and experimental results were compared and an agreement was shown. Theoretical model for ultrasound pressure field was realized by using a KZK (Khokhlov, Zabolotskaya and Kuznetsov) nonlinear parabolic equation and temperature rise in phantom tissue caused by absorption of HIFU energy is often described using Pennes' bioheat transfer equation.

ÖZET

MEDİKAL UYGULAMALARDA KULLANILAN ULTRASONİK DÖNÜŞTÜRÜCÜLERİN KARAKTERİZASYONU VE ETKİLERİNİN FANTOM DOKUDA ARAŞTIRILMASI

Bu tezin genel amacı yüksek yoğunluklu tıbbi uygulamalarda kullanılan odaklanmış ultrason (HIFU) dönüştürücüleri karakterize etmek ve fantom dokudaki etkisini araştırmaktır. HIFU dönüştürücülerin iki türü, elektrik akustik ve termal yöntemlerle karakterize edilmiştir. HIFU dönüştürücülerin anlık giriş elektrik gücünün ölçülmesi için yeni bir yöntem kullanılmıştır. Amaç uygulanan elektrik enerjisine karşı üretilen ultrasonik güçler arasında bir ilişki kurmak ve HIFU dönüştürücülerin etkinliğini ölçmektir. Ultrasonik basınç ölçüm sistemi, TÜBİTAK UME Ultrasonik Laboratuvarı'nda tasarlanmış ve üretilmiştir. Sistem, su deposu, konumlandırma sistemi, ölçüm cihazları ve kontrol/yazılım bölümlerinden oluşur. Basınç alanının ölçülmesi ve 2-eksen ve 3-eksen haritalama incelenerek HIFU tarafından yayılan alan araştırılmıştır. Fantom dokuda sıcaklık ölçüm düzeneği kurulmuştur. TÜBİTAK UME Sıcaklık Laboratuarı'nda üretilen iki sıcaklık sensörü kullanılmıştır. Pt100 (Platin dirençli termometre) sıcaklık sensörleri ve ısılçiftler fantom doku içine yerleştirilmiştir. Sıcaklık değişimi ve sıcaklık dağılımı araştırılmıştır. Ultrasonik güç, elektrik gücü, ultrasonik basınç ve sıcaklık artışı arasındaki ilişkiler sunulmuştur. Literatürde mevcut teorik model ile deneysel sonuçlar karşılaştırılmış ve uyum gözlenmiştir. Ultrason basınç alanı için teorik model, KZK (Khokhlov, Zabolotskaya and Kuznetsov) doğrusal olmayan parabolik denklemi ve fantom dokudaki sıcaklık artışına sebep olan genellikle Pennes' bioheat transfer denklemi ile açıklanan HIFU enerji emilimi kullanılarak gerçekleştirilmiştir.

TABLE OF CONTENTS

LIST OF FIGURES

LIST OF TABLES

LIST OF SYMBOLS / ABBREVIATIONS

a	Absorption in dB/m
β	Nonlinearity parameter
c	Speed of sound in tissue, 1540 m/s
Cb	Temperature of blood, ºC
C_s	Specific heat of tissue in J/(kg-°K)
f	Frequency in Hertz, Hz
F	Force in Newton, N
g	Accleration of gravitiy, 9,8023 m/s^2
I	Current in Ampers, A
K_s	Tissue thermal conductivity in W/(m·K)
λ	Wavelength in Meter, m
L	Inductance in Siemens, Ω
m	Mass in Kilogram, kg
P,W	Power in Watts, W (Elecrical or ultrasound)
Pelk	Elecrical Power in Watts, W
Pult	Ultrasonic Power in Watts, W
p	Pressure in Pascal, Pa
p2	Second harmonics of fundamental pressure
p3	Third harmonics of fundamental pressure
p4	Fourth harmonics of fundamental pressure
p5	Fifth harmonics of fundamental pressure

p+	Peak compressional pressure
p-	Peak rarefactional pressure
p_{pp}	Peak-to-peak pressure
p(x)	Axial pressure in x direction
p(y) or p(z)	Transversal or radial pressure in y or z direction
Q_V	Rate of heat generation by external heat source.
Q_m	Rate of heat generation per tissue unit volume
ρ	Density, kg/m^3
R	Resistance in Ohms, Ω
V	Voltage in Volts, V
W_b	Specific heat of blood in J/(kg-°K)
Z	Impedance in Ohms, Ω
z_{foc}	Focusing depth, m

BIPM	Bureau International des Poids et Mesures
BHT	The bioheat transfer equation
CIPM	Comité International des Poids et Mesures
CW	Continuos wave
DNA	Deoxyribonucleic acid
FUS	Focused ultrasound surgery
GUM	Guidelines of uncertainty in measurements
HIFU	High Intensity Focused Ultrasound
IEC	International Electrotechnical Commission
ISO	International Organization for Standardization

KZK	Khokhlov, Zabolotskaya and Kuznetsov
LabVIEW	Laboratory Virtual Instrument Engineering Workbench
LiNbO3	Lithium Niobate
MRI	Magnetic Resonance Imaging
OIML	International Organization of Legal Metrology
Pt100	Platinum resitance thermometer
PVDF	Polyvinylidene Fluoride
PZT	Lead (P), Zirconate (Z) Titanate (T), Piezoceramic
RFB	Radiation Force Balance

1. INTRODUCTION

Cancer remains an important health problem all over the world. An important approach of fight against cancer is the discovery of novel techniques for diagnosis and treatment [1,2,3]. Accurate diagnosis and treatment methods will empower the therapy for the patient. Therapeutic ultrasound techniques in especially cancer treatment need to be supported by metrological tools in order to establish the safe use of ultrasound. HIFU transducer that produces up to few hundreds of Watts power in MHz frequencies is used as novel technique in cancer therapy in medicine. In order to characterize the ultrasound field radiated by an ultrasound transducer (i.e.HIFU), many scientists and researchers are realizing new studies [4-8]. During HIFU treatment, the temperature and ultrasound field distribution play an important key role. In order to ensure safe and efficient treatment, the temperature and ultrasound field distribution should ideally be known. Ultrasound field, temperature rises and temperature distributions must be measured with sufficiently high accuracy, so as to warrant a safe medical application. Mapping temperature distribution in tissue when ultrasound applied will ensure to use it safely and effectively.

Ultrasound is used for a wide range of different treatments: high intensity focused ultrasound, lithotripsy (kidney stones removal and including similar devices for tendon repair at bone surfaces), physiotherapy (e.g. sports injuries), enhanced bone repair and wound healing, fat removal, and various cosmetic purposes [9-13].

Field structure of such transducers, which is the most critical criterion for image quality of medical devices, mainly depends on geometrical configuration of transducers and their focal point. For these reasons careful metrological characterization of HIFU transducers, including field mapping is a matter of great importance.

Despite the fact that basic characterization of the acoustical output parameter for therapeutic ultrasound devices made progress and first international standard are under development [14]. The metrological basis –meaning reliable measuring procedures and models- for the determination of these parameters in tissue is under investigation.

It is widely described in scientific literature, that ultrasound waves generate heating effects in human body [15-17]. The amount of ultrasound power radiated by the transducers as a consequence the heating effect on tissues is proportional to the magnitude of driving electrical signal. Records related to the heating of specific regions in human body up to 85°C depending on the exposed ultrasonic power and focusing conditions are available in many publications [18,19]. Therefore in order to make correct treatment, exact knowledge about exposure of relevant region and proper penetration of ultrasonic radiation is required. This information has to be accompanied by the absolute value of ultrasonic power radiated by HIFU transducer determined during measurements traceable to national standards.

It is well known, that maximum ultrasonic power from HIFU transducers could be obtained on their focal point. Significant deviation from this maximum value can be found out of the focal point and on the axis different from the axis of maximum radiation. Therefore, exact determination of the focal distance and results of field characterization of HIFU transducers enable indispensable information for engineers engaged in design of medical devices with HIFU transducers.

The main objective of this thesis is metrological characterization of HIFU transducers, which includes determination of a resonance frequency, range dependent power measurements, radiation transfer rate measurements and 3D scanning of the ultrasonic field generated by a HIFU transducer, while near (Frensel) and far (Fraunhofer) field regions of transducers, and their focal points have been identified after modeling.

Measurement systems constructed at TÜBİTAK Ulusal Metroloji Enstitüsü (UME). Acoustic powers were measured in strong focusing fields up to 100 W in the frequency range 0,5 MHz to 3,0 MHz and the spatial distribution of pressure in these fields were quantified. Also the temperature rise in the focal region has been investigated by means of thin wire thermocouples and resistance thermometers.

In the first method, the total acoustic power produced by the HIFU transducer will be measured in the primary Radiation Force Balance (RFB) system. In the same system instantaneous input electrical power was also be measured.

Ultrasound power produced by the HIFU transducer was measured in the primary radiation force balance (RFB) system. The ultrasound power is radiated to an absorbing or conical reflecting target that is suspended to a balance. A change in apparent mass of target is measured and the ultrasound power is calculated by the formula shown in Equation 1.1.

$$Pult=F.c=mgc \qquad (1.1)$$

F is force, m is mass, g is acceleration of gravity and c is speed of sound (depend on the water temperature) in water in Equation 1.1. Instantaneous input electrical power is measured by using voltage and current probes. The electrical power is calculated by means of formula shown in Equation 1.2.

$$Pel=V.I.cos\theta \qquad (1.2)$$

θ is the phase angle between voltage and current in Equation 1.2.

In the second method, pressure field produced by the HIFU transducer have been determined by needle and $LiNbO_3$ (Lithium Niobate) transducers in the automated scanning system. The experimental results have been compared with theoretical approximations depending on the KZK equation [20,21].

In the third method, the temperature distribution produced by a HIFU (High Intensity Focused Ultrasound) transducer have been investigated by different set ups using different type temperature sensors (thermocouple and PT100) in the automated scanning system. The maximum temperature, the temperature change and the temperature distribution due to applied ultrasound power have been characterized. The temperature measurements were carried out in water and in a phantom gel (tissue mimicking material) that has very similar human tissue/body characteristics. Automated scanning system with the water tank (200 cm x 100 cm x 100 cm dimensions) can move 150 cm, 70 cm and 70 cm with accuracy of 100 μm.

The most important character of HIFU transducer is its temperature rise effect in tissue since it burns out the cancer cells in tissue. Ultrasound field was characterized by two types

of sensors. A HNA sensor manufactured by ONDA Corp-USA is a thin (400 µm active element in diameter and 1,2 mm case in diameter) sensor for high power field measurements [22]. This transducer was mounted at one end of the water tank and hydrophone was mounted at the other side of the moving translation stage. Ultrasonic field was measured with the controlling computer LabVIEW program (Laboratory Virtual Instrument Engineering Workbench).

The temperature measurements have been carried out by different types of sensors. Thin thermocouple and Pt100 sensors were used and the results were compared. Thermocouple temperature sensors have been produced at UME Temperature Laboratory. In order to use multisensors at the same time, a rigid frame was produced at UME workshop. The temperature measurements will be traceable to ITS-90 scale (International Temperature Scale of 1990) that facilitates the comparability and compatibility of temperature measurements between -272,5 °C and 1085 °C. The temperature distribution in the tissue can be calculated by the Pennes' bioheat transfer equation [23].

1.1   ULTRASOUND

The frequency of sound waves that a healthy human can hear is between 20 Hz and 20 kHz. Ultrasound has a higher frequency than normal hearing. Ultrasound used for medical purposes is from 1 MHz to 20 MHz frequency range.

Sound waves are generation of high pressure and low pressure pulses traveling through a medium. The high pressure areas (compression) are where the particles have been squeezed together; the low pressure areas (rarefaction) are where the particles have been spread apart as seen in Figure 1.1.
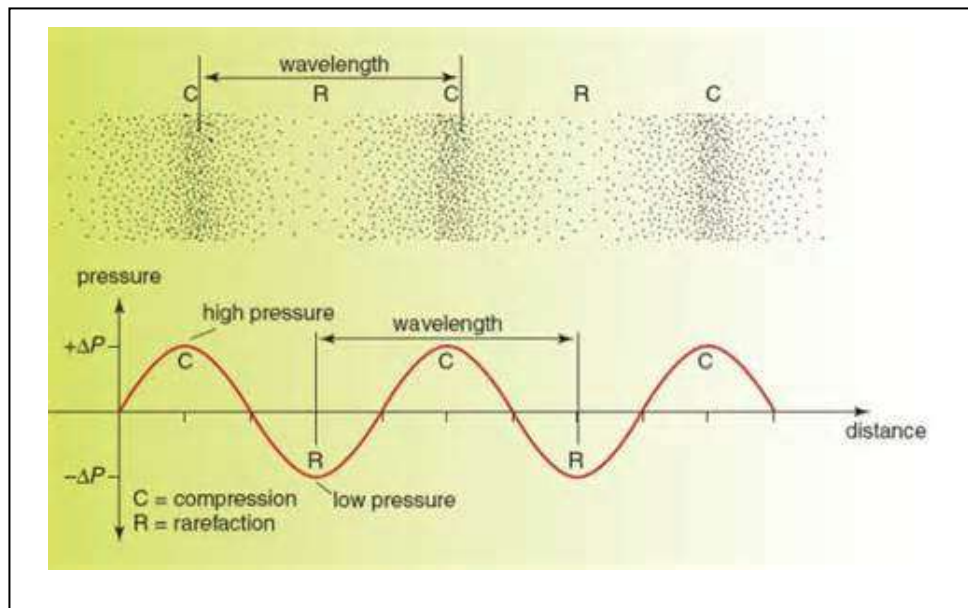
Figure 1.1. High pressure (compression) and low pressure (rarefaction) areas in sinusoidal form

Ultrasound pressure like sound pressure is the pressure deviation from the local ambient pressure caused by a high frequency sound wave. The International System of Units (abbreviated SI from French: Le Système international d'unités) unit for sound pressure is the Pascal and symbolized as Pa.

Ultrasound waves are produced by ultrasonic transducers which are made of PZT (Lead-Zirconate-Titanate) or crystal. Ultrasonic transducers are reciprocal sensors which converts mechanical vibrations to electrical signals and vice versa as seen in Figure 1.2.

Sound and pressure waves play an important role in a number of medical diagnostic and treatment technologies and many of them exploit the piezoelectric effect in one way or another. When materials such as ceramics, bone and DNA are mechanically stressed, they accumulate an electrical charge. Conversely, by applying an external electric field these materials, we can induce a change in their static dimensions. This inverse piezoelectric effect is used in the production of ultrasonic sound waves.
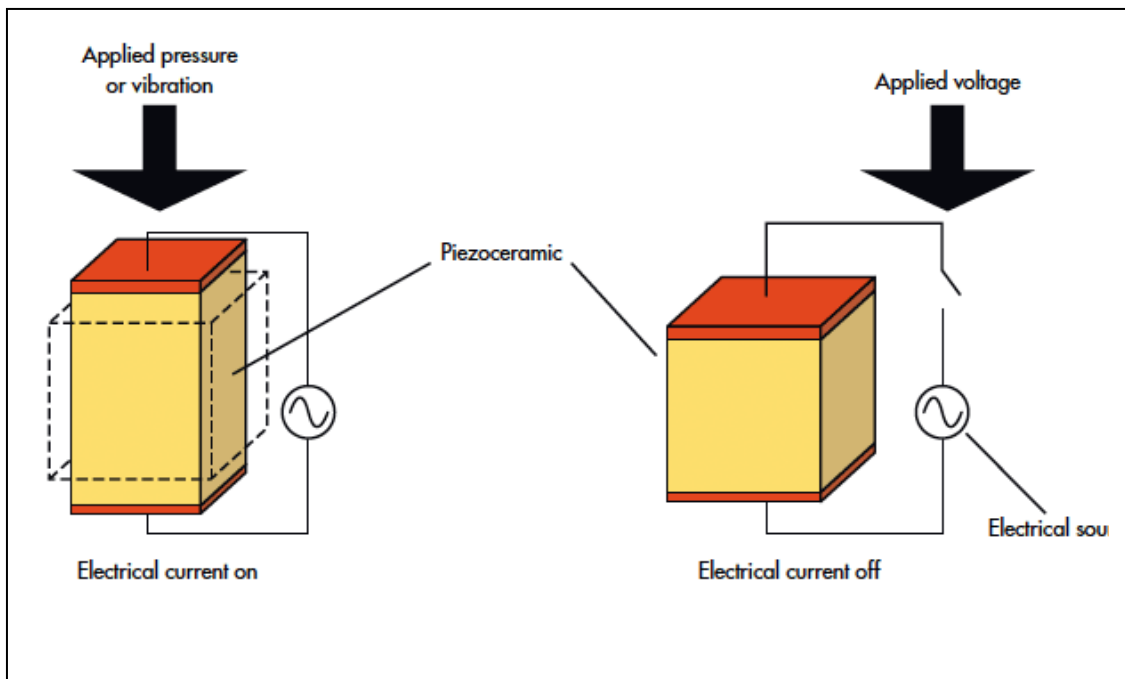
Figure 1.2. PZT scheme

Geometrical structure determines the properties of acoustic field including near, focal and far field regions. This geometrical structure with boundary conditions satisfies the solution of acoustic wave equation in these boundary conditions.

1.2   ULTRASOUND IN MEDICINE

Ultrasonography is a medical imaging technique that uses high frequency sound waves and their echoes. It is generally known as a safe application, since it does not use ionizing radiation, which can pose hazards such as chromosome breakage and cancer development. Ultrasonic energy has two potential physiological effects, which are the one is heating and the other is cavitation. Ultrasound energy produces a mechanical pressure wave through soft tissue. This pressure wave may cause microscopic bubbles in living tissues and distortion of the cell membrane. When ultrasound energy transmitted through the body, it heats the tissue. Heating effect is typically negligible as the normal tissue dissipates most of the heat for lower pressures that is radiated by diagnostic devices, but with high

intensity and focusing, it can cause small pockets of gas in body fluids or tissues to expand and contract/collapse in a phenomenon called cavitations [24, 25].

Focused high-energy ultrasound pulses can be used to destroy calculi such as kidney stones and gallstones into fragments small enough to be passed from the body without undue difficulty, a process known as lithotripsy [25].

Treating the cancer tumors and other disorders by means of a process known as high intensity focused ultrasound, also called "focused ultrasound surgery" (FUS) [26]. Generally lower frequencies than medical diagnostic ultrasound is used between 250 Hz and 2 MHz, but at the significantly higher time-averaged intensities as seen in Figure 1.3. The treatment process is generally visualized and guided by magnetic resonance imaging (MRI) and ultrasonography.
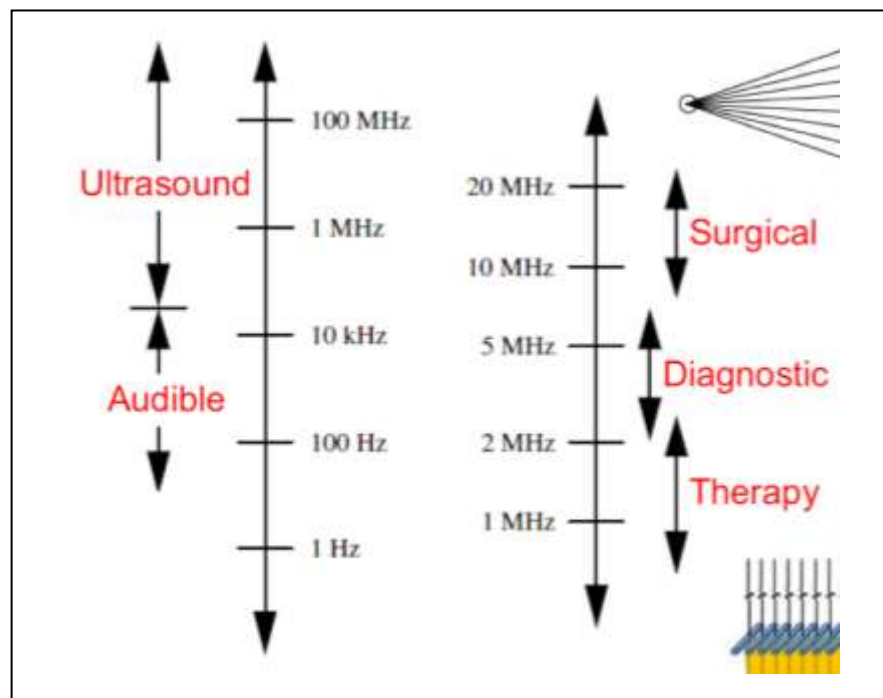
Figure 1.3. Medical ultrasound spectrum

Ultrasound pressure waves between 2 MHz and 18 MHz ranges are routinely used in diagnostic medical imaging and easily penetrate tissue to provide real-time images.

Ultrasound travels about five times as fast in water (around 1500 m/s) than it does in air (around 300 m/s) and brain tissue behaves pretty much like water.

Typical diagnostic ultrasonic applications operate in the frequency range of 2 MHz to 18 MHz. Higher frequency sound waves have a smaller wavelength and thus are capable of reflecting or scattering from smaller structures. Higher frequency sound waves also have a larger frequency dependent attenuation coefficient and thus are more readily absorbed in tissue, limiting the depth of penetration of the sound wave into the body [27].

Ultrasonography is effective for imaging soft tissues of the body. Superficial structures such as muscles, tendons, testes, breast, thyroid and parathyroid glands, and the neonatal brain are imaged at a higher frequency (7 MHz to 18 MHz), which provides better axial and lateral resolution. Deeper structures such as liver and kidney are imaged at a lower frequency 1 MHz to 6 MHz with lower axial and lateral resolution but greater penetration There are many applications of ultrasound in medicine for diagnostic and treatment in literature [27-36] as listed below.

- Ultrasound imaging
- Physiotherapy
- Ultrasound treatment
- Tissue burning
- Bone healing
- Cleaning teeth in dental hygiene.
- Drug delivery

1.3   HIFU TRANSDUCERS AND TECHNOLOGY

Generally HIFU transducers are made of a piezoceramic (PZT) or piezocomposite material and have the shape of a spherical shell. Figure 1.4 shows a schematic of geometrically focused spherical concave shell transducer as first suggested by Lynn *et al.* in 1942 [37]. The Existing focal point is located close to the geometrical center of curvature and the increase in the intensity at the focal spot can easily be a factor of thousands as compared to non-focused plane waves. Commonly used spatial maximum intensity levels for HIFU

ablation are around 1000 W/cm^2 to 3000 W/cm^2, whereas the intensity levels used for diagnostic ultrasound are around 0,1 W/cm^2 to 0,5 W/cm^2 [38, 39].
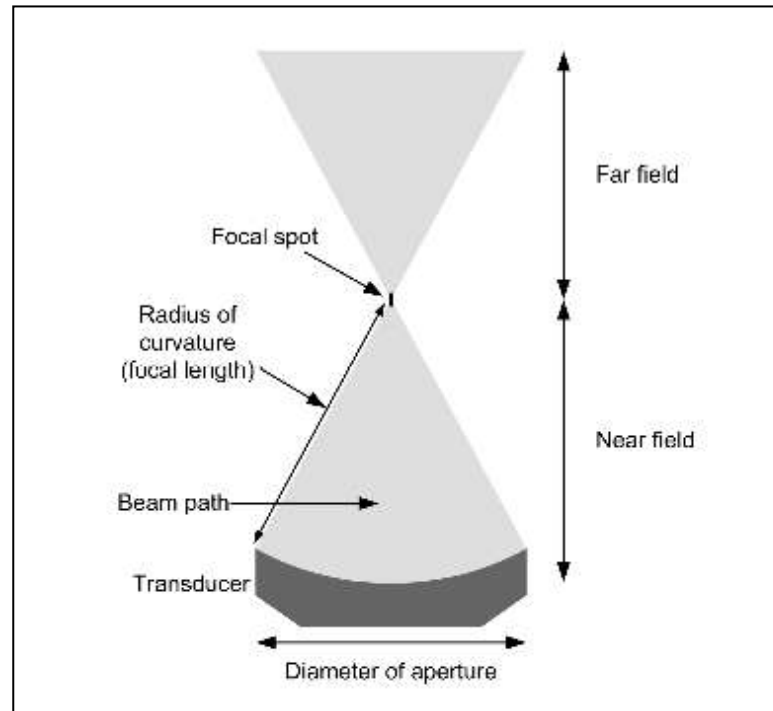
Figure 1.4. Schematic of a spherical shell transducer
(The ellipsoid focal spot (in black) is in scale with the radius of curvature and aperture.)

Diagnostic ultrasound is furthermore applied in short bursts of a few microseconds, whereas HIFU is applied continuously for several tens of seconds. The size of the ellipsoid focal spot is determined by the ratio of the transducer radius of curvature and the diameter of the aperture, and is also linearly dependent on the wavelength. The wavelength λ is in turn determined by the chosen frequency f according to $\lambda=c/f$, where c is the speed of sound in the target tissue, which is typically close to that of water in human soft tissues *i.e.* approximately 1540 m/s.

For a typical HIFU transducer with a 12 cm radius of curvature and 13 cm aperture diameter, the ellipsoid focal spot had a width and length of approximately 1 mm and 7 mm, respectively, when the transducer was operated at 1,2 MHz. In general, the ultrasound frequency used for HIFU therapy depends on the target and the required penetration depth, with transducers typically using frequencies in the range of 0,8 MHz and 1,6 MHz,

whereas intracavitary transducers for such applications as prostate ablation use higher frequencies in the range of 2 MHz to 4 MHz [39-41].

The focused beam causes localized high temperatures of between 40°C and 90°C (or even higher) in an elliptical region as small as 1 mm to 2 mm (in diameter) and 5 mm to 10 mm (in length) visualized as reddish ellipse in Figure 1.5. The high temperature, maintained for a few seconds, produces a well-defined region of necrosis. This procedure is referred to as ultrasound ablation. [42].
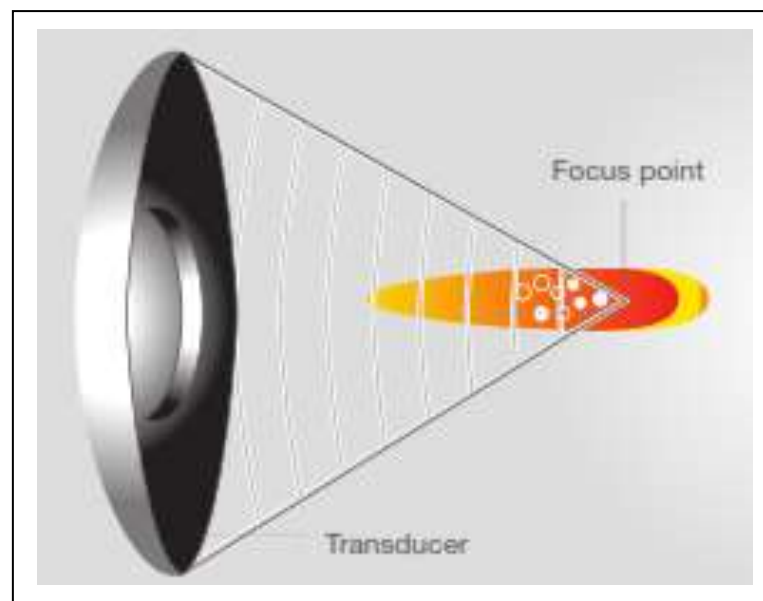
Figure 1.5. HIFU transducer focused by concave shape PZT

High intensity pressure field can be produced mainly by three ways. In most cases PZT's are used for transmitting sound waves. Technically, the acoustic waves are focused by a spherical arrangement of the ultrasound transducers or by adapting the relative phases of a transducer array (phased array). In general, an acoustic lens is placed in front of the transducer to increase the small volume of the focus.

In first technique for producing a high intensity field, a disk shape PZT is used with an acoustic lens (a polystyrene lens) to collimate the beam in a focus as shown in Figure 1.6 and Figure 1.7.
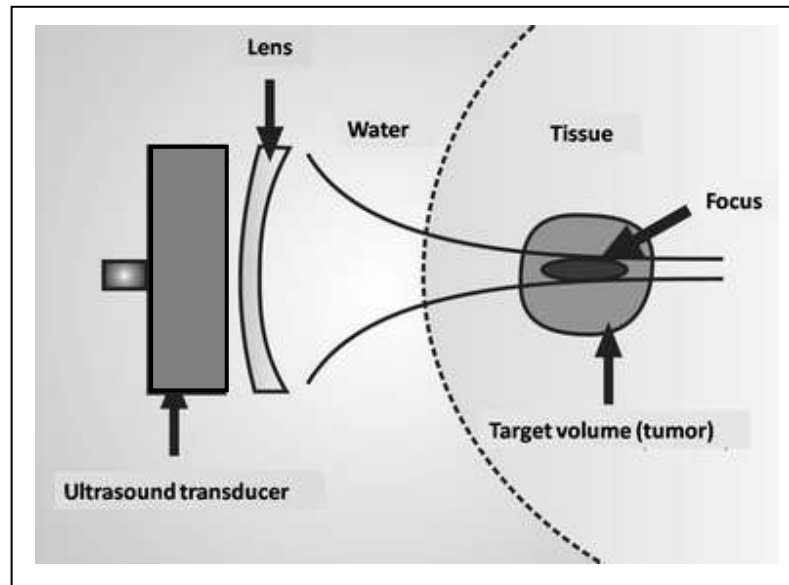
Figure 1.6. HIFU transducer focused by concave shape PZT

However it is an easier way for producing focused field, some amount of energy is lost since acoustic lens acts as an absorber in the region away from the center points.
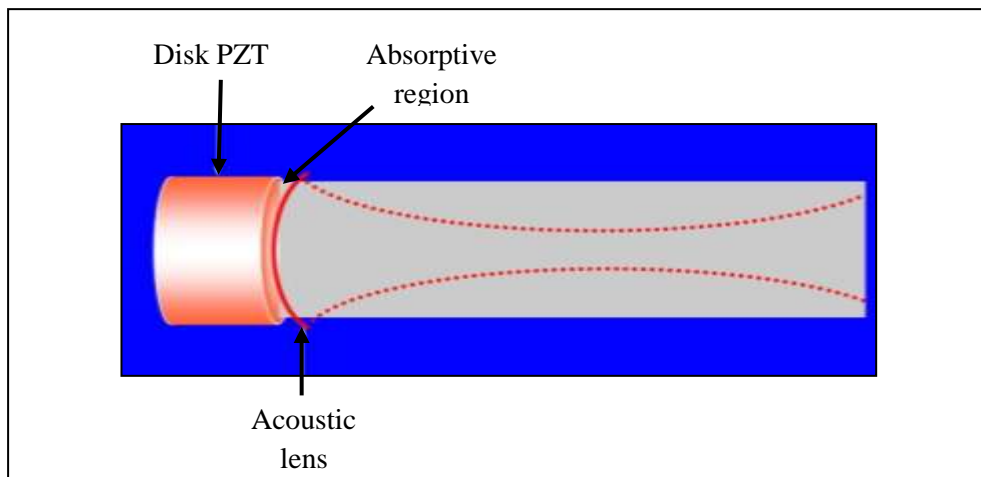
Figure 1.7. HIFU transducer focused by using acoustic lens

Second technique to produce a high intensity field, is constructing the transmitter in concave (bowl) shape. Concave shape accumulates the sound field in a point where is called focus point as it is seen in Figure 1.8.
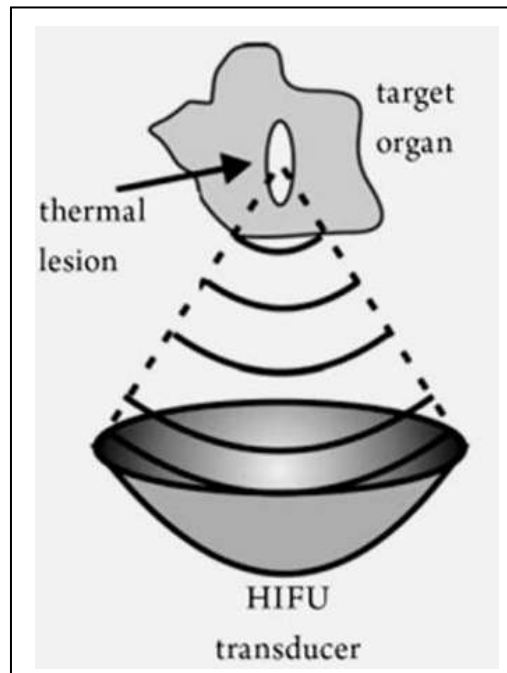
Figure 1.8. HIFU transducer focused by concave (bowl) shape PZT

Third technique to produce a high intensity field, is constructing multi-element transmitters in a disk or partially concave shape as it is seen in Figure 1.9. In this model focal point can be adjusted. High-intensity focused ultrasound developed for medical applications employ phased-array transducers in which an array of small size piezoelectric transducers are used to produce multiple pressure waves whose phase is adjusted electronically by introducing delays in the electrical pulses that generate the pressure waves. By coordinating these delays, the focal point -point of highest pressure and thus highest temperature in the tissue- can precisely be controlled [40].

This design may consist of few hundreds of mini transmitters. The driving, controlling and matching the transmitters need for high technology and tricky business [40].
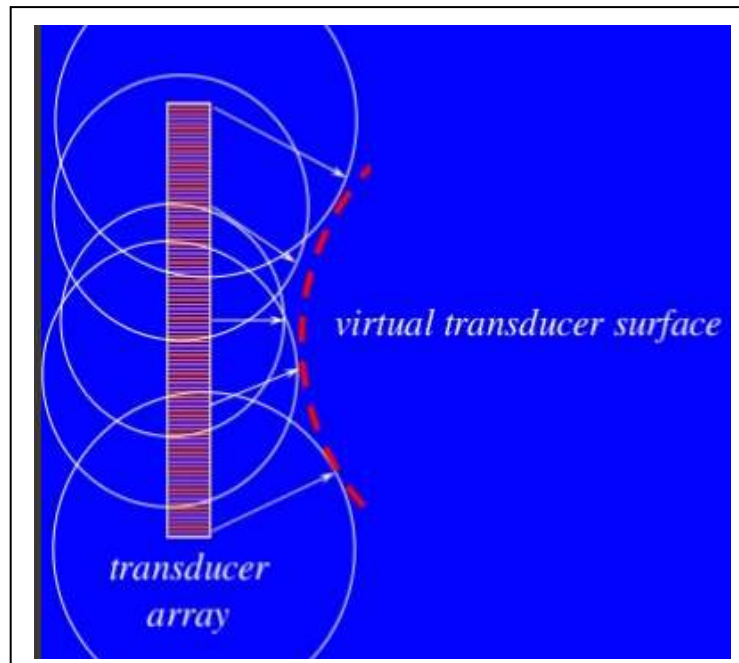
Figure 1.9. HIFU transducer focused by phase shifting for multiple PZTs

Focused ultrasound is a highly precise medical procedure that applies high-intensity focused sonic energy to locally heat and destroy damaged tissue through ablation. HIFU is a hyperthermia therapy, a class of clinical therapies that use temperature to treat damaged tissue. HIFU is also one modality of therapeutic ultrasound, involving minimally invasive or non-invasive methods to direct acoustic energy into the body. In addition to HIFU, other modalities include ultrasound-assisted drug delivery, ultrasound hemostasis, ultrasound lithotripsy, and ultrasound-assisted thrombolysis.

Clinical HIFU procedures are typically performed in conjunction with an imaging procedure to enable treatment planning and targeting before applying a therapeutic or ablative levels of ultrasound energy. HIFU is an approved therapeutic procedure for the treatment of cancers of the brain, breast, liver, bone, and prostate [41].

HIFU transducer that has been used for measurements in this thesis is shown in Figure 1.10. On the left hand side is the Sonic Concepts HIFU transducer with a hole for diagnostic purposes. It has a separate matching unit that acts for fundamental frequency and third harmonic generation as it is seen in right hand side of Figure 1.10. Sonic

Concepts HIFU transducer is a made of concave shape PZT and more details about this type HIFU taransducers can be found in reference [43].

Figure 1.10. HIFU transducers used in measurements covered by this thesis

In Figure 1.11, Precision Acoustics HIFU transducer is shown. It is made of a disc shape PZT with an acoustic lens in front. The matching network was embedded just behind the transducer backing [44].

Figure 1.11. HIFU transducers used in measurements covered by this thesis

Some other types of HIFU transducer pictures can also be seen in Figure 1.12. Two similar transducers with and without a hole in the center that were used in this thesis study are shown in (a) and (b) in Figure 1.12. Measurement and clinical purpose HIFU transducers (smaller ones) can be seen in (c) of the same figure.

| a-HIFU transducer without a hole for diagnostic purposes | b- HIFU transducer witha hole for diagnostic purposes | c- HIFU transducers for clinical applications |
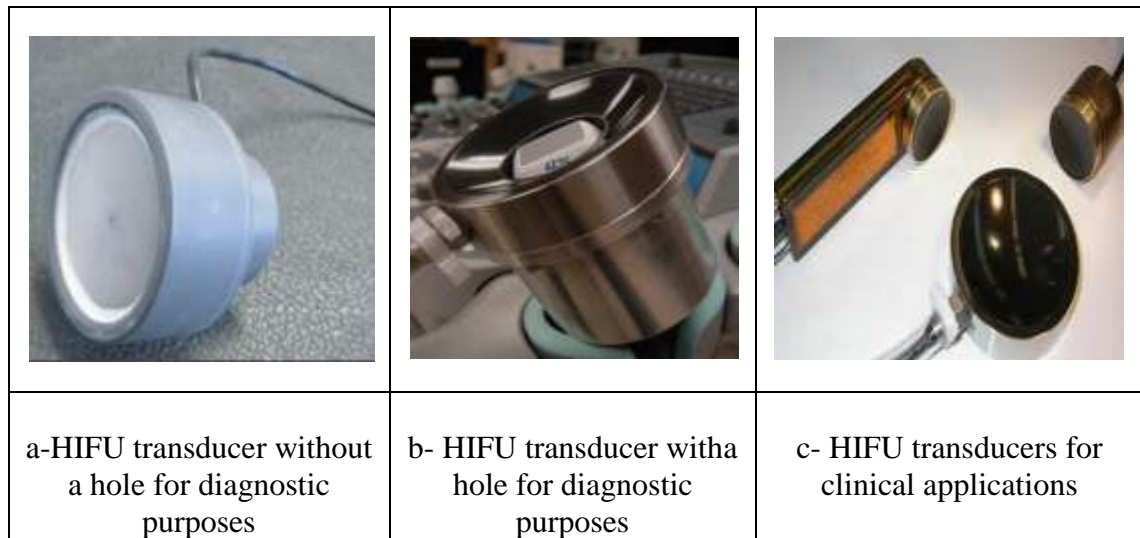
Figure 1.12. Single element HIFU transducers

Phased array HIFU transducer pictures can be seen in Figure 1.13. [43,45]. Upper one named as (a) in the figure is a rectangular PZT elements fabricated together and formed as a concave shape to produce a focal point. Lower ones named as (b) and (c) in the same figure are 256 circular PZT elements fabricated together and formed as a concave shape to produce a focal point.

a- Rectangular PZT elements fabricated together and formed as a concave shape

b- Circular PZT elements fabricated together and formed as a concave shape (prototype)

c- Circular PZT elements fabricated together and formed as a concave shape
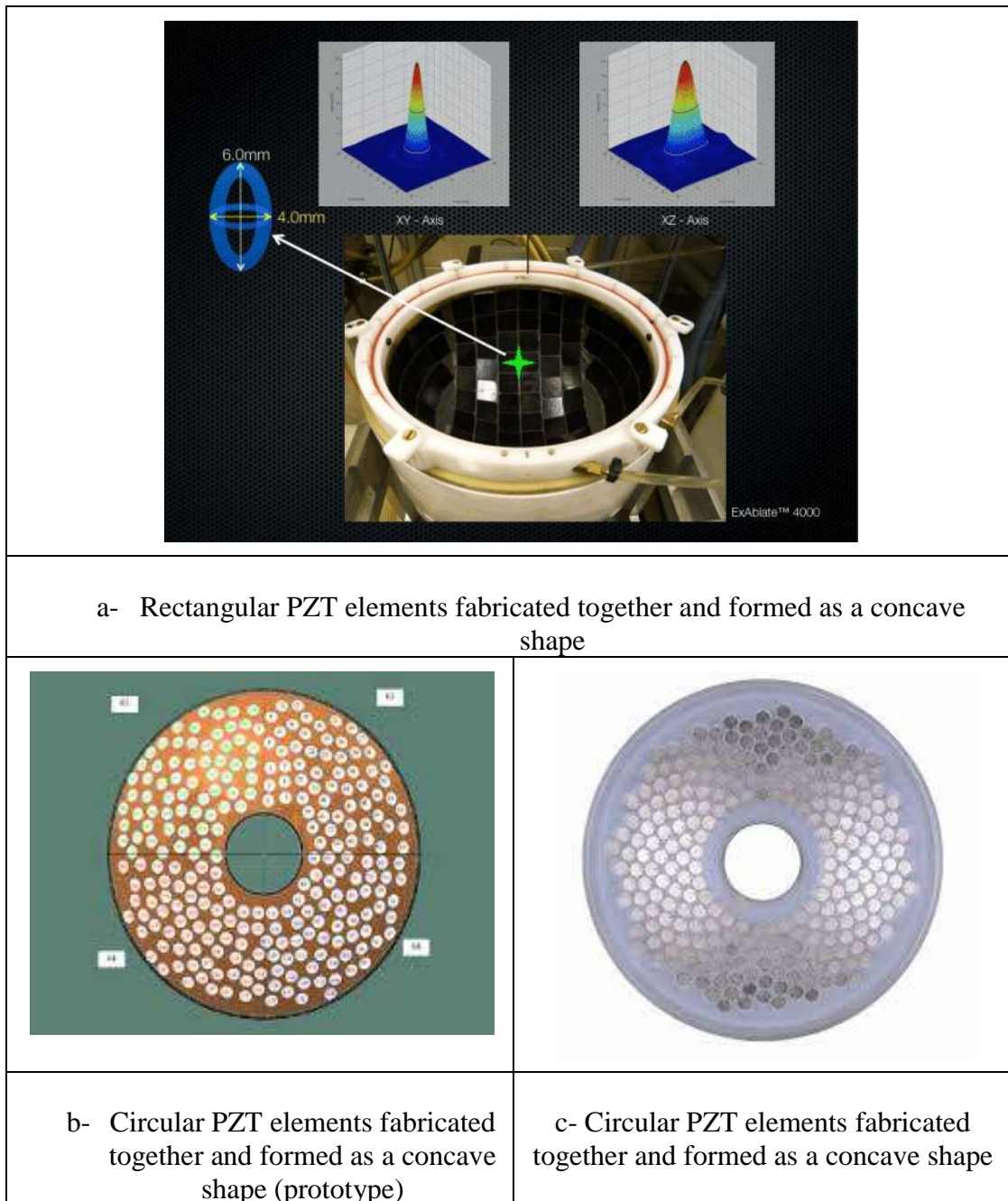
Figure 1.13. Phased array HIFU transducers

Application of HIFU can also be seen in Figure 1.14 and Figure 1.15 [46-47]. In Figure 1.14, two MR guided HIFU treatment system can be seen. Tumor is diagnosed by using MRI scanning. On the left hand side, HIFU transducer is located inside the bed for internal tissue treatments in the body. On the right hand side, HIFU transducer is used for applications for the head. Brain tumors inside the head are treated by HIFU.

Figure 1.14. Treatment with HIFU systems

In Figure 1.15, Ultrasound guided HIFU treatment system can be seen. This system is used for prostate cancer treatments [48]. Patient lies on the table (blue pad) in fetal positon. HIFU transducer penetrates through the rectum to come as close as possible to prostate region. Diagnostic imaging ultrasound probe, first visualize the cancer tissue, and then HIFU transducer burn the cancer tissue by moving in three dimension. Treatment takes 1 or 2 hours depending on the size of the lesion and patient goes back home just after the treatment.

Figure 1.15. Prostate treatment with HIFU systems

The biophysical effects of high-intensity ultrasound were first studied extensively in 1927 by Wood and Loomis [49]. They observed that planar ultrasound waves, propagating in parallel towards the target, could rupture biological cell membranes provided the intensity was sufficiently high. This observation triggered a lot of interest and the first recorded mention of the possibility of using ultrasound for cancer treatment was made in 1933. In 1942, Lynn et al. suggested that a geometrically concave transducer could be used to increase the local intensity by focusing the ultrasound waves, while keeping the intensity low in surrounding areas [37]. This allowed for inflicting tissue damage to a well-defined deep-seated focal spot while sparing surrounding tissue. Although a substantial amount of research was performed toward clinical applications (mainly ablation of the central nervous system) during the following decades, HIFU did not gain widespread clinical acceptance as a technique for local hyperthermia or tissue ablation mainly due to a lack of suitable guidance.

The generation of HIFU and the interaction of HIFU with biological tissue are also briefly described as they constitute the foundation for any HIFU therapy and are furthermore

necessary background in the discussion of the different sonication strategies and methods of feedback control. The book Physical principles of medical Ultrasonics compiled by Hill, Bamber, and ter Haar, can be recommended for more information on therapeutic ultrasound and the interaction of ultrasound with biological tissue [40].

2. ELECTRICAL AND ULTRASONIC POWER MEASUREMENTS

Important parameters to measure are the total power from HIFU transducer and instantaneous input electrical power. It is critical to measure the voltage and the current (to calculate the power) at MHz frequencies. A new measurement system at TÜBİTAK UME Ultrasound Laboratory has been built and improved for this purpose. Instantaneous input electrical power was measured by using voltage and current probes. The electrical power is calculated by using below equatoion (2.1).

$$P = V.I.cos\theta \tag{2.1}$$

In the equation (2.1), θ is the phase angle between voltage and current. An efficiency value that is the ratio of ultrasound power and input electrical power was given so that the end user will apply correct ultrasound power. All measurements at different systems and manufacturing of some sensors and set ups have been realized at TUBİTAK UME laboratories. As a result, the high power ultrasound field radiated by HIFU transducer that is used for cancer therapy, has been investigated experimentally and compared with available theoretical models in literature by thermal and ultrasound methods, in order to characterize the HIFU transducer and establish the safe and effective use of it. All measurements are traceable to national standards. The goal of this thesis is to investigate temperature and ultrasound field effects of ultrasonic transducers used in human body for cancer therapy. It is also very important measure the voltage and the current (to calculate the power) for ultrasonic transducers used in cancer therapy at MHz frequencies.

Instantaneous input electrical power has been measured by using voltage and current probes in the new system constructed at at TÜBİTAK UME Ultrasound Laboratory. The electrical power was calculated with three methods. Measurements were realized for two HIFU transducers whose resonance frequencies are 0,93 MHz and 1,10 MHz correspondingly. Details of measurement system, measurement results and uncertainty of measurements have been given in this study.

Parameters of the electrical power measurements had been well defined in low frequency applications. When the interested frequency level is higher than 100 kHz voltage, current

and impedance measurement results are easily affected input impedance of the measurement equipments. Input impedance of the measurement equipment and impedance of the transducer are contained resistive, capacitive and inductive components and these components are changed with frequency significantly.

Voltage across the ultrasonic transducer generally can be measured with oscilloscopes or RF voltmeter at the interested frequency region. Input impedance of the measurement equipment can be 50 Ω or 1 MΩ. If the transducer has got purely resistive component in this case only numerical corrections are necessary for between the input impedance of the measurement device and output impedance of the transducer. This correction term is negligible at 1 MHz frequency level. When the input impedance of the measurement equipment contained capacitive component, therefore it should be calculated and whether it should be taken account or not in the phase calculation.

2.1 ELECTRICAL POWER MEASUREMENT SYSTEM

Power measurement set-up of the ultrasonic transducer is shown in Figure 2.1. The connections on power amplifier were depicted in Figure 2.2. The output of the power amplifier was directly connected to a magnetic coupled current probe. It was coupled to the terminal of the power amplifier as shown in Figure 2 and current values are determined from its transformer current ratio and output voltage across its resistor. Magnetically coupled current probes generally have differential input features without creating any phase error between the voltage, V and current, I. Ultrasonic transducer was connected to the one port of Tee BNC (Bayonet Neill–Concelman) which is definition point for all electrical measurements. The other port of the Tee BNC was used for the voltage measurements. Voltage and current measurements are done by employing oscilloscope into the measurement system.

Agilent 4294A is used for the two terminal impedance measurements. Reference point for the two terminal impedance measurement is one port of the Tee BNC. The calibration of the impedance analyzer was realized at this point. List of devices used in the set up in Figure 2.1 are tabulated in Table 2.1.

Table 2.1. Devices used in electrical and ultrasonic power measurement set up

Name of device	Manufacturer and type
Generator	Agilent 33250A
Power Amplifier	ENI-150 W (Watts) and E&I-500 W
Oscilloscope	Agilent 500 MHz, 2GSa/s
Current Probe	Agilent 1147A compatible with Agilent oscilloscope
Impedance Analyzer	Agilent 4294A
HIFU transducers	Sonic Concepts and Precision Acoustics
Balance	Mettler Toledo PR2004
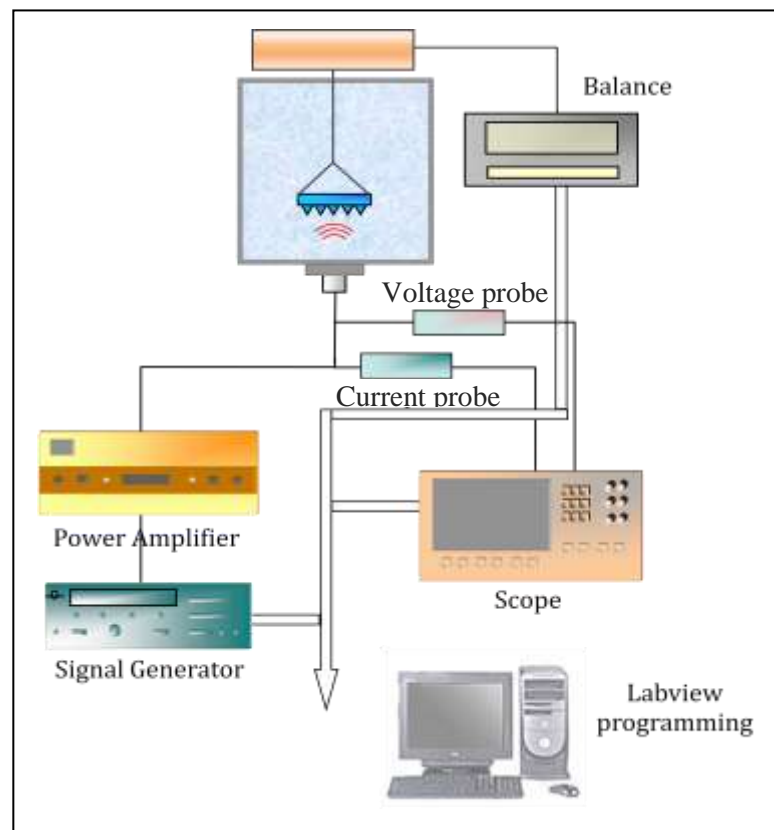
Figure 2.1. Electrical and ultrasonic power measurement set-up

Figure 2.2. Connections on power amplifier output to current and voltage probes.

An equivalent electrical network is seen in Figure 2.3. In the circuit diagram, C is the HIFU transducer main capacitance which produces ultrasonic energy, L_s is the self inductance of the two electrodes of the C capacitor, R_s is the resistivity of the two electrodes of C capacitor. R_p represents dielectric isolation resistance of capacitor that causes leakage current and it resulted in loss in the ultrasonic energy. By employing matching network, efficiency of the transmitted ultrasonic energy could be increased and harmonic components of the input electrical signal could be decreased.
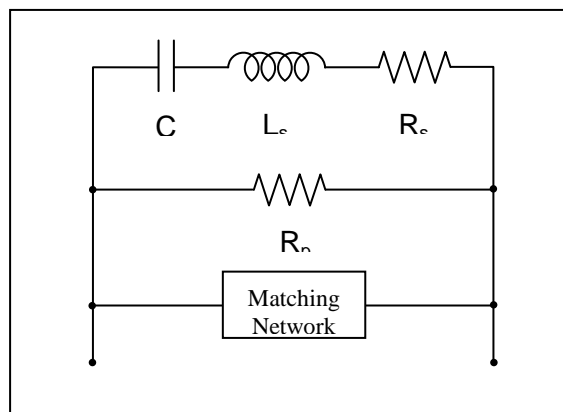
Figure 2.3. An equivalent electrical circuit diagram of HIFU transducer

Measurements have been carried out in the measurement system at TUBITAK UME Ultrasound Laboratory. All measurements were performed in controlled laboratory conditions with temperature and humidity stability of 23 °C ± 1,0°C and 50 % ± 10% respectively. Ultrasonic power measurement system has been located on a heavy granite marble in order to diminish the effect of vibration during measurements. Ultrasonic power measurements were realized in radiation force balance system according to IEC 61161 standard [50].

3. PRESSURE FIELD CHARACTERIZATION

The scattering of ultrasound due to tissue inhomogeneities will affect the energy of the propagating wave, since the scattering will redirect and disperse the ultrasound waves out of the main beam. For linear mediums, the attenuation of the propagating pressure caused by both absorption and scattering can be written as ashown in equation (3.1).

$$p(x)=p_0\,exp(-\alpha x) \tag{3.1}$$

In equation (3.1), p_0 is the initial pressure profile directly outside of the transducer surface, and x is the distance travelled by the ultrasound in the tissue with an attenuation coefficient $\alpha = \alpha_a + \alpha_s$ that contains both an absorbing (α_a) and scattering (α_s) component. Higher ultrasound frequencies cause an increase in attenuation, with the relationship being approximately linear for most biological soft tissues within the frequency range of interest for therapeutic HIFU.

When the literature survey was carried out, many studies, researches and thesis on the subject of HIFU transducer characterization can be found. Radiation force balance and hydrophone techniques are very popular techniques to characterize the HIFU field in a liquid medium. In these techniques, the ultrasonic power and intensity distribution have been determined, respectively [51]. A non-invasive method for characterizing HIFU fields in a liquid medium was recently developed by Hariharan et al (2008) [52]. The technique involved measuring the velocity induced in the liquid by transfer of momentum from the ultrasound beam to the absorbing liquid. An iterative numerical algorithm was used to calculate the acoustic intensity field giving rise to the measured streaming field [53].

One must be taken into account with the method is its ability to measure pressure components at power levels where acoustic non-linearity is significant. At low acoustic pressures, e.g. those mainly used in ultrasound imaging, propagation of acoustic waves is assumed to be a linear process [53]. But at high pressures, like those used in HIFU applications, linear approximations become useless and the non-linear terms should be accounted for in the propagation model.

At high pressures, ultrasonic waves traveling in the medium (i.e. water), change its shape (form) due to differences in the velocities of different portions of the wave spectrum. The positive (upper) portion of the sound wave which represents the compression phase travels much faster than the negative (lower) portion which corresponds to low density rarefaction phase. This causes the sinusoidal waves to steepen resulting in the formation of distorted wave forms. The amount of distortion depends mainly on the pressure of the wave and the nonlinearity of the medium. If the intensity is high enough, the sine waves can be completely distorted to form saw tooth waves.

For higher intensities of ultrasound waves, nonlinear propagation effects increase and result not only in waveform distortion and generation of higher harmonics, but also at sufficient levels, in the formation of shock waves [54,55]. In nonlinear acoustic theory, amplitude-dependent propagation effects are well described [56].

Although shock wave formation was not explicitly considered, nonlinear acoustic propagation has previously been studied and shown to have negligible effects on HIFU treatments. [57-58]

Ultrasonic pressure field models were investigated for finite amplitude ultrasonic waves in water propagation of focused structures [59]. Similar study were conducted by Şahin for circular and rectangular structures [60]. These studies had significant improvements in the field of acoustics. In these studies, theoretical and experimental results are compared and the results have been confirmed as compatible. Baker and Şahin (1994) have developed a new model for the rectangular focused transducers and some experimental data is presented [61,62]. Baker et al. (1995) A new theoretical model and experimental data were published in compliance with the published results [63]. Theoretical and experimental studies in two and three dimensions of the ultrasonic fields were studied [64-66].

Howard S.M and Zanelli C. I [66] have used a needle type hydrophone for measurements of HIFU field. Design and development of HIFU transducers were published by Schafer M.E. and others [67]. In this study, reflective target was used in the ultrasonic power

measurements and Pulse-Echo method was used for the characterization of PVDF hydrophone.

In the early 1970s, Khokhlov-Zabolotskaya and Kuznetsov have produced a famous equation known by their names abbrevations KZK for the non-linear wave equation including non-linear effects of acoustic waves, diffraction and dissipation [1,2]. Many researchers study to solve this KZK equation analytically [18,68].

3.1 THEORETICAL ASSUMPTIONS

Theoretical model has been used for circular source geometry [62]. All sources were assumed to be centered at the origin of the Cartesian coordinates and lie in the $\sigma=0$ plane. The initial boundary condition at $\sigma=0$ is that the particle velocity had constant unit amplitude u_0 over piston faces and vanished beyond the boundary of both sources. Similarly, the initial condition has unit amplitude and zero phases for the fundamental and the magnitudes of the all harmonics retained in the calculation were set to zero. It was also considered that the nonlinear propagation occurs in a thermo viscous medium, such as water. Under these considerations, the KZK equation that consistently accounts for nonlinearity, attenuation and diffraction was used.

$$\frac{\partial^2 W}{\partial \sigma \, \partial \tau} = \alpha r_0 \frac{\partial^3 W}{\partial \tau^3} + \frac{r_0}{2l_d} \frac{\partial^2}{\partial \tau^2} \left(W^2\right) + \frac{1}{4} \nabla_\perp^2 W \tag{3.2}$$

In above equation (3.2);

$W=u/u_0$ is the normalized particle velocity,

u is the fluid velocity in the direction of propagation,

u_0 is the characteristic velocity amplitude,

$\sigma=z/r_0$ is the normalized axial distance on the acoustic axis,

α is the absorption coefficient,

$\tau=(wt-kz)$ is the retarded time,

$l_d=1/\beta \varepsilon k$ is the acoustic shock distance,

β is the nonlinearity parameter,

ε is the acoustic mach number,

k is the acoustics wave number.

r_0 is the axial distance

$$\nabla_{\perp}^2 = \frac{\partial^2}{\partial x^2} + \frac{\partial^2}{\partial y^2} \qquad (3.3)$$

In above equation (3.3), the transverse Laplace operator defined in Cartesian coordinates.

Available theoretical models for the solution of the KZK equation can only be achieved by numerical methods [59, 60, 62]. It assumes a solution in the form of a Fourier series with amplitudes and phases that are functions of the spatial coordinates x, y and σ.

$$\begin{aligned} W(x,y,\sigma,\tau) &= \sum_{n=1}^{\infty} \left\{ W_n(x,y,\sigma) Sin\left[n\tau + \psi_n(x,y,\sigma)\right] \right\} \\ &= \sum_{n=1}^{\infty} \left\{ g_n(x,y,\sigma) Sin(n\tau) + h_n(x,y,\sigma) Cos(n\tau) \right\} \end{aligned} \qquad (3.4)$$

In above equation (3.4), n is the harmonic number,

W_n is the velocity amplitude in the Fourier expansion of W,

g_n and h_n are Fourier coefficients for the nth harmonics,

ψ_n is the phase of the nth harmonics.

Numerical modeling of experimental conditions was performed using a KZK-type nonlinear parabolic equation, generalized for the frequency-dependent absorption properties of the propagation medium:

$$\frac{\partial}{\partial \tau}\left[\frac{\partial p}{\partial z} - \frac{\beta}{\rho_0 c_0^3} p \frac{\partial p}{\partial \tau} - L_{abs}(p)\right] = \frac{c_0}{2} \Delta_{\perp} p \qquad (3.5)$$

In above equation (3.5), p is the acoustic pressure,

z is the propagation coordinate along the axis of the beam,

c_0 is the ambient sound speed .

Focused transducers can be modeled by knowing the source parameters, such as the main working frequency, the radius of curvature and the effective operational aperture of the source. The radius of curvature and the diameter of the transducer were nominally stated by the manufacturer as 62,6 mm and 64,0 mm, respectively. However, knowledge of these parameters still does not allow modeling the source as a uniform piston: the transducer housing, surface waves and inhomogeneity of the piezoceramic might limit and distort the exact uniform vibration of the source.

Therefore, it is necessary to first obtain the effective operational aperture and the radius of curvature of the source. To simplify the problem, the source was modeled as a curved uniform piston using nominal measures of curvature and aperture, and the axial and transverse pressure plots were calculated in the linear regime and compared with the measurements. The exact source geometry to be used in the model was then determined by adjusting the curvature and aperture to best fit the measured focal region.

Waveforms simulations in axial and transversal (radial) directions were performed with the HIFU-Simulator, which is a freely distributed MATLAB-based software package [69]. Material parameters of the measurement environment (water in this case) were adjusted in the software as the following: speed of sound c_S=1482 m/s, (in water), density ρ=10^3 kg/m^3, ultrasound absorption at 1 MHz $\alpha_{1\text{ MHz}}$=0,217 dB/m, exponent of absorption versus frequency η_1=2 and nonlinearity parameter β=3,5.

Transducer parameters also adjusted like; radius a_{act}, focusing depth z_{foc}, fundamental frequency f_0, acoustical power P_{ac}; Computational parameters also adjusted like; radius of the computational domain $R=a_{\text{act}}$, length of the computational domain $Z=2 \cdot z_{\text{foc}}$, number of considered harmonics K=100 are needed.

Besides data considering thermal aspects, the peak compressional pressure values $p+$, the peak rarefractional pressure values $p-$, the intensity I, as well as the pressure waveform $p(t)$ at the focus are available as output data. Due to the parabolic approximation of the KZK equation, the validity of the simulation software is limited to transducers with an f-number bigger than 1,37.

This code determines many important characteristics of continuous wave, high-intensity focused ultrasound (HIFU) beams and their heating effects [70]. This is done by integrating the axisymmetric KZK equation from the frequency-domain perspective. This results in a spatial distribution of pressure of each harmonic, taking into account beam diffraction, interference effects, power law frequency-dependence of absorption and the corresponding phase velocity dispersion, and the nonlinear effects of higher harmonic generation/wavefront steepening. From these pressure fields the temporal average intensity and heating rate are calculated. The heating rate distribution may then be used as a source for the bioheat transfer (BHT) equation, which may be integrated to determine the temperature and thermal dose distributions. [70].

The features of the simulator are as the following;

- use in MATLAB environment (The MathWorks, Inc., Natick, MA).
- Frequency-domain representation is suited for continuous wave simulations and roughly square-envelope pulses for which the pulse duration is much longer than the acoustical cycle.
- Accommodates arbitrary power-law frequency vs. absorption relationship. The corresponding phase velocity dispersion necessary to maintain causality is determined using an approximation of the Kramers-Kronig relations.
- Accommodates any axisymmetric transducer pressure distribution.
- Perfectly matched layer absorbing boundary conditions prevent spurious results caused by artificial boundaries.
- Includes bioheat transfer equation solver to determine temperature and thermal dose information.
- Automatically produces plots of many important quantities (pressure, intensity, heating rate, temperature rise, and thermal dose).
- Spatial distribution of positive pressure, negative pressure, intensity, heating rate, temperature rise, and thermal dose are accessible so the user may post process or further analyze the output.

The code comes pre-configured to perform an example run which may facilitate the user's familiarity with the software. The two main parts are the propagation code and the heating

code. To run the example simulation, command is typed at the MATLAB prompt as shown below.

$$[z,r,H,I,Ppos,Pneg]=axisymmetricKZK(); \qquad\qquad (3.6)$$

This starts the HIFU beam simulation with the parameters indicated in the following Table 3.1 [70].

Table 3.1. Parameters used in the model

Item	Parameter	Symbol	Value	Unit
Material 1	small-signal sound speed	c_1	1482	m/s
	mass density	ρ_1	1000	kg/m^3
	absorption at 1MHz	α_1	0,217	dB/m
	exponent of absorption vs. frequency curve	η_1	2	-
	nonlinear parameter	β_1	3,5	-
	material transition distance	z	5	cm
Material 2	small-signal sound speed	c_2	1629	m/s
	mass density	ρ_2	1000	kg/m^3
	absorption at 1MHz	α_2	58	dB/m
	exponent of absorption vs. frequency curve	η_2	1	-
	nonlinear parameter	β_2	4,5	-
Transducer	Radius	a	2,5	cm
	focusing depth	d	8	cm
	Frequency	f	1,1e6	Hz
	Power	P	100	W
Computational domain	max radius	R	A	cm
	max axial distance	Z	2d	cm
	number of harmonics	K	128	-

Figure 3.1 shows the waveform at the focal point. Sinusoidal waveform has been distorted at the focal since the nonlinear propagation and diffraction in water (or in tissue).
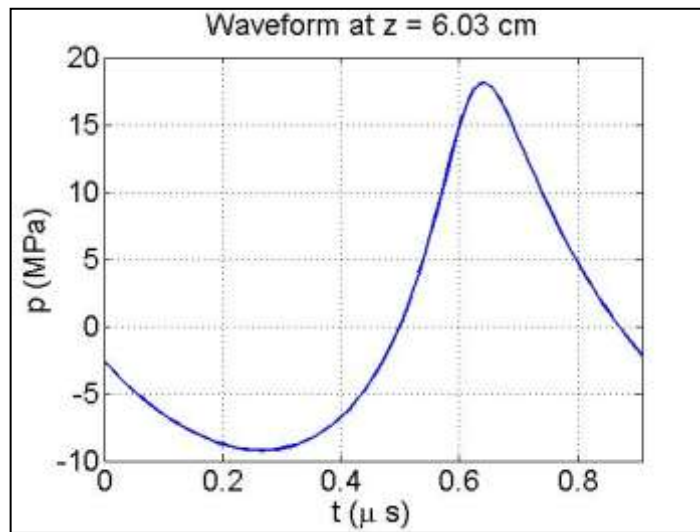
Figure 3.1**.** Time waveform (on axis) at distance where peak pressure occurs

Besides it generates an asymmetric distortion of pressure waveforms, higher harmonics and narrow harmonic beam widths also occurs as it is seen in Figure 3.2 for radial propagation and in Figure 3.3 for axial propagation.
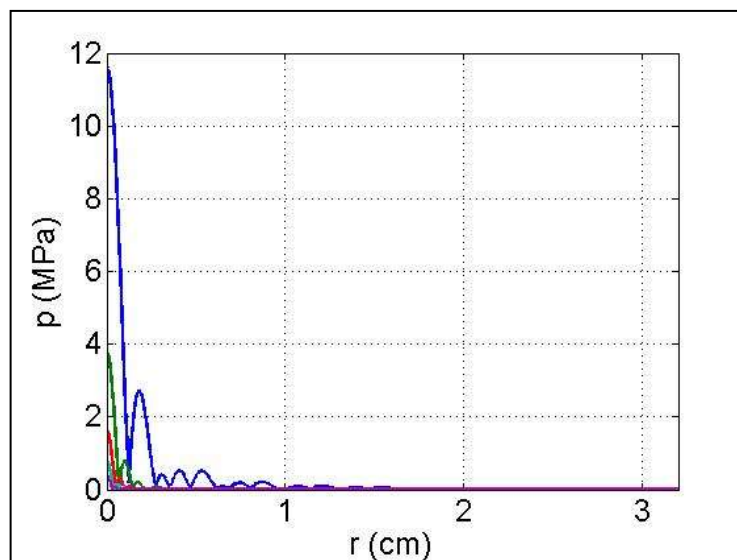
Figure 3.2**.** Radial pressure amplitude of the first five harmonics at focus
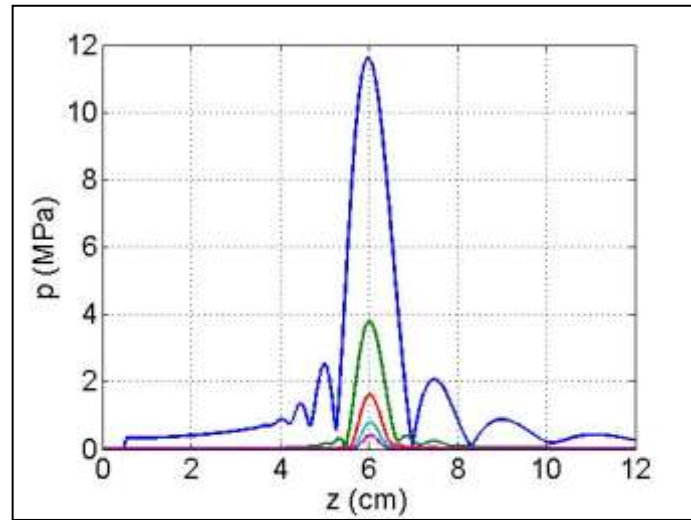
Figure 3.3. Axial pressure amplitude of the first five harmonics

Figure 3.4 shows the peak compressional pressure and peak rarefactional pressure as a function of axial distance, z from the surface of HIFU transducer.
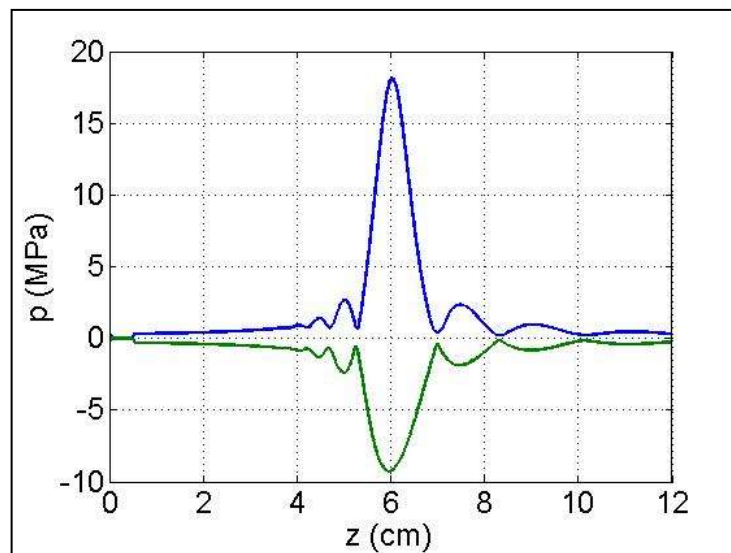
Figure 3.4. Axial peak compressional and rarefactional pressures

3.2   MEASUREMENT SYSTEM SPECIFICATIONS

3.2.1   HIFU Transducer

The H-102 transducer by Sonic Concepts is a highly efficient transducer intended for HIFU field investigations. Its fundamental frequency is 1,10 MHz, active radius is 70 mm, focal point is 62,6 mm and has a 15 mm central opening for imaging as it is seen in Figure 3.5. The transducer is used with a matching box terminated to 50 Ω. The acoustic output is stable over the radiating surface. The measured efficiency of the transducer with the matching network is typically over 80% across the fundamental frequency.

Figure 3.5. The H-102 transducer with impedance matching unit

3.2.2   HIFU Hydrophone

HNA-0400 hydrophone from ONDA Corp. (Sunnyvale, CA, USA) as seen in Figure 3.6 is designed to be used in high pressure ultrasound fields like HIFU transducers produce. It is a commercially available HIFU hydrophone, consisting of a sensing PZT (Lead Zirconate Titanate – namely called Piezo-electric ceramic) element with a diameter of 400 μm, which is protected by a metallic coating with a thickness of 30 μm [23]. It is a needle type of hydrophone that eliminates errors arising from reflections from measurement environment. It has a nominal sensitivity of 70 nV/Pa.
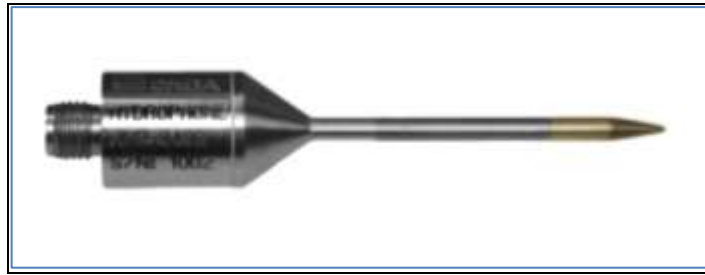
Figure 3.6 The HIFU hydrophone

Frequency characteristics of the hydrophone are given in manufacturer data sheet between 1 MHz and 20 MHz as seen in Figure 3.7.
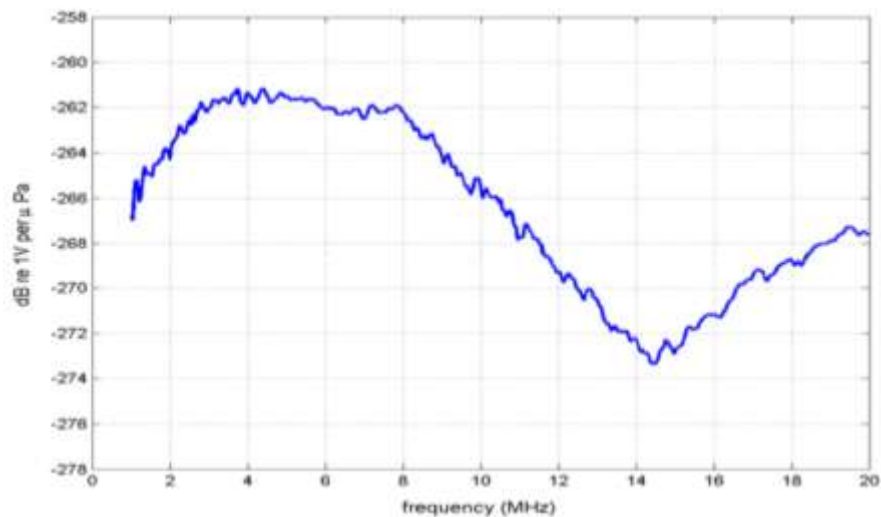
Figure 3.7 Frequency response curve for HNA-0400 hydrophone

3.2.3 Measurement Tank

HIFU transducer and receiver hydrophone were mounted inside the water tank whose dimensions are 200 cm (length), 100 cm (height) and 100 cm (depth). A scanning system that have a two arm, one of which has motion capability in three direction x (horizontal) ,y (horizontal) and z1 (vertical) and the other has motion capability in turning along itself (w) and vertical (z2) were used to scan the field. HIFU transducer were mounted on the arm-II of the scanning system and receiver transducer were mounted on the arm-I. Scanning measurement results were analyzed by a Labview programme.

Measurement tank has been designed and produced for mounting the transducers and hydrophones in different arms which are controlled individually, as seen in Figure 3.8. Water tank and positioning system have no mechanical contact to each other so that preventing any vibration through out the movent in water. Positionning system has been produced by steel and joint by steel soldering technique. Water tank was made of three layer of laminated glass and mounted and isolated by using special silicon joint material. Water tank is seen in white color, frame of the positioning system is seen in black in Figure 3.8.
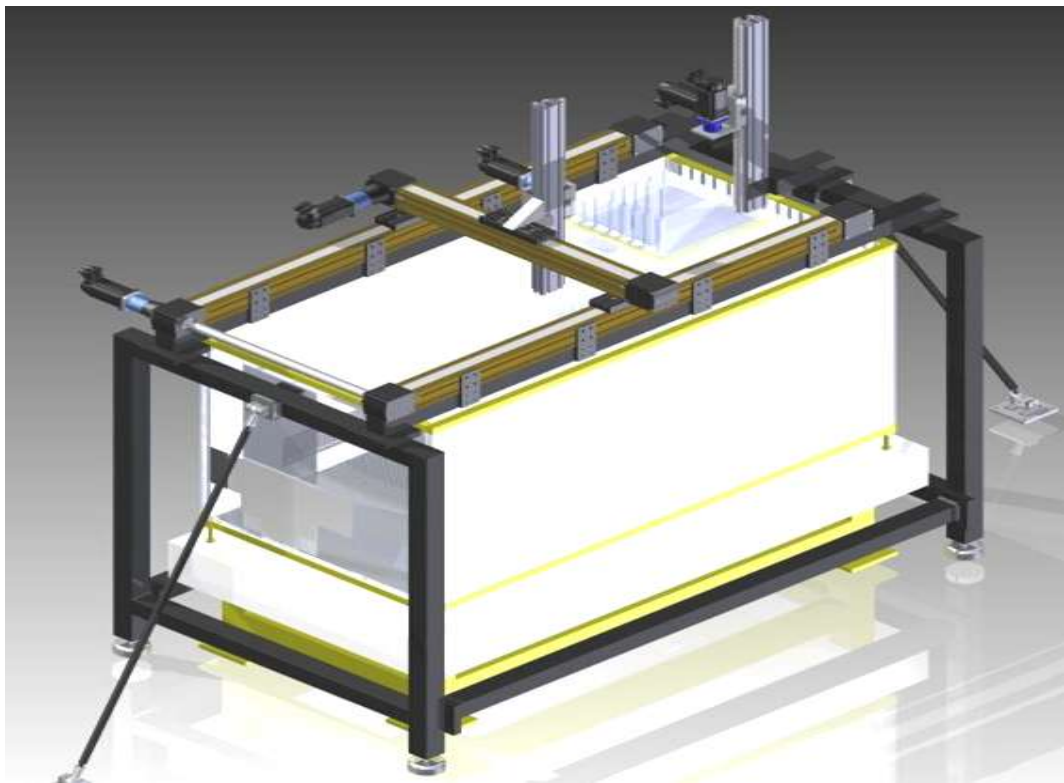
Figure 3.8. Sketch of the water tank for HIFU pressure measurements

HIFU pressure measurements have been realized in the system shown in Figure 3.9. All measurements were realized inside the degassed, deionised and distilled water since the water environment simulates the human body characteristics (as the human body contains 2/3 of water).
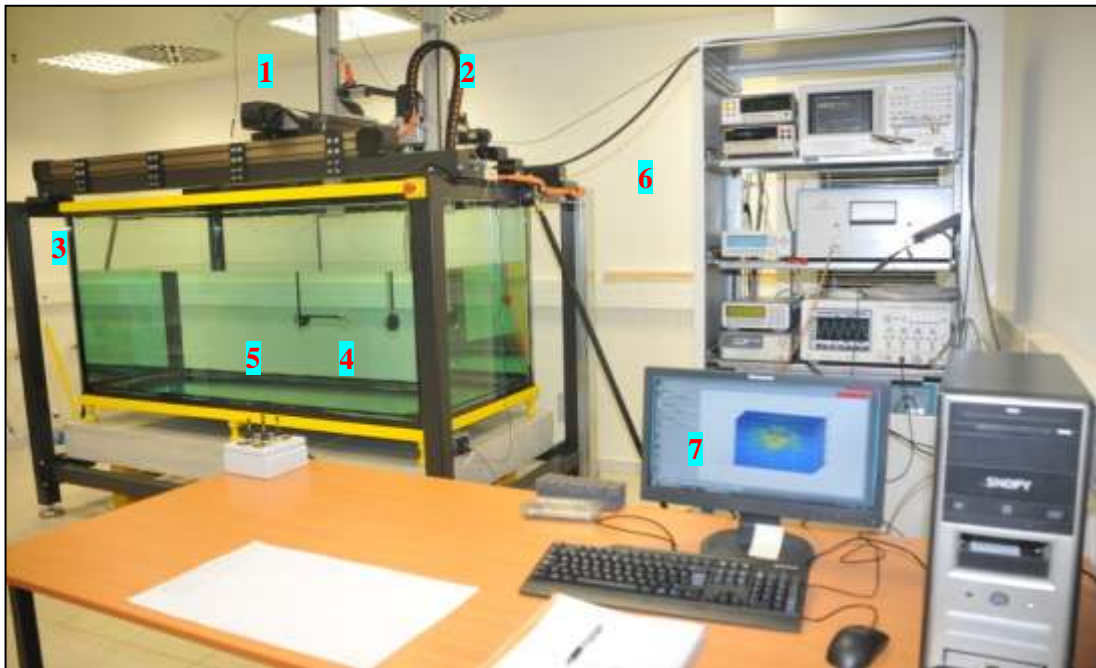
Figure 3.9. Photograph of the home-made water tank and measurement system for HIFU pressure measurements

Positionning system that is seen in Figure 3.9 have two arms as it was stated before. Arm1 is numbered as 1 and 2. HIFU transducer labelled as 4 in the picture was mounted in Arm-2 (labelled as 2 in the picture) and hydrophone labelled as 5 in the picture was mounted in Arm-1.HIFU transducer and hydrophone were located inside the water. Drivers, amplifiers and automatic control of the positioning system were located in a rack labeled as 6 in the picture. Signal generator, oscilloscope, power amplifier and other measurement devices were also located in same rack. Positioning system and measurements were controlled by a software in a Labview programme labelled as 7 in the same Figure 3.9.

HIFU transducer at the working frequency was mounted on specially designed holders and placed, horizontally inside the water. Receiver hydrophone was placed through the axial distance corresponding to the focal plane. Separate holders were used to mount for transducers and hydrophones. Special care was taken in making sure that no air bubbles were present inside water and at the surface of the source or the receiver. Residual bubbles were removed with a thin wire by manually.

HIFU transducer was fed via signal generator and power amplifier in the resonance (working) frequency. The pressure transmitted by HIFU transducer was measured by receiver hydrophone.

Signal from the power amplifier of various power levels was fed directly to the oscilloscope by using a probe (1:10 attenuator) in order to test the harmonics produced by the power amplifier and verify that the harmonics generated only represent the nonlinear acoustic field. Probe was connected directly to the 1 MΩ termination of the oscilloscope. Then the signal output of the power amplifier was applied to the HIFU transducer. The high intensity and focused ultrasound field generated by the HIFU source was determined by the needle hydrophone at transducer surface and focal plane, respectively.

Receiver hydrophone was aligned on the acoustic axis, in order to make sure that the measurements were taken at a point around the focus. A voltage of 100 V RMS (root mean square) was applied to the 1,10 MHz HIFU transducer electrical terminals from the power amplifier. A matching box was used to match the acoustical and electrical gain curves. No preamplifier was used behind the HIFU receiver hydrophone. Only original cable delivered by the manufacturer (Onda Corporation, Sunyvale, USA) and a 50 Ω cable (75 cm long) provided by the NI was used with analyzer card.

The signal was captured and analyzed by the commercially available LabVIEW 8.1 software (National Instruments). LabVIEW is a system-design platform and development environment for a visual programming language from National Instruments. It is originally released for the Apple Macintosh in 1986. LabVIEW is commonly used for data acquisition, instrument control, and industrial automation on a variety of platforms including Microsoft Windows, various versions of UNIX, Linux etc.

Firstly, user interfaces (called front panels) were created into the development cycle. VI (virtual instruments) was organized by using block diagram, front panel and connector panel as it is seen in Figure 3.10. The front panel was built by using controls and indicators. Controls were used as inputs and indicators were as outputs. All measurement block diagram containing the graphical source code were organized in the back panel. All of the objects (signal generator, analyzer etc.) were placed on the front panel. The back

panel also contains structures and functions which perform operations on controls and supply data to indicators. The structures and functions are found on the Functions palette and can be placed on the back panel. Both time and frequency domain information were recorded using LabVIEW software. The pressure-time signal was then processed to obtain the amplitude by LabVIEW.
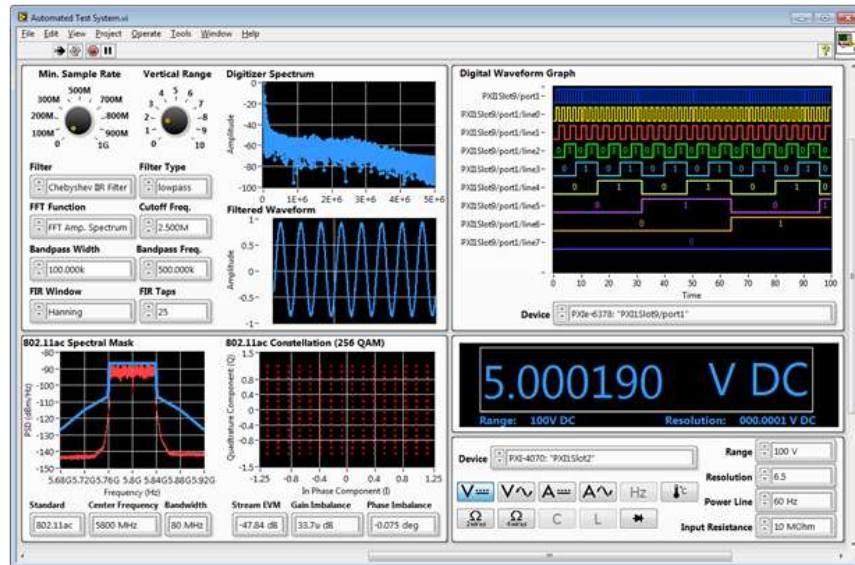
Figure 3.10. LabVIEW software

LabVIEW program specifications was detailed in Apendix A.

Ultrasound field scanning system specifications are listed below;

- Tank Dimensions; 200 cm (length) x 100 cm (width) x 100 cm (depth)
- Scanning region: 150 cm x 70 cm x 70 cm
- There are two arms; one has x, y, z (depth) direction motion and the other has z (depth) and turning motion
- Positioning accuracy is 100 μm and 0,01 °
- Fully automated system synchronized with measurement system
- The translation stage was controlled by a Labview based program which also allowed a joystick control. The driving signal was generated a signal generation card (-National Instruments, NI PCI-5412) [71] and output from the

hydrophone was fed directly into a DSO (digitizing signal oscilloscope card, (NI PCI-5105) [72]. The controlling program executed a "capture-analyze-move" cycle, allowing a large number of measurements to be made.

- Measurement parameters:
- Ultrasound pressure field measurements,
- p1, (and harmonics, p2, p3, p4, p5), p+, p-
- 2D and 3D mapping is possible

The HIFU transducer used is a single element spherically focusing piezoceramic transducer with a hole in the center for imaging (H-102, Sonic Concepts) and have parameters is given as it follows;

- the source radius is r0 = 32 mm,
- the focal length is F = 62,6 mm, and
- the main frequency is f0 = 1,10 MHz

The transducer was driven in a "burst" mode; to avoid signal disturbances due to the acoustic reflections from the walls of the water tank and surface of water. Because the ultrasonic transducers have a very high gain in air, they are heated quickly and can easily be broken.

Short pulses series (30-cycle excitation) was fed in the transducer by a function generator card (NI-National Instruments) through a linear RF amplifier (ENI-Electronics and Navigation Industry).

- τon= 10 cycles = 9,1 μs for f = 1,10 MHz
- pulse repetition period: T = 5 ms,
- pulse repetition frequency: PRF = 200 Hz,
- duty ratio: D = 1,8·10^{-3} for f = 1,10 MHz

An ideal tone burst signal is shown in Figure 3.11 and a snap shot picture taken from oscilloscope display is shown in Figure 3.12. It is a tone burst signal terrain of 20 pulses in 1 s.
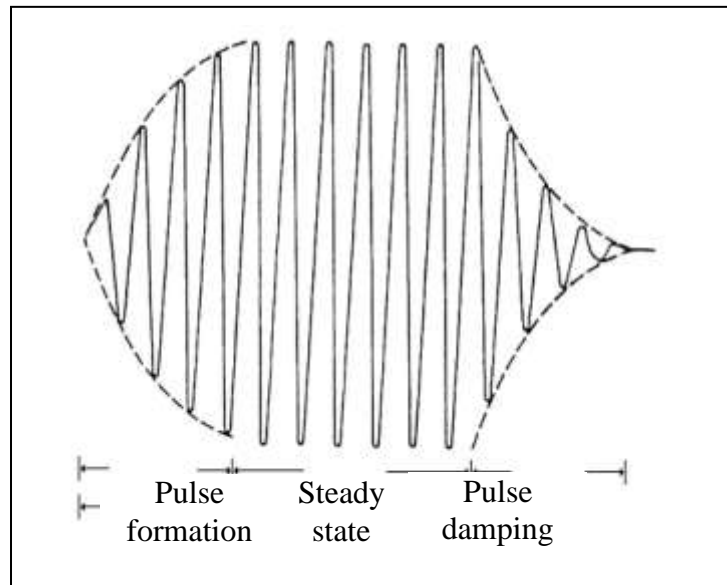
Figure 3.11. An ideal tone burst signal
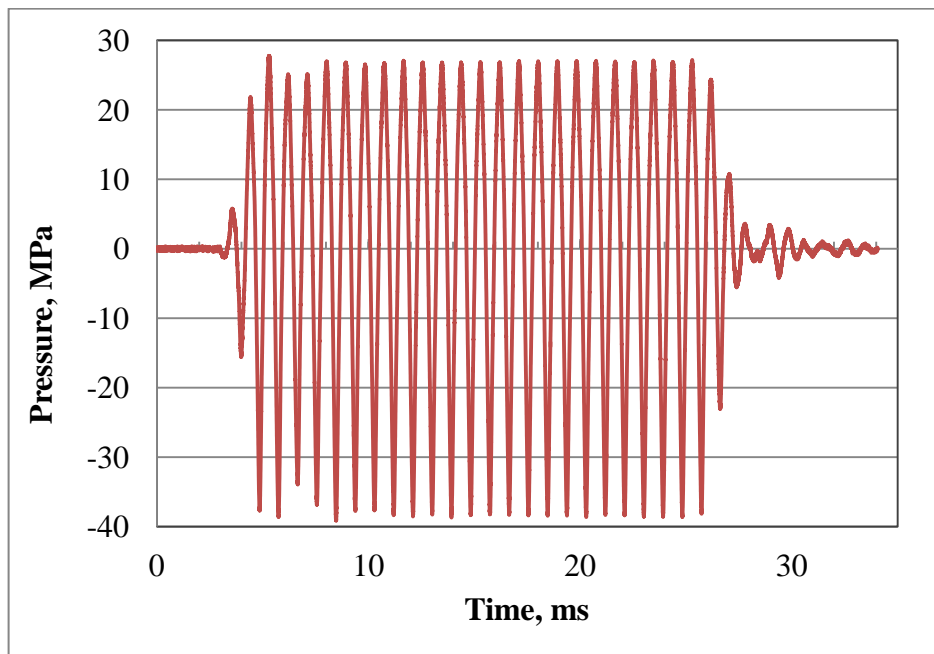
Figure 3.12. A tone burst signal taken from oscilloscope

The measurements of the ultrasound field were carried out with a needle hydrophone (Onda Corparation). The hydrophone was attached to a 3-axis, computer-controlled positioning system for alignment with the ultrasound source. The hydrophone signals were

recorded by NI signal analyzer card with a sample rate of 500 MS/s and a data length of 25000 points per waveform.

For each waveform, the following parameters have been calculated:

- $p+$= peak-compressional acoustic pressure max(p(t))
- $p-$= peak-rarefactional acoustic pressure –min(p(t))
- p (pp) = peak-to-peak pressure pc+pr

All of the experiments were performed in a large water tank at room temperature (23 °C). The water was deionized and degassed prior to measurements to limit the development of cavitations.

3.2.4   Alignment of the System

There are a number of important factors that can influence the measurement results as follows;

- Alignment of the transducers
- Environmental conditions (i.e. water)
- Stability of the measurement system
- Vibration of the tank
- Low signal from receiving transducer
- Electrical noise from motors

Alignment of the transducers:

One of these factors is the method by which the hydrophone is mounted. Poor alignment will affect the response of a hydrophone, the degree of influence depending on its directional response at the measurement frequency. Misalignment may be caused by the use of a mounting pole that is not straight, leading to an error in hydrophone position and potentially an error in hydrophone orientation. The accurate alignment of needle hydrophones is essential for accurate acoustic measurements. The transducer was scanned along the axis to locate the focal distance as seen in Figure 3.13 and Figure 3.14. The focal

distance was estimated by a scan along the acoustic axis of the transducer with a step size of 0,5mm and is identified as 62,6 mm for Sonic Concepts

HIFU transducer. Alignment has been explained step by step as follows;.

- HIFU transducer face was mounted perpendicular to the positioning system rod with a perpendicular fixture.
- Receiver hydrophone (Onda Corporation) was mounted perpendicular to HIFU transducer face with a perpendicular fixture.
- Zeroing between the HIFU transducer and receiver hydrophone was adjusted by getting the both transducers as close as possible (slightly touching)
- Receiver hydrophone was adjusted manually (with a joystick) to be in the center of the HIFU transducer. This adjustment as can be seen in Figure 3.13 was checked by eye.
- Positioning system was set to zero automatically by software, in this position.
- Receiver hydrophone was positioned at 20 mm, 40 mm, 60 mm, 80 mm and 100 mm away from the HIFU transducer face (x-axis).
- HIFU transducer was fed by a signal generator and power amplifier assembly at around 100 Watts electrical power. Electrical power was measured simultaneously by current and voltage probes and an oscilloscope.
- Y-axis (z-axis is constant) was scanned between -10 mm and 10 mm in 1 mm steps at each x distance between HIFU transducer and receiver hydrophone. The acoustical pressure was measured and recorded automatically at each position.
- After all measurements were finished, y-axis values were drawn at each x- axis position in order to see the maximum peaks.
- Measurements were repeated for z-axis while y-axis was constant at x-axis positions.
- Positioning system were aligned (moved −y and +y and −z and) to see the maximum in the center.
- Then positioning system was set to zero again automatically by software, in this new position.
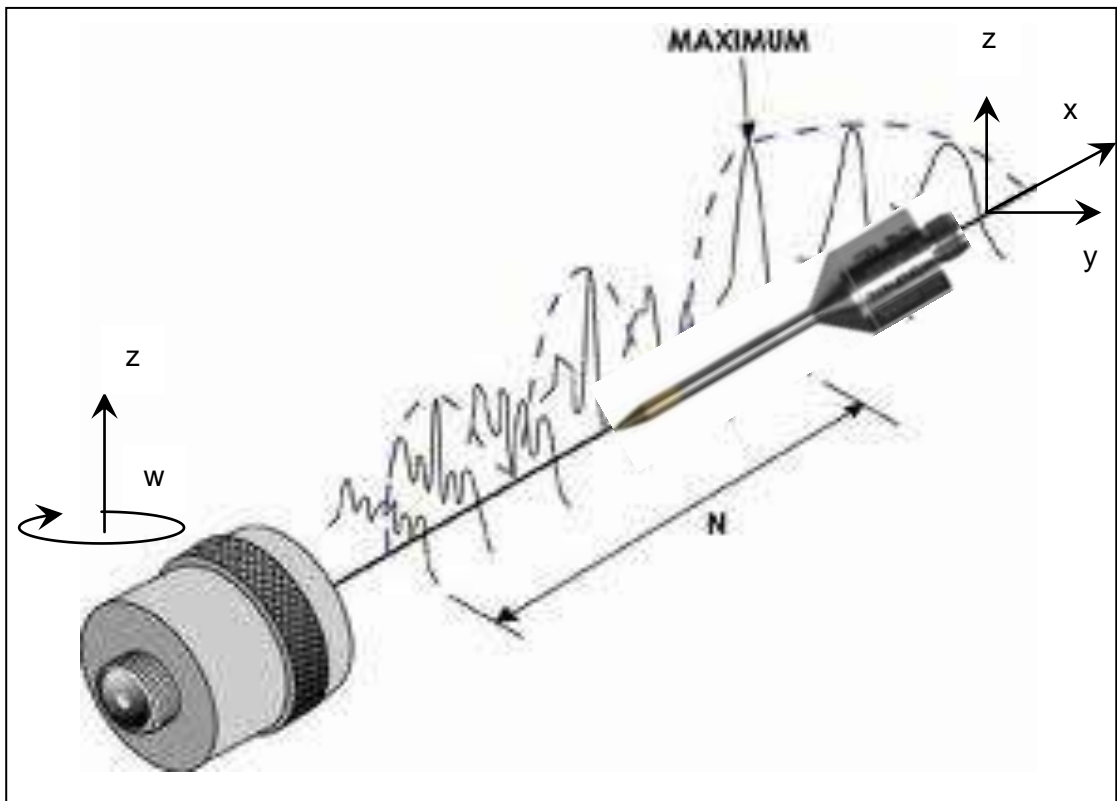
Figure 3.13. Alignment of the transducer and hydrophone
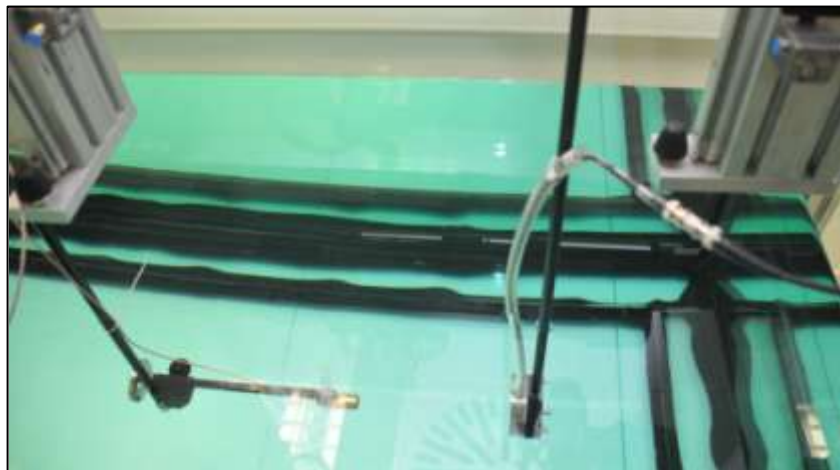
Figure 3.14. Mounting of the carbon-fiber rods in two arms

In case of misalignment, it is most probable to have unexpected results as it can be seen in Figure 3.15, Figure 3.16 and Figure 3.17. In Figure 3.15, the fundamental peak hasn't got a sharper shape and the maximum is not clear. Also second and third harmonic don't have a single peak, around the focal plane.
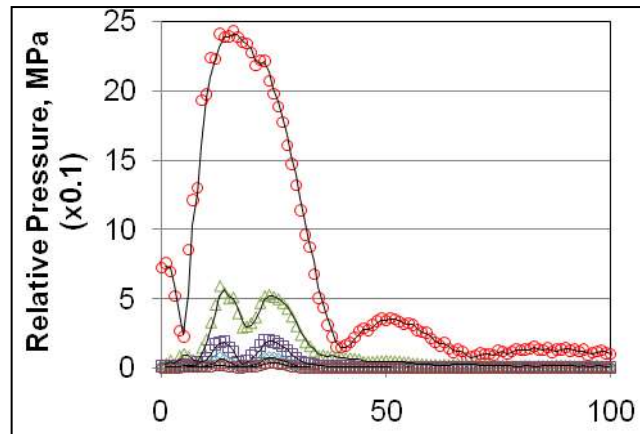
Figure 3.15. Ultrasound peak pressure variations on acoustic axis

In Figure 3.16, peak compressional pressure P+ and peak rarefactional pressure P- haven't got single peaks.
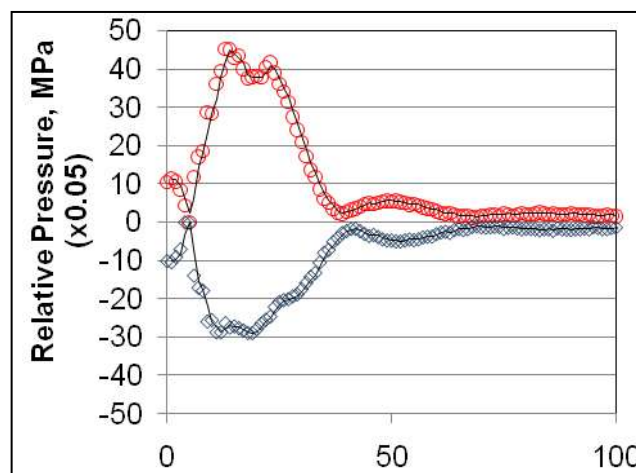
Figure 3.16. Ultrasound peak compressional and rarefactional pressure variations on acoustic axis

In Figure 3.17, the maximum pressure field is not clearly resolved in the expected focus.
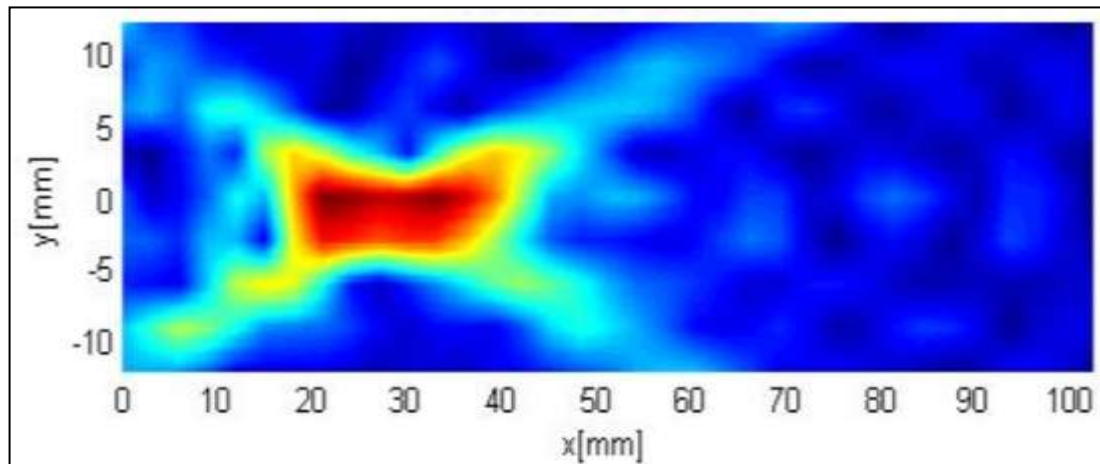
Figure 3.17. HIFU pressure field- preliminary measurement results

Environmental conditions:

Distilled, Deionised and degassed water were used inside the tank. Water used in ultrasound measurements must have some specifications published in [73]. 5 micron and 1 micron filters, UV lamp were used for distillation. So inorganic compounds such as metals (iron and lead) and nitrate and hardness (calcium and magnesium) were removed out of water. Water temperature was monitored during the measurements.

Stability of the measurement system:

Some designs were made to mount the transducers to obtain stability and suitable for needle hydrophone. Carbon-fiber tubes (cylindrical) were used to mount the transducers to positioning system's post. Carbon-fiber is a lightweight fiber used in advanced composites.

Also, L shaped mount is used to fix the needle hydrophones so that it is positioned in exactly the same place within the acoustic field.

Vibration of the tank:

Vibration of the water during the measurements imposes some instability problems. In order to avoid this problem, water tank and precise positioning system were built

separately without any mechanical contact between them except floor. Water tank was maintained on one ton of a heavy (~ 4000 kg) marble block its steel legs were standing on the isolation material as it is seen red rectangle in Figure 3.18. Therefore, the vertical movement of the system was minimized. Water tank was stabilized also with supporting adjustable steel rods in both sides in order to minimize lateral motions as it is seen in blue rectangle in Figure 3.18.
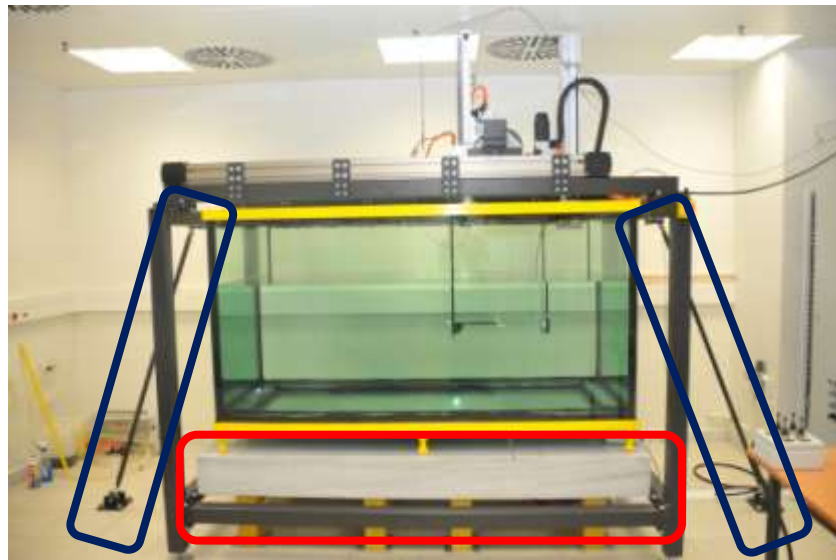
Figure 3.18. Water tank and positioning system stability

Low signal from receiving transducer:

The cable between receiving hydrophone and analyzer where is mounted on the computer case, was very long (3 m), because of the physical distance. Computer was brought nearer to the hydrophone so that shortest cables without extra connector are used. Only transducer cable whose length is 50 cm and original cable (NI, IREX 0749) of NI oscilloscope card whose length is 80 cm were used. In this way, lost in the signal through cable is diminished and signal-to-noise ratio was increased. Amplification of the signal was observed and compared by using longer and shorter cables.

Electrical noise:

Positioning system has 5 servo motors for 5 axes. They have high frequency electrical white noise that affects the reading values on oscilloscope. Effect of electrical noise from

DC motors can be seen in yellow sinusoidal signal in Figure 3.19. In order to avoid this noise, positioning system was switched off before each measurement.
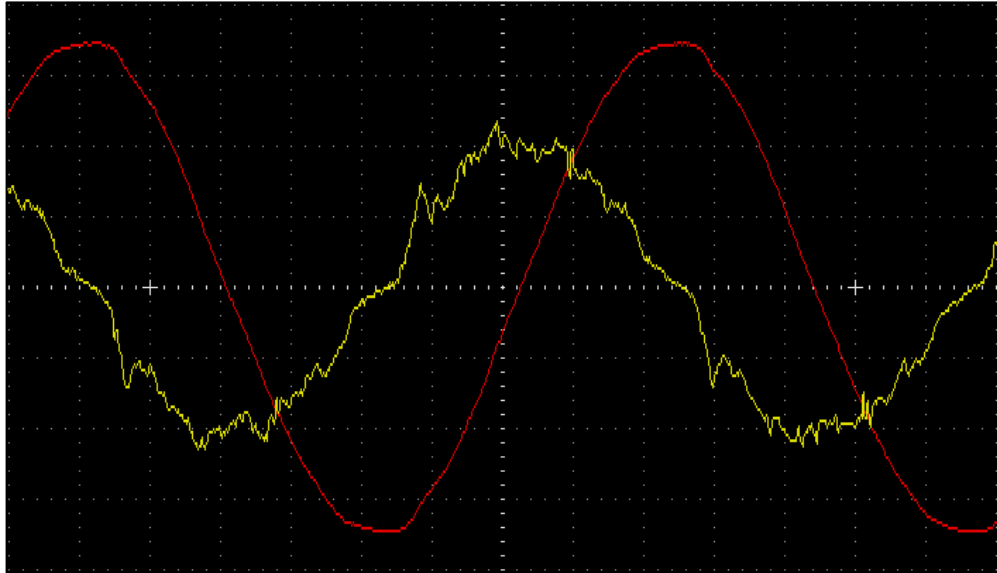
Figure 3.19. Measurement signal with and without electrical noise

Cleaning of the transducers:

Before puttin the HIFU transducer and hydrophone were in to the water, they are cleaned with an oil solving detergent in order to remove oil and dusts. Because oil and dust increase the cavitations inside the water that affects the measurement results.

4. TEMPERATURE DISTRIBUTION CHARACTERIZATION

As ultrasound propagates through biological tissue it loses energy, or becomes attenuated, partially through absorption and partially through scattering and due to nonlinearity. The fluctuations in pressure induce vibrational and rotational motion of the tissue molecules that in turn causes a rise in temperature depending on the frequency and absorption coeffficient of the medium (such as water or tissue). This phenomenon can also be interpreted as absorption and conversion of mechanical ultrasound energy into heat energy.

Very fast energy transmission during HIFU procedure affects a drastic rise in local tissue temperature of the order of 60 °C. For such high pressures, one can be thought a burning if a care would not be taken. High pressure and high dosage may cause an unexpected damage to healthy tissues. On the other hand, lower dosage of energy results in inadequate destruction of the tumor in the tissue. For effective treatment and patient safety during HIFU application, energy should be delivered at the exact target with the correct dosage level. In order to determine the accurate thermal effects generated by the HIFU radiation within the propagation medium, it is highly necessary to conduct accurate temperature measurements. Therefore, analytical methods of characterization of the HIFU thermal distribution in a solid medium (such as in a tissue phantom) are required. Characterization involves determination of the thermal distribution with respect to its distribution in space (spatial measurement) as well as its variation with time (temporal measurement) and also assessment of the lesion size.

In this part of the thesis, improved and accurate methods to assess the HIFU thermal effects in tissue mimicking materials have been studied. An important tool for the characterization of a HIFU transducer is the determination of the temperature effect in the tissue phantom. Although the tissue media have significantly different properties than liquids especially the acoustic absorptive, the similar tissue mimicking materials are on the market [23].

When the literature is searched for HIFU transducer characterization by means of thermal ways, a number of studies can be found. In this study accurate and convenient techniques

for characterizing the thermal field distribution generated by the HIFU transducer in solid tissue media are studied. Characterization of the HIFU thermal field distribution involves a number of investigations performed in a tissue-mimicking material. These include quantification of temperature rise (in spatial and temporal coordinates) and lesion volume in a tissue-mimicking material. Method for assessing the HIFU induced thermal effect in tissues has been discussed in this study.

Thin wire thermocouples embedded in tissue mimicking materials have been popularly used for measuring the HIFU induced transient temperature rise by focusing the beam on the thermocouple junctions at selected power levels. Thomas et al studied acoustic cavitation activity in polyacrylamide and agar-graphite phantoms [28]. Temperature rise was measured using embedded E type thermocouples of diameter 0,13 mm. Similarly, Wu et al (2004, 2007) used a tissue mimicking phantom with embedded thermocouples, to study acoustic cavitation, in HIFU ablation [74,75].

In a study, temperature rise in a tissue mimicking material modified to include an artificial blood vessel, is measured with thermocouples embedded in the material close to the vessel [76]. The purpose in that study was to investigate the effect of blood flow on HIFU procedures.

The insertion of thermocouples in real tissues is an invasive process and hence inconvenient in in-vivo studies involving anaesthetized animal specimens. Besides, technical difficulties associated with the use of thermocouples, limit their use. For HIFU studies, thin wire thermocouples (of diameter 20 µm to75 µm) are used. These are fragile thermocouples and vulnerable to breakage due to mishandling.
HIFU is being used in clinical treatments to coagulate benign or malignant tissue by thermal procedures [77,78].

4.1   TEMPERATURE DISTRIBUTION MODEL

The temperature rise caused by absorption of HIFU energy is often described by using Pennes' bioheat transfer equation that takes into account the heat diffusion as well as heat loss through perfusion [23].

The temperature distribution in the tissue can be calculated by the Pennes' bioheat transfer equation.

$$\rho_s C_s \frac{\partial T}{\partial t} = K_s \nabla^2 T - W_b C_b (T - T_\infty) + Q_m + Q_v \tag{4.1}$$

In equation (4.1), ρ_s : the tissue density,

t : time,

C_s : the specific heat of tissue,

K_s : the tissue thermal conductivity,

W_b : the blood perfusion rate,

Cb : the specific heat of blood,

T : the temperature of tissue,

T_∞ : the temperature of blood,

Q_m : the rate of heat generation per tissue unit volume,

Q_V : the rate of heat generation by external heat source.

A focused transducer was used in the study so that the sound beam may be considered perpendicularly incident on to the water-phantom tissue interface along z-direction. The boundary condition on the front face parallel to the x-y plane is:

$$C_n\left(x, y, z_1^+\right) = C_n\left(x, y, z_1^-\right) \times \frac{2\rho_2 c_2}{\rho_1 c_1 + \rho_2 c_2} \tag{4.2}$$

In equation (4.2), $\rho_1 = 993$ kg/m^3, $c_1 = 1520$ m/s, are density and sound velocity of water, respectively and $\rho_2 = 1775$ kg/m^3, $c_2 = 3380$ m/s, are density and sound velocity of phantom tissue, respectively; $z1$ is distance from the transducer to the interface between water and phantom tissues.

In Pennes' model [23], it is assumed that the temperature of water is constant and the temperature distribution is continuous through the phantom tissue-water interface. Using Pennes' bioheat equation, the temperature distribution inside the phantom tissue as well as in the tissue can be determined [70].

Because the experiment was performed on biological tissues in vitro, the heat flow from blood circulation does not exist so that W_b can be neglected, Q_m can also be neglected in dead tissues. Therefore, the Pennes bioheat equation can be simplified to

$$\rho_s C_s \frac{\partial \overline{T}}{\partial t} = K_s \nabla^2 \overline{T} + Q_v \qquad (4.3)$$

In equation (4.3), $T = T - T_0$, T_0 is the temperature before heating.

4.2   TEMPERATURE MEASUREMENTS

Under the effect of ultrasound radiation, the temperature in the tissue rapidly elevates to values high enough to cause cell death or necrosis within the tumor [79]. The main advantage of HIFU application is its ability to penetrate deep into the body and deliver thermal energy to a specific target with sub millimeter accuracy [80]. Studies showed that HIFU ablation is an effective treatment way for uterine fibroids, a procedure that has been approved by the US Food and Drugs Administration (FDA) [81]

Huang et al (2004) have proposed a 'standard' method. They describe correction of the viscous heating artifact in tissue phantoms in HIFU fields [82]. Temperature rise versus time was measured in tissue with an absorption coefficient similar to that of soft human tissue. In order to apply it to measurements made in biological tissue, a phantom material with acoustic and thermal properties which closely match those of the tissue would be required.

HIFU sonications are targeted at selected locations within a 3D array of 8 thermocouples embedded in a solid medium [83]. The temperature rise is measured by an invasive method, using thermocouples embedded in a tissue mimicking phantom when an ultrasound was directed. Knowledge of the beam location enables removal of positioning error from the raw data as our TMM is opaque.

A variety of HIFU ablation procedures are performed for the fixed transducer position. The HIFU source is a 1,10 MHz HIFU transducer (Onda Corp, Sunnyvale CA) of focal length 62,6 mm and radius 70 mm. Tissue temperature rise is recorded during and after sonication, by using a multi channel Black Stack (Hartman Scientific model) and a computer program which is done in Hyper terminal [84].

In the literature by Parker K, J. and Friets E. M., during each of the experiments, the transducer is operated for 30 seconds and then switched off. The duration is typical of HIFU procedures. In the first set of experiments, the HIFU beam is focused on the thermocouple located 2 mm away from the vessel. Transducer acoustic powers of 10,3 W, 17,3 W and 24,8 W were generated. These powers yield focal intensities in the range of 495 W/cm^2, 832 W/cm^2 and 1192,8 W/cm^2 respectively [89].

4.2.1   Phantom Specifications

The primary objective of a thermal therapy is to increase the temperature of tissue beyond a threshold (usually 50 °C - 90 °C) to induce permanent tissue damage to achieve therapeutic benefit. Much effort has been made in developing tissue equivalent phantom materials to accurately predict and capture the extent of heat evolution and thermal damage. In order for any heat sensitive gel to be feasible and clinically acceptable, it must meet the following requirements;

- Tissue equivalency in thermal and optical properties,
- thermal stability at high temperatures, and
- capability of capturing the heat damage three dimensionally to allow for comparison between thermal therapy devices.

Further, an ideal thermal phantom material must be reproducible, inexpensive, and easily fabricated. Finally, the most ideal thermal phantom would satisfy all of the previously mentioned requirements and use relatively nontoxic substances so that phantom creation can be carried out in clinical setting without elaborate laboratory setup and safety precautions.

A gel-based tissue-mimicking material was used that simulates the thermal and acoustic properties of human soft tissue as seen in Figure 4.1. On the left side of the figure, thermocouple is positioned in the center on the plastic cube-vessel. On the right side of the figure thermocouple is inside the gel phantom. They show the placement of the thermocouples relative to the vessel, as well as the HIFU transducer described subsequently.

Figure 4.1. Picture of the thermocouple and tissue phantom

Thermocouple sensors were tightened with a thin wood pieces (teeth stick) and slowly inserted thorough the gel that is a soft material. The process is acted as slow as possible in order not to leave an air between thermocouple and the gel.

A test tank was designed with a 6 mm glass rod positioned horizontally, so that when the rod was eventually removed from the solidified tissue-mimicking material, a vessel in the form of a rectangular void resulted.

The phantom specifications were tabulated in Table 4.1. Tissue phantom must satisfy the real human tissue specifications like sound attenuation coefficient, density and thermal conductivity.

Table 4.1. Phantom specifications

Item	Value
Density	1060 kg/m^3
Phase velocity	1600 m/s
Attenuation Coefficient	0,6 dB/(cm-MHz)
Specific Heat	3850 J/(kg-°K)
Thermal Conductivity	0,55 W/(m-°K)
Optical	Turns permanently opaque when temperature reaches a threshold of 70 °C
Size	101 mm x 101 mm x 51 mm polystyrene box and 58 mm x 58 mm x 79 mm polystyrene box

Temperature reading system:

Black Stack (Hartman Scientific model) is a unique modular design that consists of a base controller, thermocouple and resistance sensor connection modules as named "temperature reading" in Figure 4.2 [84]. Additional 8 moduls can also be attached. Temperature is calculated according to the standard tables for type B, E, J, K, N, R, S, T, and gold-platinum thermocouples Adjustments to the standard curve can be made for improved accuracy. The Black Stack has a built-in clock and the base controller includes one built-in serial RS-232 port. It has short term resistance accuracy is 0,00025 Ω between 0 Ω and 25 Ω with the temperature coefficient of 0,5 ppm/°C.

4.2.2   Temperature Measurement System

A system has been constructed for temperature field distribution characterization measurements as seen in, Figure 4.2, Figure 4.3, Figure 4.4 and Figure 4.5.

HIFU transducer was placed at the bottom of the water tank. Then the phantom gel with temperature sensor was located on the top of the HIFU transducer as it is seen in Figure 4.2. All assembly was inside the water, in order to simulate the real human body conditions. Then the phantom gel was arranged so that the temperature sensor is matching to the focal point produced by the HIFU transducer. A 1,10 MHz concave focused transducer with a focal length of 69,2 mm, diameter of 60 cm and a central aperture of 5

cm, was used as the HIFU source in all cases. The drive voltage and current were monitored using a digitizing 1 GHz oscilloscope. Exposures were made in degassed water at room temperature. All wire thermocouples were inserted into tissue phantom perpendicular to the beam axis.

At the same input power condition for HIFU transducer, phantom gel was re-oriented in three dimensions by means of a 3-D manual arm in order to measure the highest temperature. In this condition, absolute temperature was measured from the applied ultrasonic power of 50 Watts.
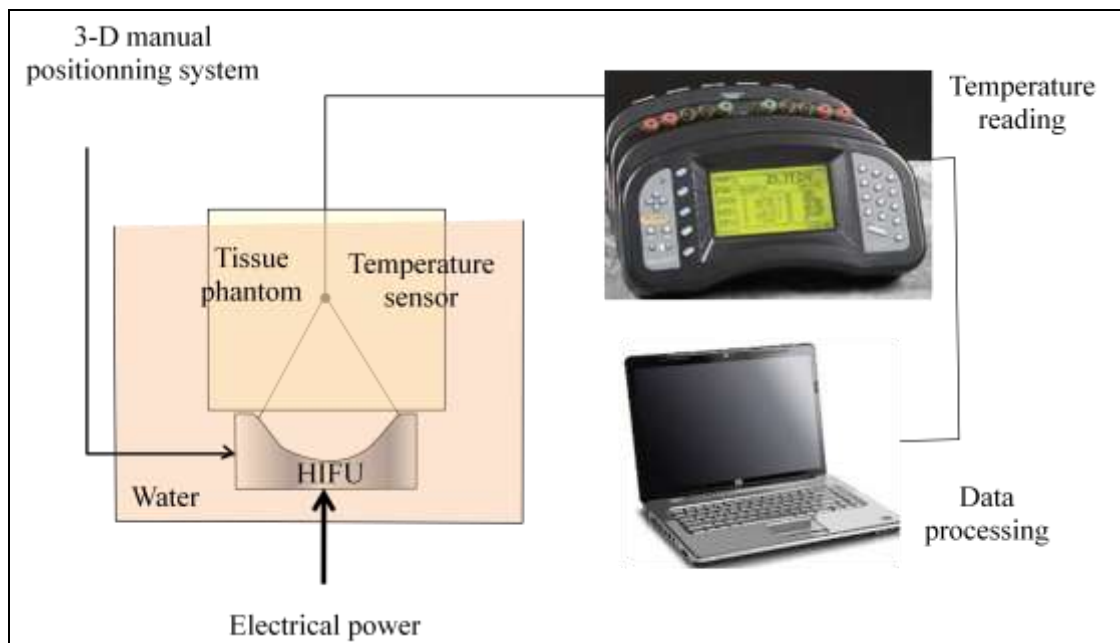
Figure 4.2. Arrangement of phantom gel with a single thermocouple
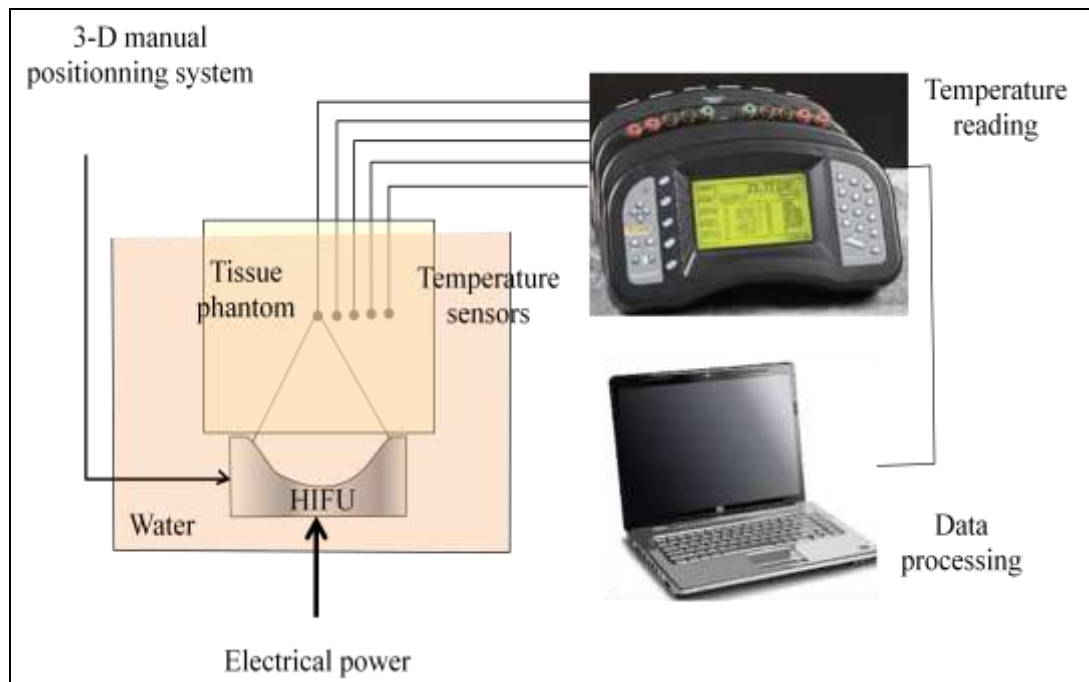
Figure 4.3. HIFU temperature measurement system in the tissue phantom
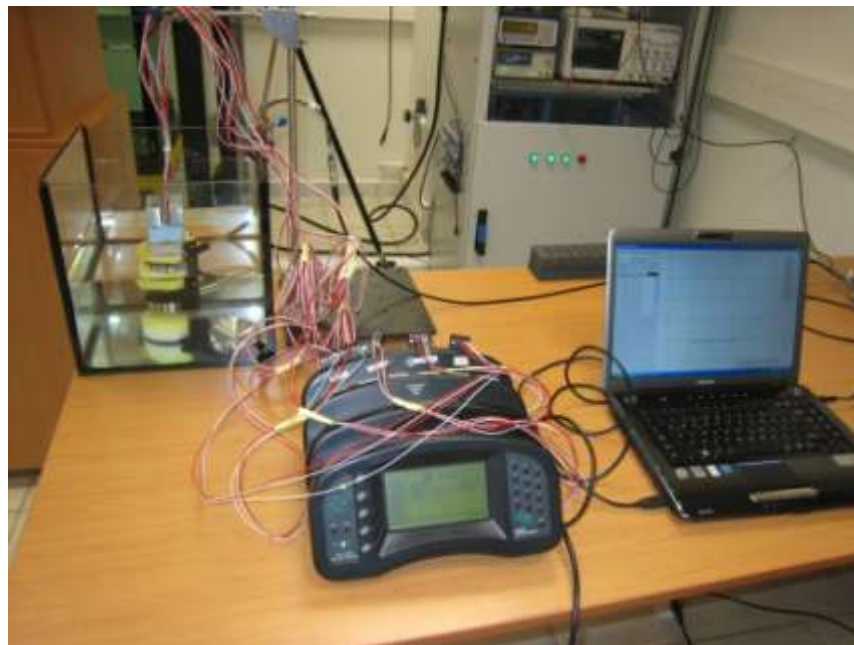
Figure 4.4. HIFU temperature measurement system in the tissue phantom
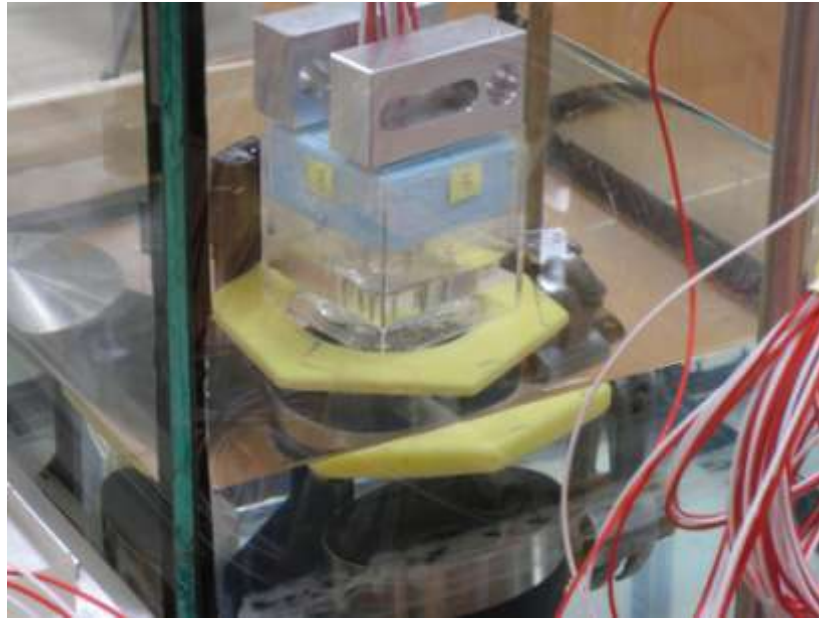
Figure 4.5. HIFU temperature measurement system in the tissue phantom

Platinum temperature sensors were inserted into the phantom tissue for HIFU temperature effect measurements. Temperature sensor elements are used successfully as components in resistance thermometers. The construction process of the elements ensures a high degree of reliability in many applications. Even in very small sizes short response times and long term stability are maintained. The temperature sensor elements produced are thin film sensors on which the temperature dependant resistant has been applied in form of a thin, layer structured platinum layer on an Al_2O_3 carrier substrate as seen in Figure 4.6.
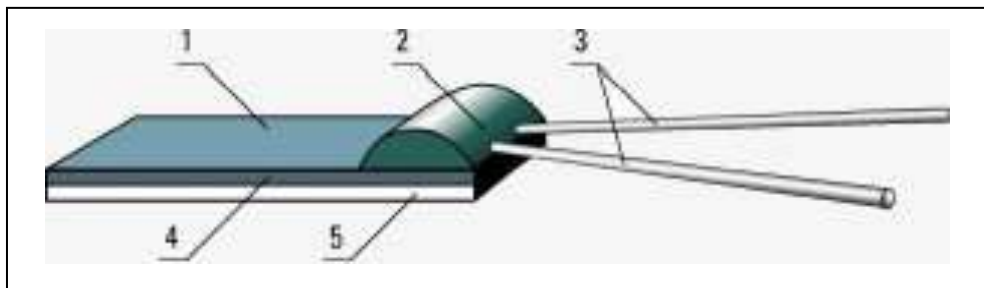
Figure 4.6. Construction of PT100 temperature sensors
(1: passivating layer, 2: locking layer, 3: connection wires, 4: structured platinum layer,
5: Al_2O_3-carrier substrate

Ultra Fine IT-Series Flexible Microprobe IT-24P is a tiny, polyurethane coated wire with polyester insulated thermocouple bead. It is designed for research applications to measure temperature in animal brains and other tissue. Ultra Fine thermocouple is fairly fragile, but very fast responding. It has a wire cross section of 0,13 mm x 0,07 mm with insulated tip maximum outside diameter of 0,23 mm.

Thermocouple was inserted into the phantom tissue for HIFU temperature effect measurements as seen in Figure 4.7. Even in very small sizes short response times and long term stability are maintained. The temperature sensor elements produced are ultra thin sensors on which the thermo viscous effect is diminished.
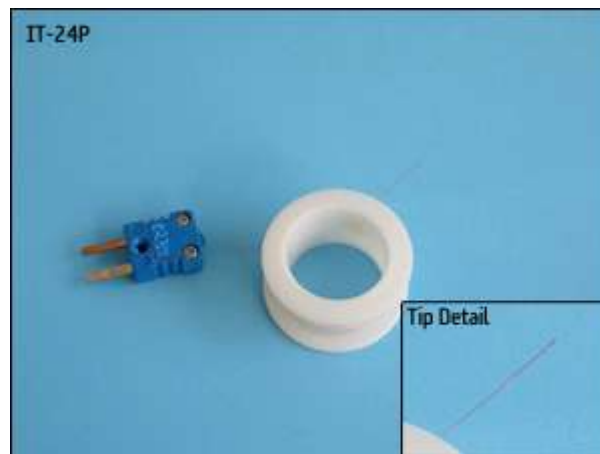
Figure 4.7. Ultra thin thermocouple sensor

5. RESULTS & DISCUSSIONS

Measurement results have been presented in three parts namely; electrical and ultrasonic measurements, pressure measrements and thermal measurements.

5.1 ELECTRICAL AND ULTRASONIC POWER MEASUREMENTS

HIFU transducers have been characterized in order to present a correlation between electrical and ultrasonic measurements.

5.1.1 Measurement results

In a purely resistive AC circuits, voltage and current waveforms are in phase. These waveforms could have sinusoidal, triangular or pulse repetition shapes. Voltage and current change their polarities at the same time in each cycle. In this condition, all the power which is applied to the load is consumed. In a purely reactive AC circuits, loads could be capacitive or inductive. Energy storage in the loads results in time difference between voltage and current waveforms. During each cycle of the AC voltage, energy is temporarily stored and later returned to its AC source. Purely resistive or purely reactive AC circuits are ideal electrical impedance conditions. But in the real case, AC circuits have resistive and reactive impedance parts. During each cycle of the AC voltage, extra energy in addition to any energy consumed is temporarily stored in the load in the forms of electric or magnetic fields. Then this extra energy is returned to the AC source later in the cycle.

HIFU impedance, Z consists of resistive, capacitive and reactive impedance parts. In this study, input electrical power of the HIFU transducer which is mainly converted into the ultrasonic energy was determined. Input electrical power of HIFU transducer was calculated with three ways. Calculated powers were denoted as *P1*, *P2* and *P3*. respectively.

In the first calculation method, electrical power *P1,* was calculated by multiplying instantaneous electrical input voltage, current and phase between them as;

$$P1 = V \cdot I \cdot cos\theta \tag{5.1}$$

In equation (5.1), the cosine of the phase angle could be represented by impedance terms, as *cosθ=R/Z.*

In the second method, electrical power *P2* was calculated by multiplying the square of instantaneous electrical input current and resistance measured with Impedance Analyzer;

$$P2 = I^2 \cdot R \tag{5.2}$$

In the third calculation method, electrical power *P3* was calculated by multiplying square of instantaneous electrical input voltage and cosine of phase angle and dividing by impedance measured with Impedance Analyzer;

$$P3 = V \cdot \frac{V}{Z}\cos\theta = \frac{V^2}{Z} \cdot cos\theta \tag{5.3}$$

Measurement results are shown in Table 5.1 for Precison Acoustics HIFU transducer that has a 0,93 MHz mechanical resonance frequency. It has an internal electrical matching network and produces the highest ultrasonic output at this frequency. Figure 5.1 shows a frequency scan between 0,8 MHz and 1,10 MHz in 20 kHz steps. Ultrasonic power and electrical power were measured simultaneously and drawn in this graph. Input ultrasonic and electrical power measurement results can be seen similarly in Table 5.2 for Sonic Concepts HIFU transducer with resonance frequency of 1,10 MHz. Figure 5.2 shows a frequency scan between 1,0 MHz and 1,2 MHz in 20 kHz steps.

Table 5.1 Ultrasonic and electrical power measurement results for Precision Acoustics HIFU transducer (Dark row for resonance frequency)

Frequency, MHz	Ultrasonic power, W	Electrical power, W						
						Deviation from average		
	PU	*P1*	*P2*	*P3*	*Average*	*P1*	*P2*	*P3*
0,85	7,6	23,4	18,4	17,4	19,7	-3,7	1,3	2,3
0,87	11,3	30,4	25,3	24,0	26,6	-3,8	1,3	2,6
0,89	19,7	41,4	38,5	35,4	38,4	-3,0	-0,1	3,0
0,91	35,0	56,7	55,6	50,3	54,2	-2,5	-1,4	3,9
0,92	39,4	61,0	64,2	56,2	60,5	-0,5	-3,7	4,3
0,93	**42,3**	**58,4**	**60,9**	**56,6**	**58,6**	**0,2**	**-2,3**	**2,0**
0,95	31,4	38,3	42,0	37,8	39,4	1,1	-2,6	1,6
0,97	17,9	24,2	25,9	23,1	24,4	0,2	-1,5	1,3
0,99	11,7	18,8	19,6	17,3	18,6	-0,2	-1,0	1,3
1,01	8,1	15,0	14,5	12,4	14,0	-1,0	-0,5	1,6
1,03	5,5	13,1	11,3	9,7	11,4	-1,7	0,1	1,7

Table 5.2 Ultrasonic and electrical power measurement results for Sonic Concepts HIFU transducer (Dark row for resonance frequency)

Frequency, MHz	Ultrasonic power, W	Electrical power, W						
						Deviation from average		
	PU	*P1*	*P2*	*P3*	*Average*	*P1*	*P2*	*P3*
1,00	37,9	44,2	49,4	46,1	46,6	2,4	-2,8	0,5
1,02	41,6	48,6	54,0	52,6	51,7	3,1	-2,5	-1,0
1,04	44,5	53,5	56,9	54,8	55,1	1,6	-2,2	0,3
1,06	48,1	58,1	60,3	58,9	59,1	1,0	-1,5	0,3
1,08	49,6	60,2	61,6	62,3	61,4	1,2	-0,3	-1,2
1,10	**50,3**	**61,5**	**64,7**	**58,9**	**61,7**	**0,2**	**-4,0**	**3,7**
1,12	49,5	60,9	63,4	57,8	60,7	-0,2	-3,5	3,8
1,14	48,9	60,4	59,1	59,0	59,5	-0,9	0,5	0,6
1,16	46,0	59,4	59,7	55,4	58,2	-1,2	-1,9	3,5
1,18	44,0	58,8	56,0	55,0	56,6	-2,2	0,7	1,9
1,20	42,3	58,0	57,0	55,4	56,8	-1,2	-0,2	1,7
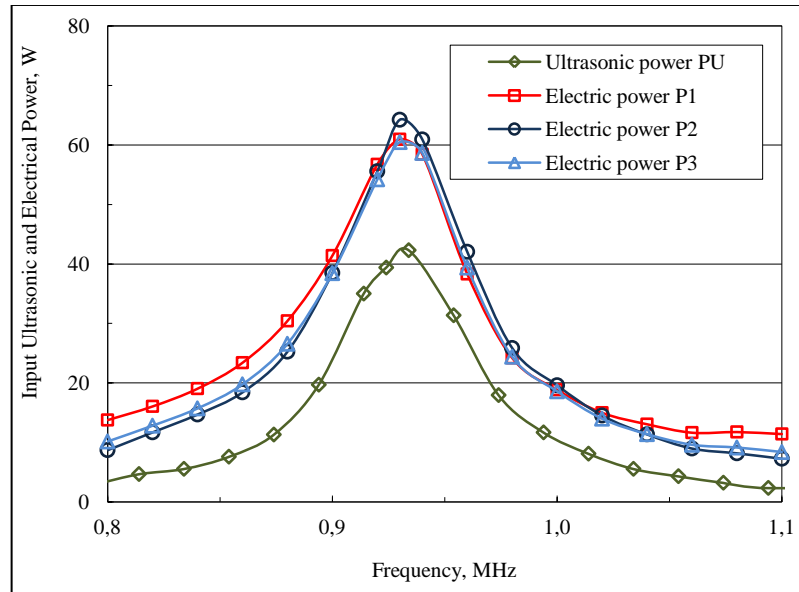
Figure 5.1**.** Ultrasonic and electrical measurement results for Precision Acoustics HIFU transducer
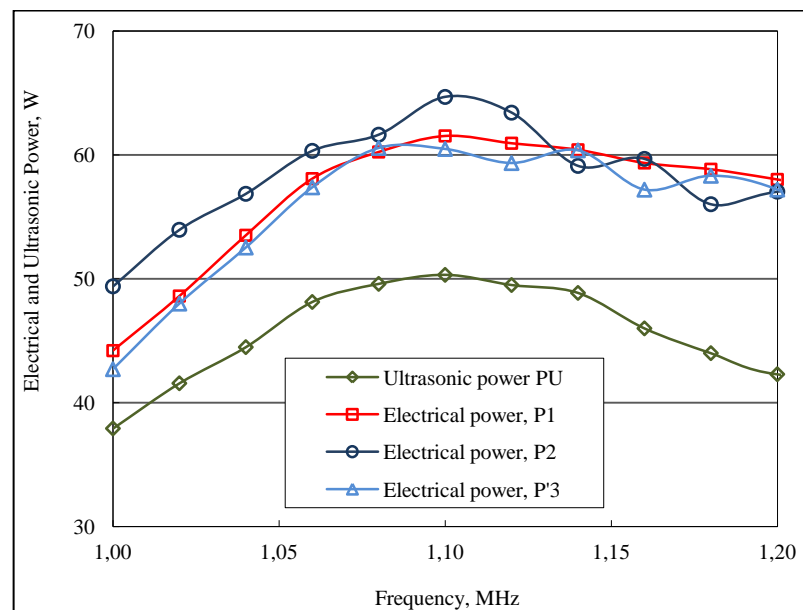
Figure 5.2**.** Ultrasonic and electrical measurement results for Sonic Concepts HIFU transducer

Figure 5.3 shows that the linearity of electrical power and ultrasonic power for different power levels. This method shows good correlation between electrical power measurements and direct measurements of the output power of the ultrasonic transducers which are

immersed into the water. During the measurements, no harmonic distortion was observed in the amplifier output at the defined output power level. Efficiencies of both HIFU transducers at resonance and around resonance frequency are between 70-80 % that is consistent with specifications declared by manufacturer in data sheets of transducers. The three calculations agree within approximately ±5% at frequencies close to resonance where the phase angle of the transducer impedance is within about ±45°. In this range, P_1, determined using the voltage and current probes, lies between P2 and P3.

The results obtained with the different methods were found to be in good agreement (± 5 %) with each other for HIFU transducer for low power levels up to 60 W. Measurement results are shown in Table 5.1 and Figure 5.1 for the (Precision Acoustics) transducer that has a 0,93 MHz mechanical resonance frequency. It has an internal electrical impedance matching network and produces the highest ultrasonic output at this frequency. Figure 5.1 shows a frequency scan between 0,8 MHz and 1,1 MHz in 20 kHz steps. Ultrasonic power and electrical power were measured simultaneously and plotted in this graph. Input ultrasonic and electrical power measurement results are shown in Table 5.2 and Figure 5.2 for HIFU transducer (Sonic Concepts) with resonance frequency of 1,1 MHz.
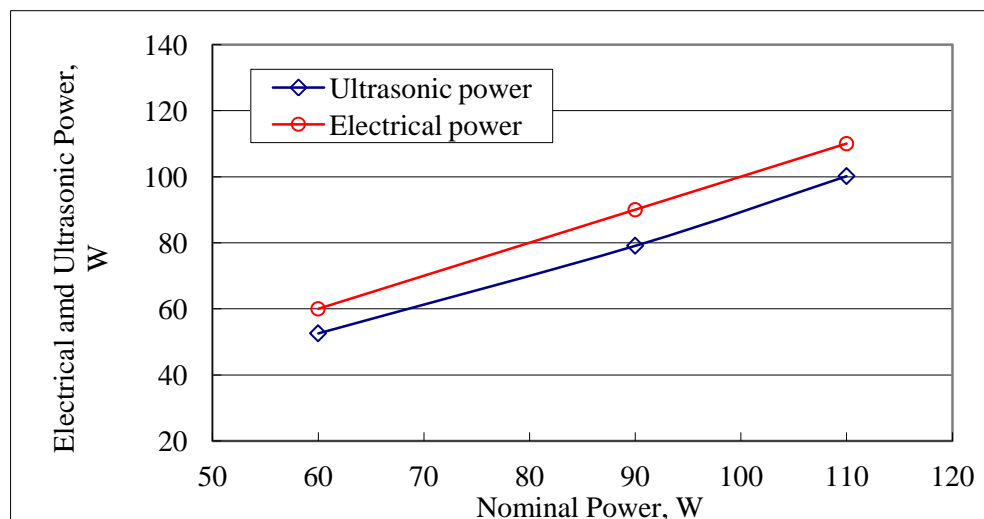
Figure 5.3. Linearity of electrical power and ultrasonic power for different power levels for HIFU transducer

5.1.2   Validation of measurements

Traceability of the measurements has been established by calibration against to electrical reference standards. The most important measurement tools in the system are the current and voltage probes. They are both calibrated against the reference standards at TÜBİTAK UME Voltage Laboratory. Amplitude and time calibration of the oscilloscope were performed at the end of cable in order to diminish the effect of the cable. Impedance analyzer was also verified by using calibrated loads which are a short circuit, an open circuit and a 50 Ω load resistance. Compatible current probe with oscilloscope was kept heated, demagnetized and leveled before the measurements according to its user manual and checked during measurements. Voltage measurements were performed with a voltage probe and the oscilloscope. Current measurements were realized with current probe and the oscilloscope that were calibrated prior to measurements. Phase measured between voltage and current signals are in correspondence with the phase measured with impedance analyzer in few degrees as seen in Figure 5.4 and Figure 5.5. Input electrical voltage, current and phase between them were measured simultaneously.
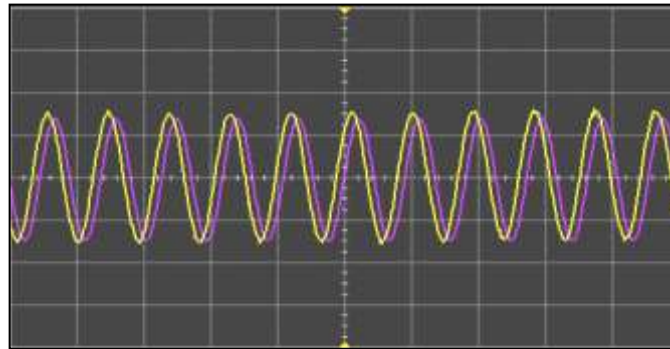
Figure 5.4**.** Captured voltage and current signals from oscilloscope
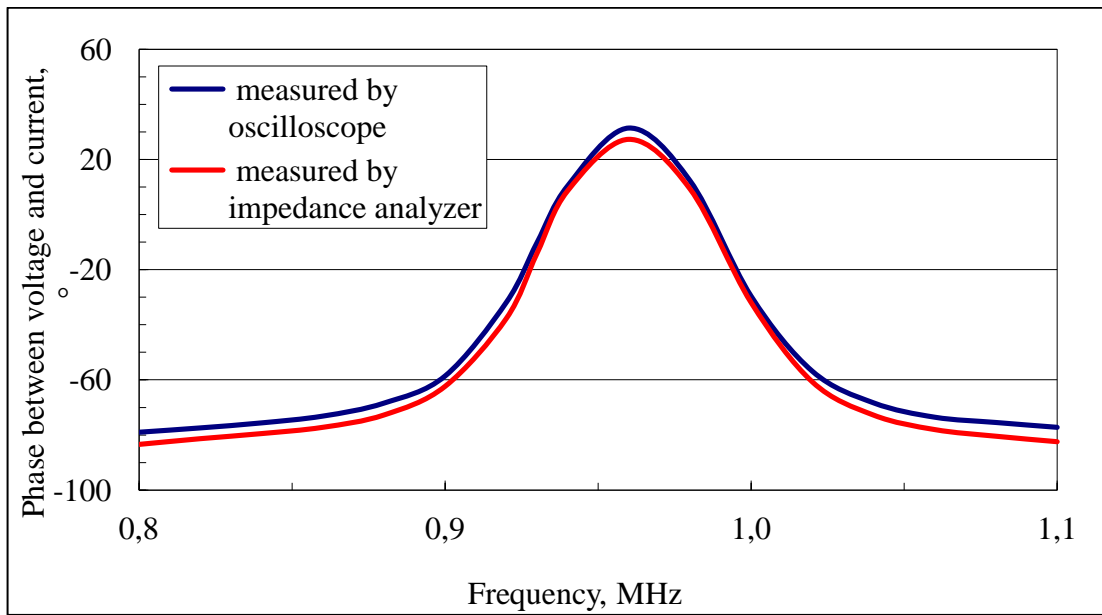
Figure 5.5**.** Difference between phases measured by oscilloscope and impedance analyzer
for Precision Acoustics HIFU transducer

5.1.3   Uncertainty of measurements

Uncertainty of measurements has been prepared according to GUM (Guidelines of uncertainty in measurements) [85]. This Guide establishes general rules for evaluating and expressing uncertainty in measurement that are intended to be applicable to a broad spectrum of measurements.

Sources of uncertainty related with voltage measurements, current measurements, cable and connection effect, phase measurement error, distortion in the signal and repeatability have evaluated in 1 MHz and 3 MHz between 60 W and 110 W. In voltage measurements, a calibrated oscilloscope and a high impedance oscilloscope probe were used. Calibration at the end of probe cable was realized at UME voltage laboratory with an uncertainty of 3,0 % declared in calibration certificate. A calibrated oscilloscope and an Agilent 1147A current probe compatible with Agilent oscilloscope were used in current measurements. Calibration at the end of probe cable was realized at UME voltage laboratory with an uncertainty of 2,0 % declared in calibration certificate. Cable and connection effects have rectangular distribution and were assessed as 0,4 %. Errors were determined from cable length by performing voltage measurements in different cable lengths. Error arising from

cable connections was estimated from experiences. Phase between voltage and current were measured by oscilloscope that is calibrated at UME voltage laboratory. Uncertainty value for time base of oscilloscope declared as 15 μs/s in calibration certificate were used. THD (Total Harmonic Distortion) in the signal in voltage and current signal displayed on oscilloscope screen was measured as 3,0 % around 60 W, 4,1 % around 90 W and 4,5 % around 110 W by using oscilloscope functions, Harmonic Distortion is assessed as rectangular distribution, Measurements were repeated 10 times and standard deviation was calculated as 1,2 % - 1,5 % between 60 W and 110 W accordingly. Detailed uncertainty budget including combined and expanded uncertainty were calculated is presented in Table 5.3.

Uncertainty of ultrasonic power measurements was already assessed and outlined in [86] as 15,2 % for 100 W at1 MHz.

Table 5.3 Expanded uncertainty for 1 MHz and 60 W, 90 W and 110 W

	Source of Error	Value, %			Probability Distribution	Divisor	Ui, %		
		60 W	90W	110W			60 W	90W	110W
1	Voltage measurements	3,00			Normal	2,00	1,50		
2	Current measurements	2,00			Normal	2,00	1,00		
3	Cable and connection effects	0,40			Rectangular	1,73	0,23		
4	Phase measurement error	0,10			Rectangular	1,73	0,06		
5	Distortion in the signal	3,00	4,10	4,50	Rectangular	1,73	1,73	2,37	2,60
6	Repeatability	1,20	1,30	1,50	Normal	1,00	1,20	1,30	1,50
	Combined uncertainty						2,78	3,26	3,51
	Expanded uncertainty (k=2)						5,57	6,52	7,02

5.1.4 Comparison between power measurements and power displaying devices

The new input electrical power measurement method was compared with power displaying devices and results were tabulated in Table 5.4. ENI (Electronic Navigation Industries) analog power display was used to measure the input electrical power as seen in Figure 5.6. E&I (Electronics & Innovation) 500 W power amplifier displays the power that is transmitted, forwarded and reflected to source as seen in Figure 5.7. It calculates the transmitted power by subtracting reflected power from forwarded power.

| Figure 5.6. Analog power display | Figure 5.7. Power amplifier and its display on top of front panel |
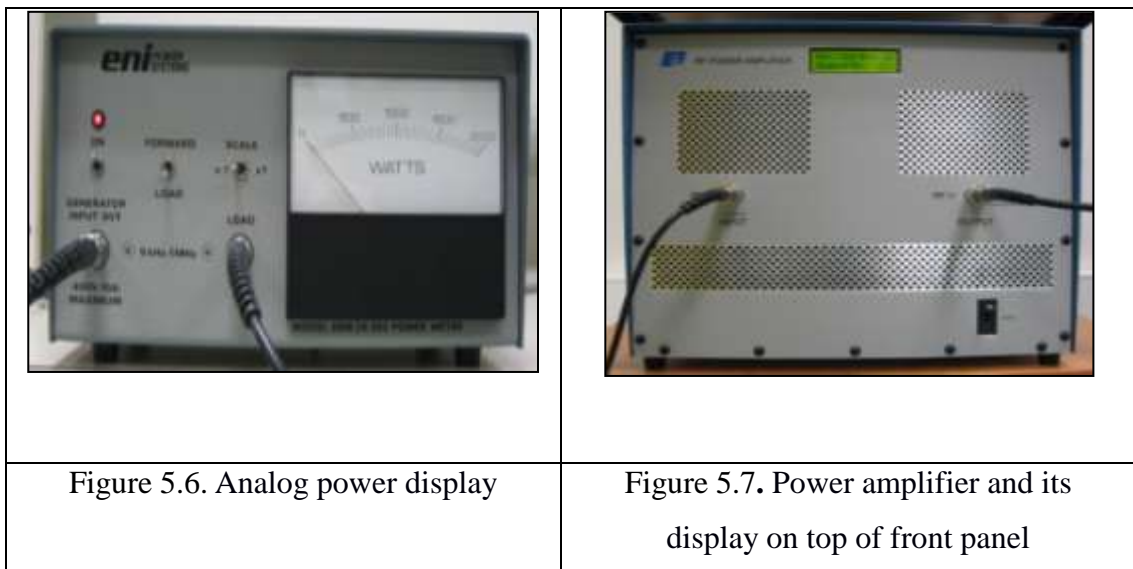
Table 5.4. Comparison results of new method and power displaying devices

Device	Power level, W		
	60 W	90 W	110 W
Instantaneous input electrical power system	$60,0 \pm 3,4$	$90,0 \pm 7,2$	$110,0 \pm 7,7$
Analog power display*	$55,2 \pm 5,0$	$85,1 \pm 7,5$	$100,1 \pm 10,0$
Power amplifier display*	$57,8 \pm 4,2$	$83,4 \pm 7,4$	$101,9 \pm 8,9$

*: the numbers following symbol ± is reading error of displays of devices.

The values stated in the table are expanded uncertainty values for the new input electrical power system. The uncertainty values in percentage 5,6 %, 6,5 % and 7,0 % that are calculated in Table 1 can be represented as ± 3,4 W, ± 7,2 W and ± 7,7 W in order to compare the results. Standard deviation was only measured for the two displays. As can be seen in above table, the results taken from new electrical power measurement system, analog power display and power amplifier display are in good agreement.

5.1.5   Electrical measurement results

Instantaneous input electrical power at MHz region has been measured by using new system established at TÜBITAK UME Ultrasound laboratory. Electrical power measurements were calculated in three different measurement methods and compared their measurement results with ultrasonic power for two HIFU transducers. Measurements were carried out at around 1 MHz for low power levels of 60 W to 110 W. Efficiencies of both HIFU transducers at resonance frequency is between 70 % and 80 % that is consistent with manufacturer specifications declared in data sheets of transducers. The three calculations are in coincidences with 5 %. The new input electrical power measurement method was compared with power displaying devices and a good agreement was achieved. It has been assessed that analog power display can be used as a secondary standard for input electrical device. New method for calculation of instantaneous input electrical power measurements of HIFU transducers has been validated by comparison of similar power displaying devices and metrological tools. Uncertainty in measurements were assessed between for 60 W and 110 W and determined as 5,6 % and 7,0 % accordingly.

An establishment of a correlation was aimed between the methods. High intensity of ultrasound beams in a tissue has numerous effects like cavitation and temperature rise. The efficiency of the HIFU transducer is described as output ultrasound power due to applied electrical power. A dependency between ultrasound power and electrical power has been established as it is seen in Table 5.5 and Figure 5.8. Blue diamonds are the difference between electrical power and ultrasound power at around fundamental frequency. It has a sinusoidal like shape with a decline behavior around fundamental frequency. This shape and behavior may need some further investigations that are out of scope of this thesis. Red

circles have more meaning than blue diamonds in the Figure 5.8. It is clearly seen that efficiency of the HIFU transducer has the maximum at the fundamental frequency which is working frequency. In fact other frequencies are less important here. We scan some frequency region around the fundamental frequency in order to show the maximum efficiency at this working frequency.

Results of the electrical measurements have been outlined in a paper [87].

Table 5.5. Difference and deviation between ultrasound power and electrical power

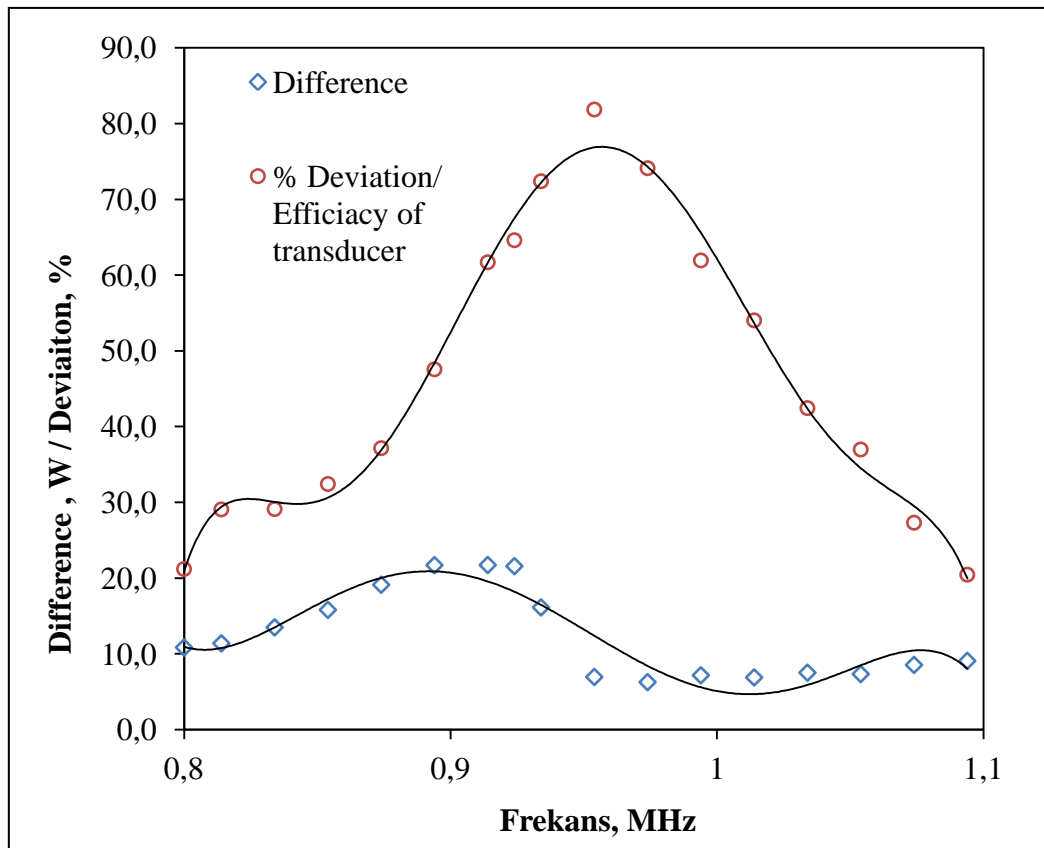| Frequency	PU	P1	Difference	% Deviation / Efficiency of transducer
MHz	W	W	W	%
0,80	2,9	13,8	10,8	21,2
0,81	4,7	16,1	11,4	29,1
0,83	5,5	19,0	13,5	29,1
0,85	7,6	23,4	15,8	32,4
0,87	11,3	30,4	19,1	37,2
0,89	19,7	41,4	21,7	47,6
0,91	35,0	56,7	21,7	61,7
0,92	39,4	61,0	21,6	64,6
0,93	42,3	58,4	16,1	72,4
0,95	31,4	38,3	6,9	81,9
0,97	17,9	24,2	6,3	74,1
0,99	11,7	18,8	7,2	61,9
1,01	8,1	15,0	6,9	54,0
1,03	5,5	13,1	7,5	42,4
1,05	4,3	11,6	7,3	37,0
1,07	3,2	11,7	8,5	27,3
1,09	2,3	11,4	9,1	20,5

Figure 5.8. Dependency between ultrasound power and electrical power

It can be stated that the efficiency of the Precision Acoustics HIFU transducer is 81,9 % at resonance frequency.

5.2 ACOUSTIC PRESSURE FIELD MEASUREMENTS

The relation between ultrasonic power and pressure may be established for low and high power levels.

5.2.1 Measurement Results

Experimental results have been compared with the theoretical model [70]. A care must be taken to compare the results at the same ultrasonic powers. Match between the primary peaks in the focus, zero point after the primary peak (focus) and extremum points in the near field are important.

A preliminary result has been taken and compared with theoretical model. Theoretical model in Figure 5.9 for axial scan was compared with experimental results in Figure 5.10 and Figure 5.11. Theoretical model in Figure 5.12 for P+ and P- was compared with experimental results in Figure 5.13 and Figure 5.14.

The general wave behaviors in Figure 5.9 created by the model and in Figure 5.12 from experiments look like comparable. Zero point after the primary peak (focus) and extremum points in the near field well matched. However fundamental peaks have similar amplitude, the focal point is somehow shifted. This might be due either to the large sensing element and the limited frequency range or to the phase response of the hydrophone, which was not available from the manufacturer.
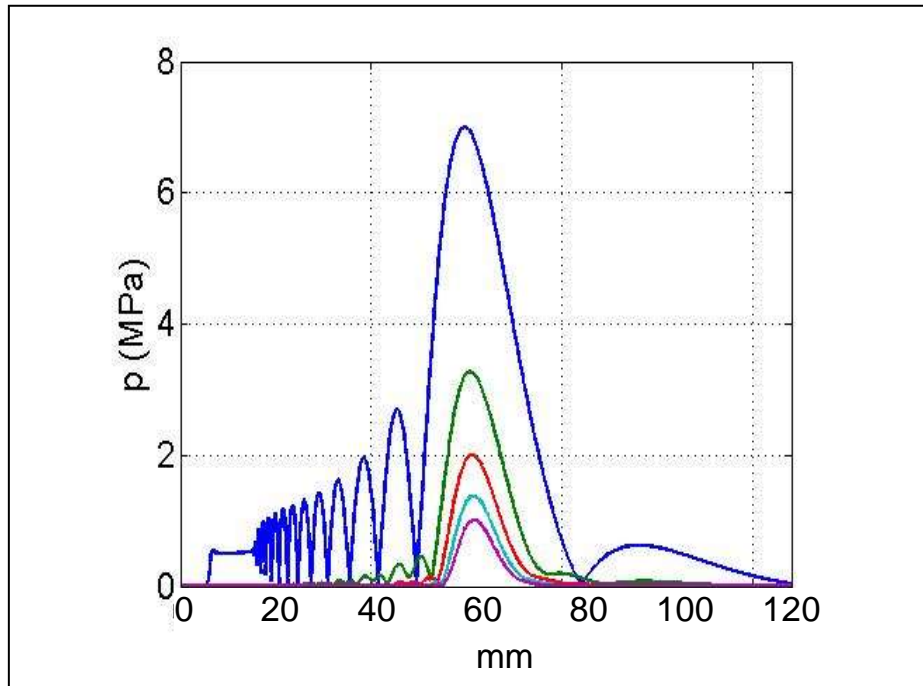
Figure 5.9. HIFU pressure field theoretical model (axial)
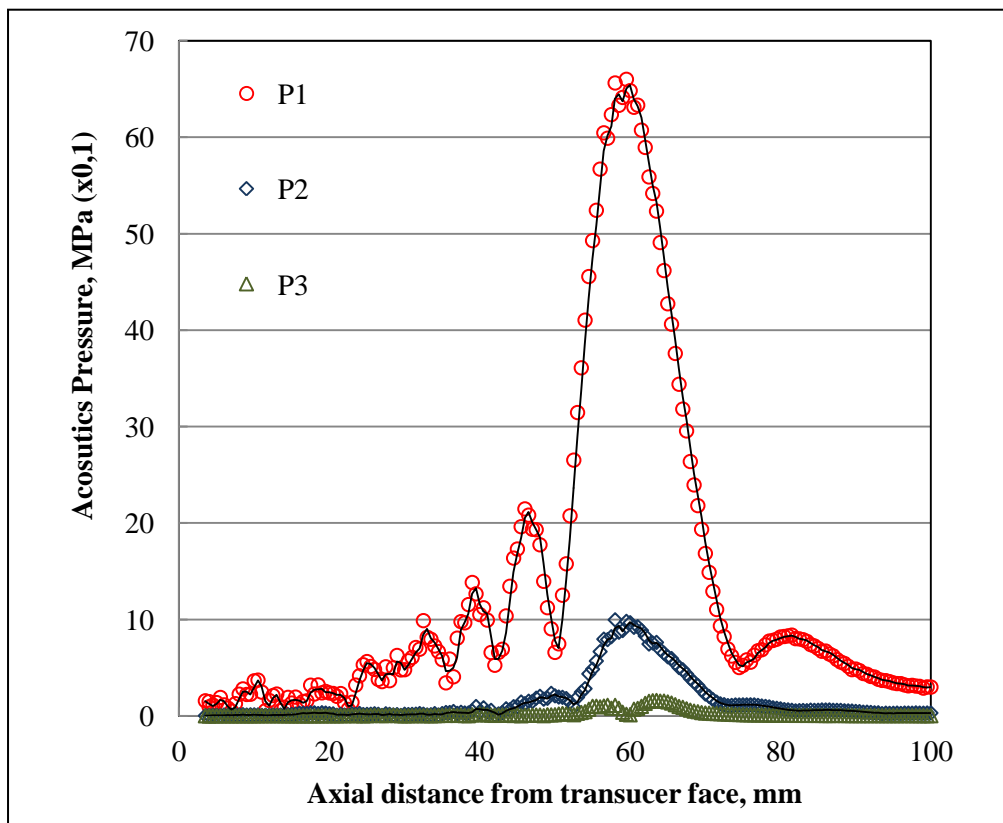
Figure 5.10. HIFU pressure field- preliminary measurement results (axial) (Sonic Concepts)
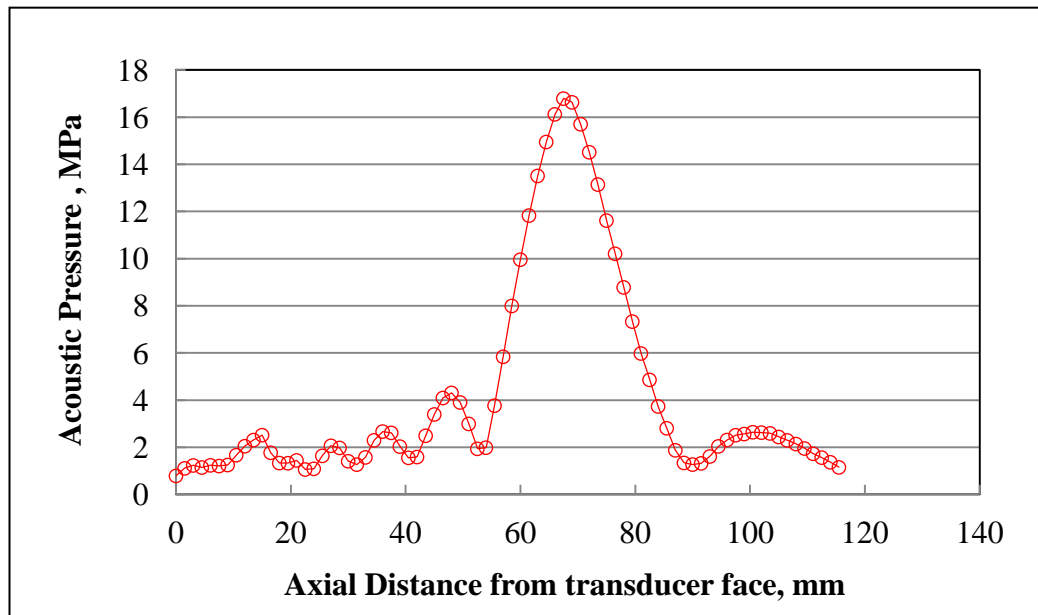
Figure 5.11. HIFU pressure field- preliminary measurement results (axial) (Precision Acoustics)

Wave behaviors in Figure 5.12 produced by the model and in Figure 5.13 and Figure 5.14 from experiments look like similar in general. In peak compressional pressure P+ curve (blue line) and in peak rarefactional pressure P- curve (green line), the focal point, zero point after the primary peak (focus) and extremum points in the near field well matched.
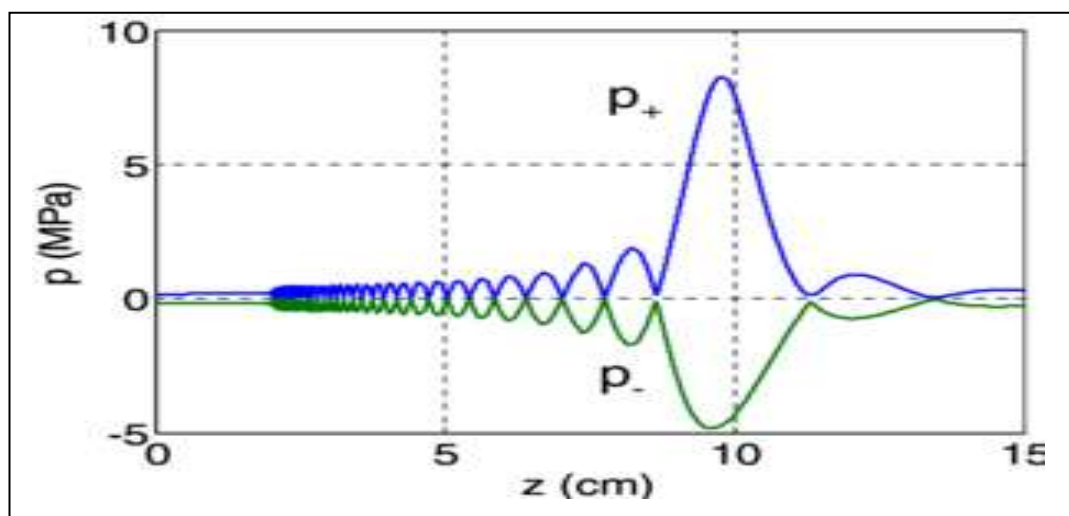
Figure 5.12. Peak compressional pressure P+ curve (blue line) and in peak rarefactional pressure P- curve(green line) produced by the theoretical model
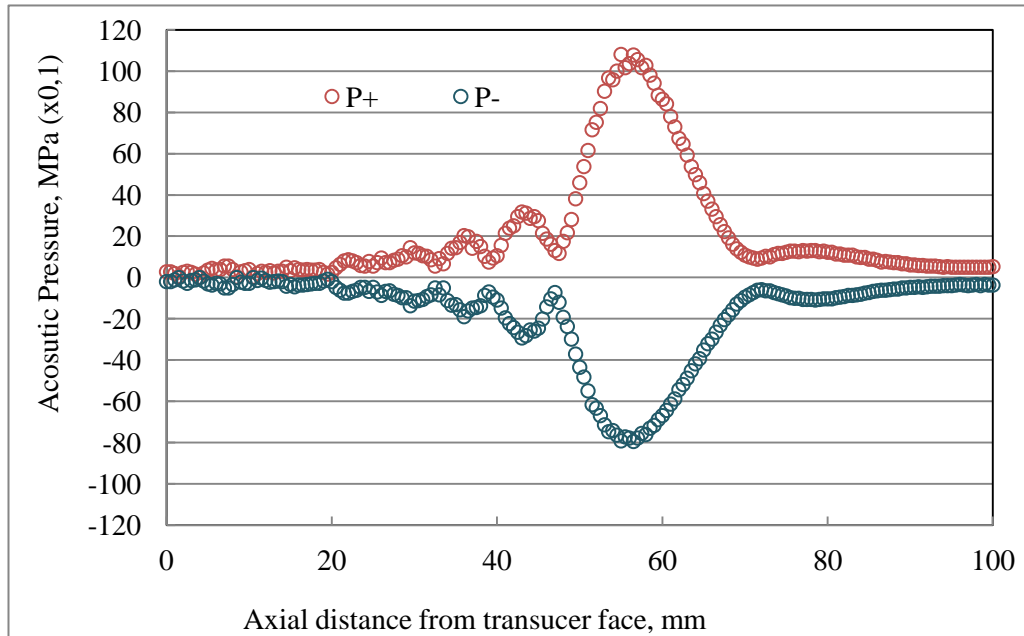
Figure 5.13. Peak compressional pressure P+ curve (red line) and in peak rarefactional pressure P- curve(blue line) for Sonic Concepts HIFU transducer
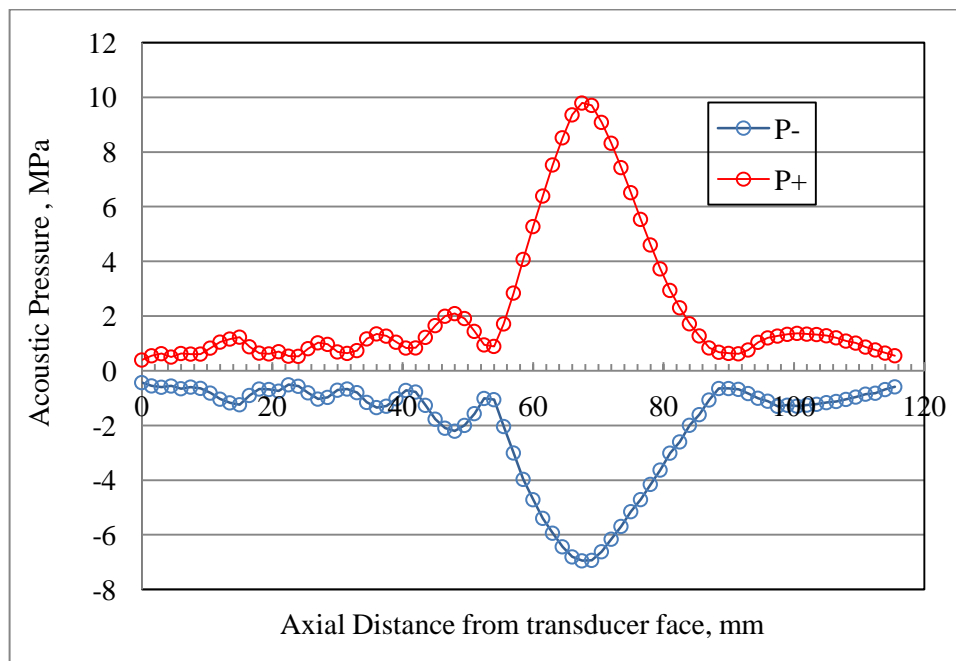
Figure 5.14. Peak compressional pressure P+ curve (red line) and in peak rarefactional pressure P- curve(blue line) for Precision Acoustics HIFU transducer

Side lobes are clearly observed at far field. The lateral beam plot at the focus is shown in Figure 5.15.
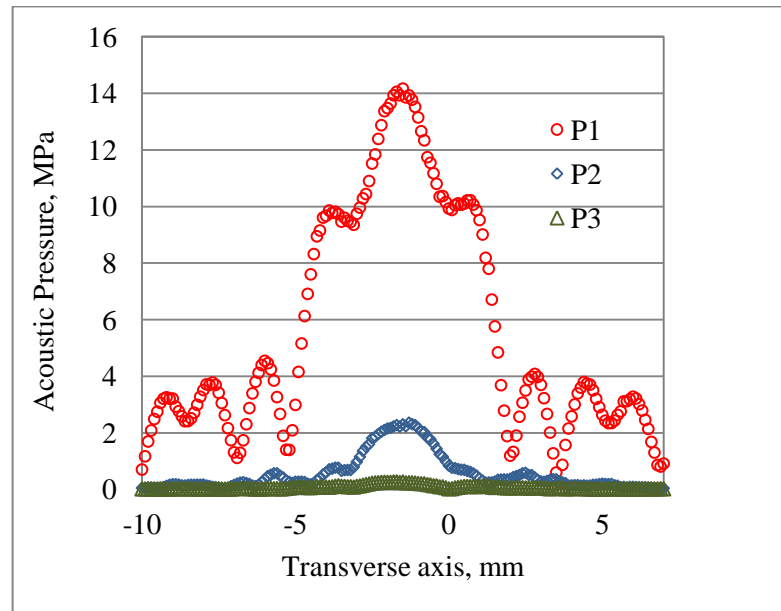
Figure 5.15. Side lobes observed at far field (Sonic Concepts)

Transversal view at the center of beam clearly has a gain as it is seen in Figure 5.16.
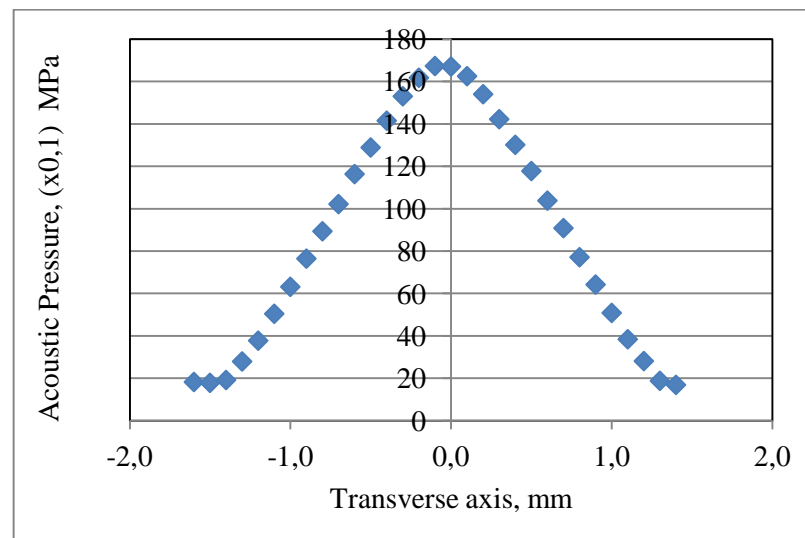
Figure 5.16. Transversal view at the center of beam for Precision Acoustics HIFU Transducer

The width and shape of the main lobe and side lobe are almost at same height. In the other lateral axis (y-axis), the sketches can be seen in Figure 5.17 for the focus, near field at 22 mm and 42 mm and far field at 82 mm and 102 mm for Sonic Concepts HIFU transducer. At focus, the side lobes are clearly resolved.
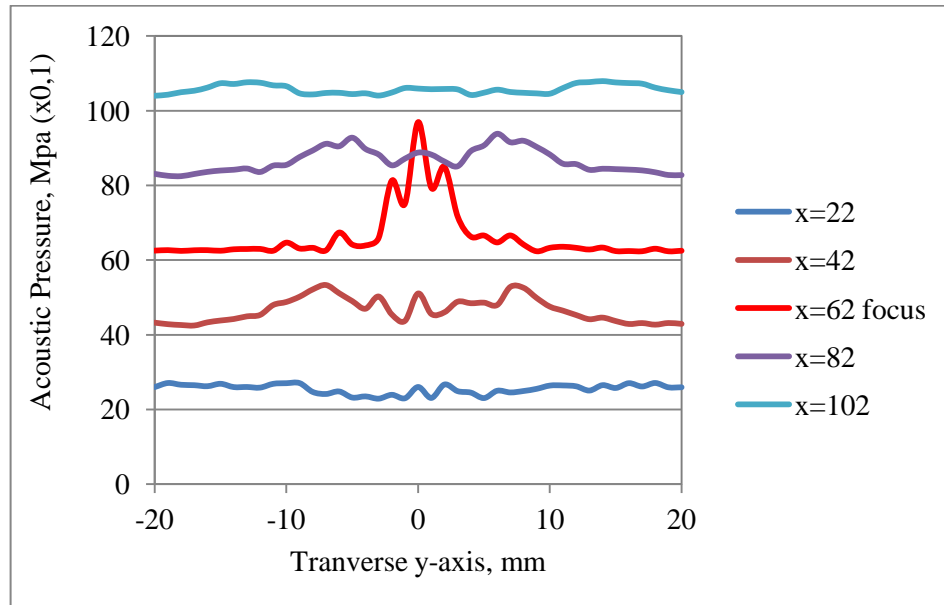
Figure 5.17. Side lobes in y-axis observed at near field, at focus and at far field for Sonic Concepts HIFU transducer

Side lobes are almost missing since in radial axis curves as seen in Figure 5.18. Lateral axis (z-axis) in the sketches can be seen in Figure 5.18 for the focus, near field at 22 mm and 42 mm and far field at 82 mm and 102 mm for Sonic Concepts HIFU transducer. At focus, high gain is resolved.
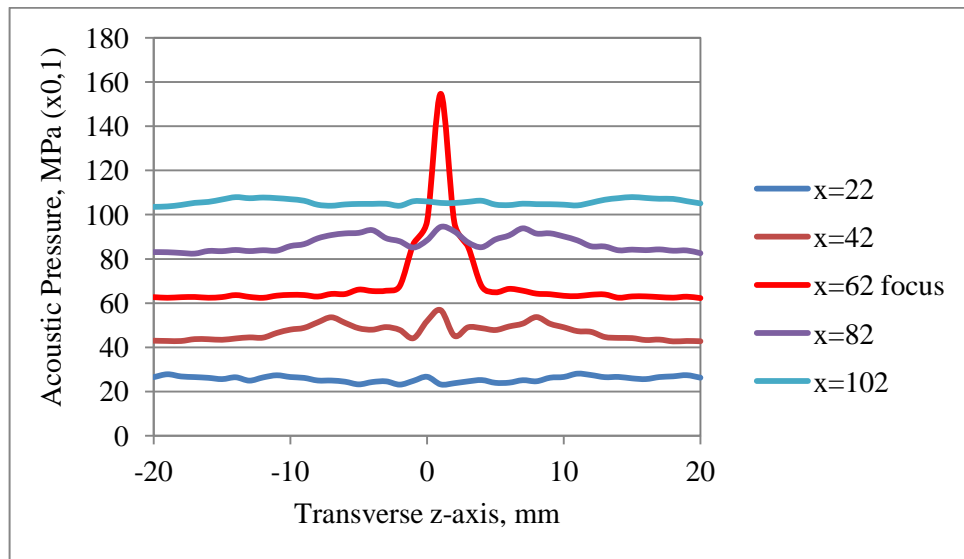
Figure 5.18. Side lobes in z-axis observed at near field, at focus and at far field for Sonic Concepts HIFU transducer

A sketch demonstrates the locations of the lateral curves up on the HIFU transducer in Figure 5.19. The pressure signal in focus has higher amplitude compared to near and far fields clearly. Height of the pressure signal in focus sharply increasing while the near and far fields have lower pressure amplitudes as seen in this figure.
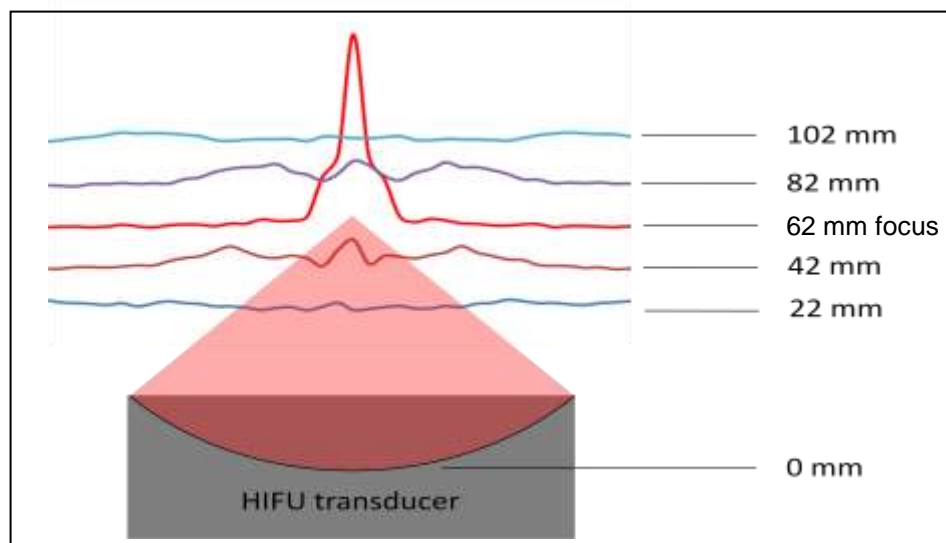
Figure 5.19. HIFU tranducer and pressure field amplitudes at near field, at focus and at far field were shown together for Sonic Concepts tranducer

2-D (two dimensional) scans through transducer face in Figure 5.20 and Figure 5.21 show the peak in focus and near and far fields clearly.
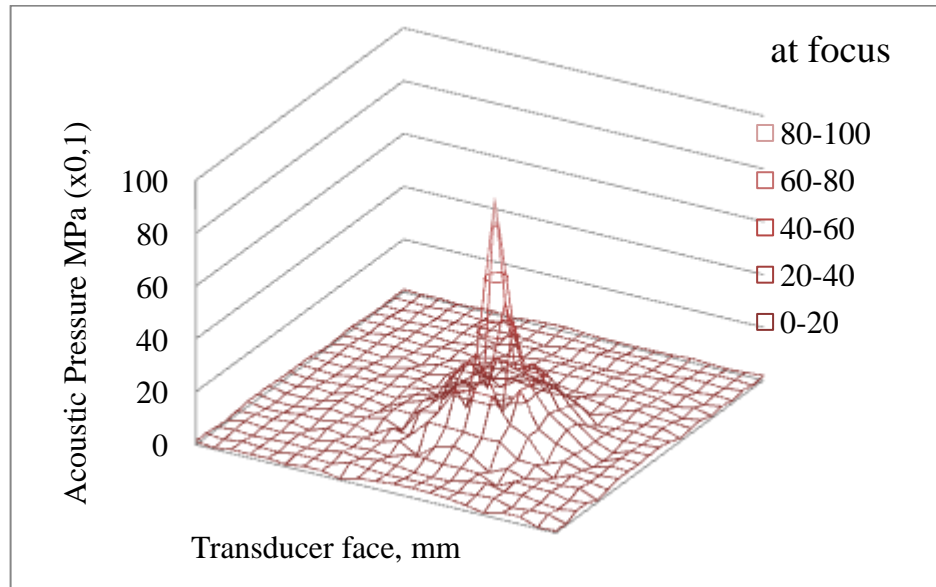
Figure 5.20. 2-D (two dimensional) scans through transducer face for Sonic Concepts
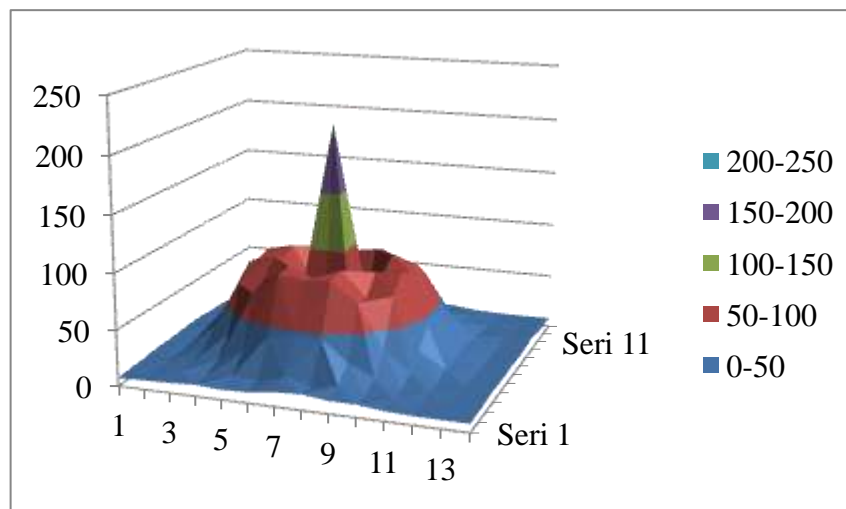
Figure 5.21. 2-D (two dimensional) scans through transducer face for Precision Acoustics

2-D (two dimensional) scans through transducer face at far filed is shown in Figure 5.22, while the main peak gets lower, side lobes starts to dominate the signal.
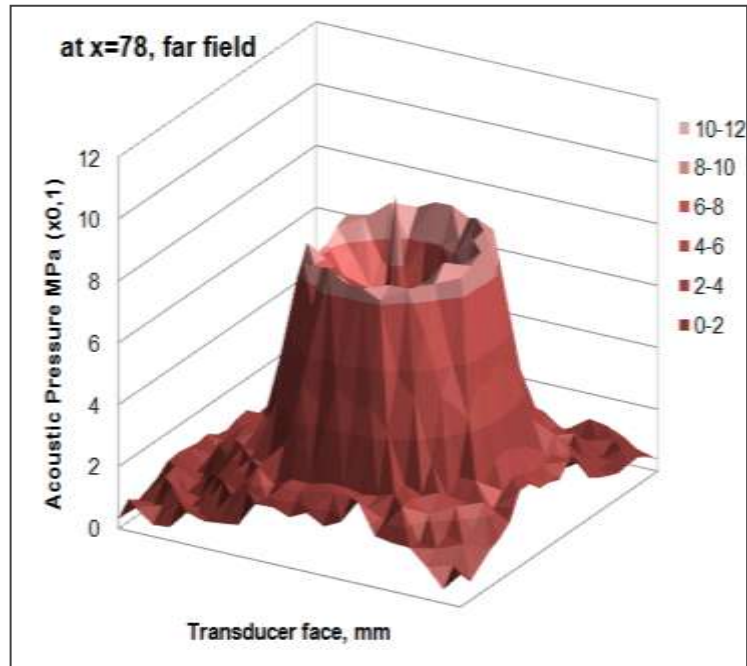
Figure 5.22. Side lobes observed at far field (Sonic Concepts)

5.2.2 Measurement uncertainty

In this section, sources of uncertainty in measurement of acoustic pressure were examined. The list of error sources that can be utilized in the calculation of the uncertainty has been assessed. The values of some uncertainty components may be very small then can be neglected. Some major uncertainty components were given here.

Sensitivity and frequency response of the receiver hydrophone;
Free field sensitivity of the hydrophone as a function of frequency is taken from the calibration chart given by the manufacturer. Uncertainty of the hydrophone is stated as 0,5 % between 1 MHz and 10 MHz.

Expanded uncertainty is stated as 95 % confidence level in calibration certificates. In other words, the value of uncertainty compound was obtained using the coverage factor k = 2,0. Also probability distribution in this component is a normal distribution.

Influence of water temperature (speed of sound);

Ambient temperature in the laboratory where all system is located was controlled by a central temperature/humidity control network. Speed of sound in water highly depends on the temperature change. Instability in water temperature around the focal region will create fluctuations in speed of sound value creating an error in measurements.

HIFU transducer and hydrophone misalignment in positioning;

One of the key factors which are creating large error is misalignment in positioning of HIFU transducer and hydrophone. Poor alignment will affect the response of a hydrophone, the degree of influence depending on its directional response at the measurement frequency. Misalignment may be caused by the use of a mounting pole that is not straight, leading to an error in hydrophone position and potentially an error in hydrophone orientation.

Expected zero distance between transducer surface and hydrophone;

Displacement between transducer face and hydrophone must be determined correctly. If the focus region is determined, the measurement hydrophone should be located as close as possible to the surface of the hydrophone. But in real case, this is not possible and a mechanical contact to HIFU transducer surface must be avoided. Alternatively, indirect techniques may be used to determine zero distance to HIFU transducer. But these techniques will always have some errors.

Reflections from water tank boundaries;

Main reflections in the water can arise mainly in three ways; one from surface of the water, the other from bottom of the tank and last one is from the edges of the tank as it is seen in Figure 5.23. Reflections from boundaries create interferences and in the signal. Although the pulse measurement technique eliminates most of those reflections, an error may be expected.
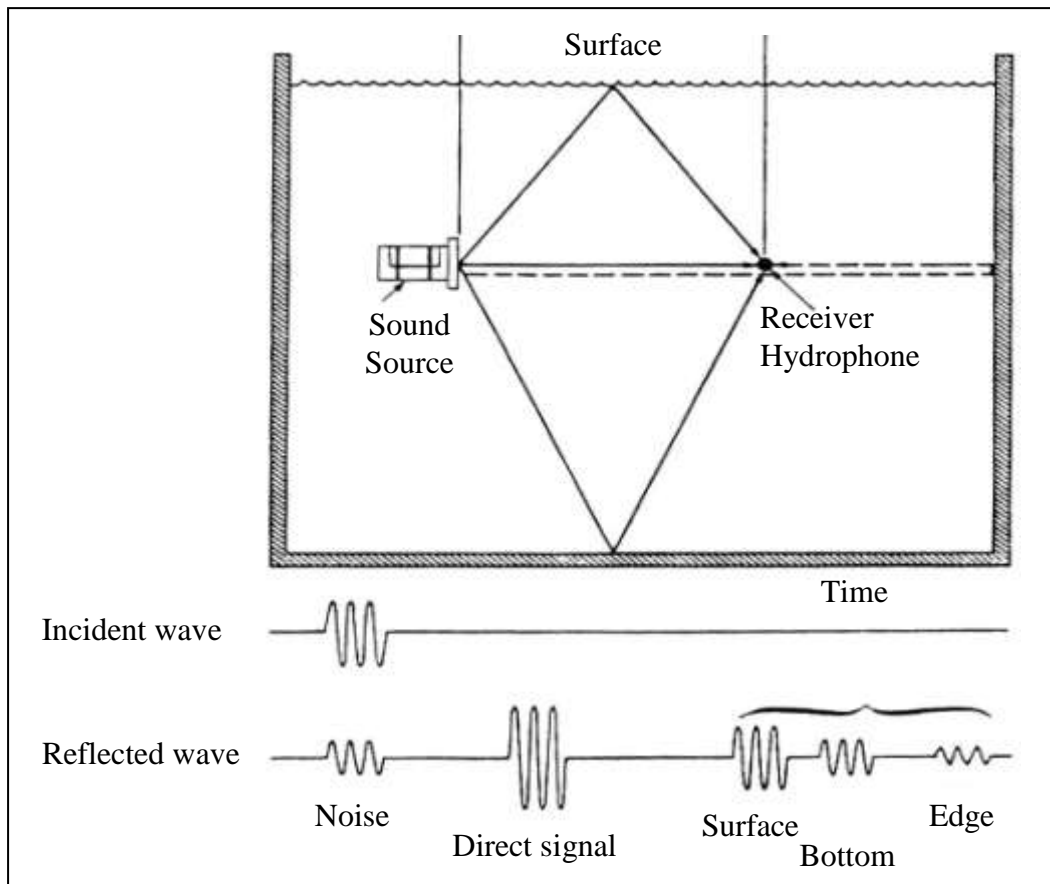
Figure 5.23. Reflections from water tank boundaries

Electrical noise;

Instability in the electrical signal to the transducer and RF signal can create fluctuations in the measured signal. Positioning system has 5 servo motors for 5 axes. They have high frequency electrical noise that affects the reading in oscilloscope.

Repeatability of measurements;

The more repeated determinations that are made the better the estimate will be expected. Repeatability uncertainty can be described as a measure of the closeness of agreement between mutually independent sound pressure determinations obtained under repeatability conditions. These are where mutually independent sound pressure determinations are obtained using the same method on a single machine at the same measurement site by the same operator(s) using the same equipment within a short interval of time. The quantity that needs to be obtained is the standard deviation of repeatability uncertainty.

All major measurement errors have been determined as it is seen in Table 5.6. Combined uncertainty of all components has been calculated as 1,4 % and expanded uncertainty has been calculated as 2,8 % for coverage factor, k=2 that corresponds 95 % confidence level.

Table 5.6 Uncertainty of acoustic pressure measurements

Sources of uncertainty	Error			Probability Distribution	Sensitivity Coefficients	Uncertainties	
Definition	Unit	Symbol	Value		Divisor	Value	Unit
Calibration of hydrophone and linearity	%	u_1	1,0	Normal	2,0	0,3	%
Calibration of analyzer (voltage)	%	u_1	0,7	Normal	2,0	0,3	%
Water temperature (speed of sound)	%	u_2	0,5	Rectangular	1,7	0,1	%
HIFU transducer and hydrophone misalignment in positioning	%	u_3	1,0	Rectangular	1,7	0,3	%
Expected surface of the transducer (zeroing)	%	u_4	1,3	Rectangular	1,7	0,5	%
Electrical noise	%	u_5	0,5	Rectangular	1,7	0,1	%
Reflections from water tank boundaries	%	u_6	0,9	Rectangular	1,7	0,2	%
Repeatability	%	u_7	0,8	Normal	1,0	0,2	%

Combined uncertainty	1,4	%
Expanded uncertainty (k=2)	2,8	%

The acoustic pressure waveforms at low powers and high powers differ meaningfully as can be seen in Figure 5.24. For low powers, the pressure waveform is more like a sinusoidal whereas it is disturbed for higher powers.

The theoretical data and experimental results have been obtained after executing operations. The results obtained by the acoustic measurements using the nonlinear field generated by the 1,10 MHz and 0,93 MHz sources are presented.

The Figures show that strong nonlinear waveform distortion and formation of a shock front are observed for the higher power levels. For smaller powers, below 10 W, the waveforms exhibit nonlinear distortions with asymmetric compression and rarefaction phases, but shock fronts are not yet produced [88].

Distortion of the sinusoidal wave form for the lower and upper power values can be clearly seen in Figure 5.24. Nonlinear distortion starts above the 10 W powers, as it is seen in a-25W and starts to turn in to a shock waveform in d-100 W in Figure 5.24. If we compare the ratio of upper part (compressional pressure) P+ and lower part (refactional) p-, we can easily see the born of shock wave form. The ratios of the P+ and P- is approximately 1,5 in a-25 W, 1,7 in a-50 W, 1,9 in a-75 W and 2 in a-100 W.

It was assumed, that cavitations might have disturbed the measurements, although degassed water has been used. Moreover, the cavitations effects might have been slowly destroying the sensor with time.
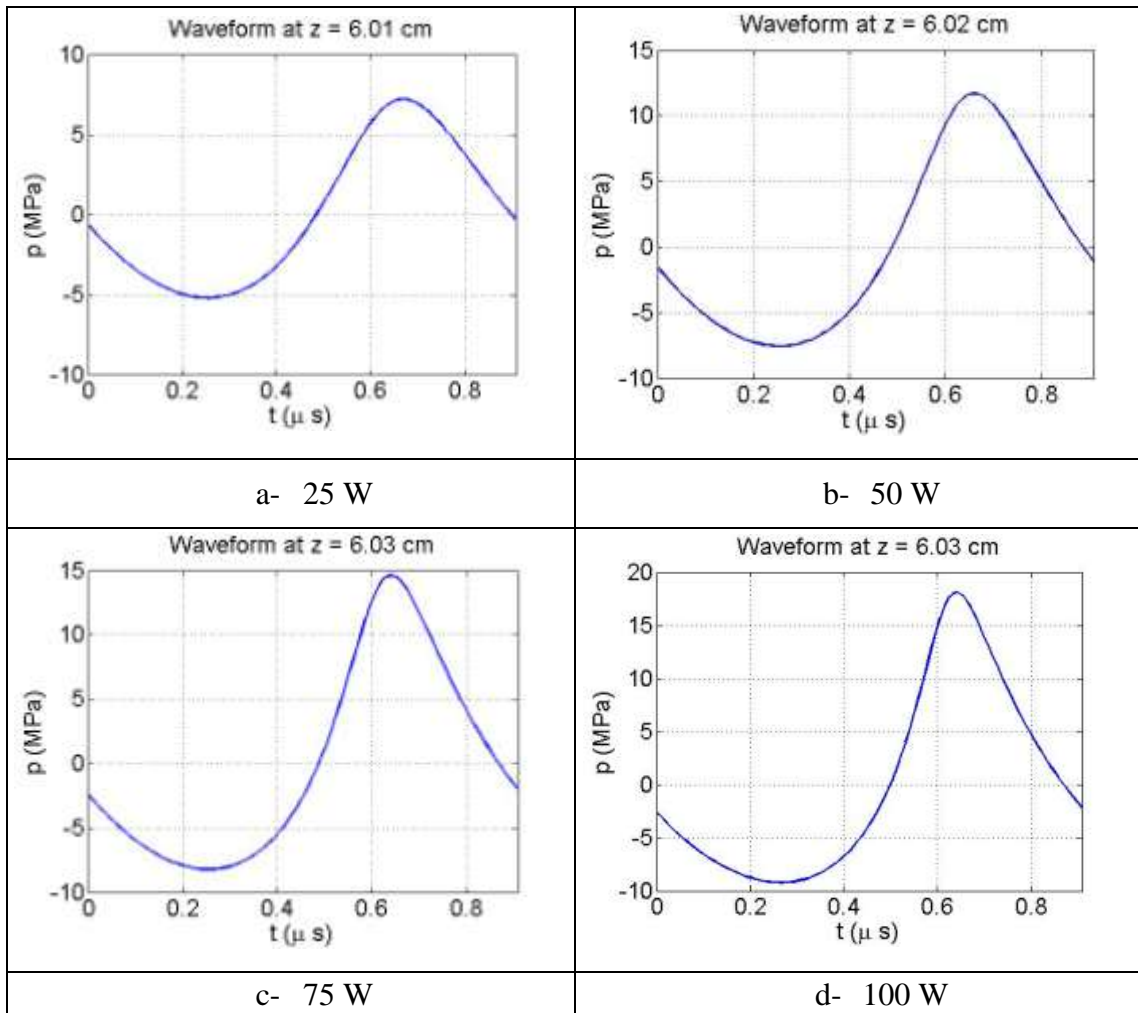
Figure 5.24. Distortion of the sinusoidal wave form for the lower and higher power levels

Shock formation is very well explained in Figure 5.25 that all the waveforms in one figure. Comparison of one cycle of the focal waveforms in a linear beam (solid curve 1) and nonlinear beams simulated in a free field in water at 25 W (curve 2), 100 W (curve 3) and 250 W (curve 4). The waveforms are normalized to the characteristic initial pressure amplitude p_0 at the face of each element and are artificially shifted by 0,15 µs relative to each other for better separation.
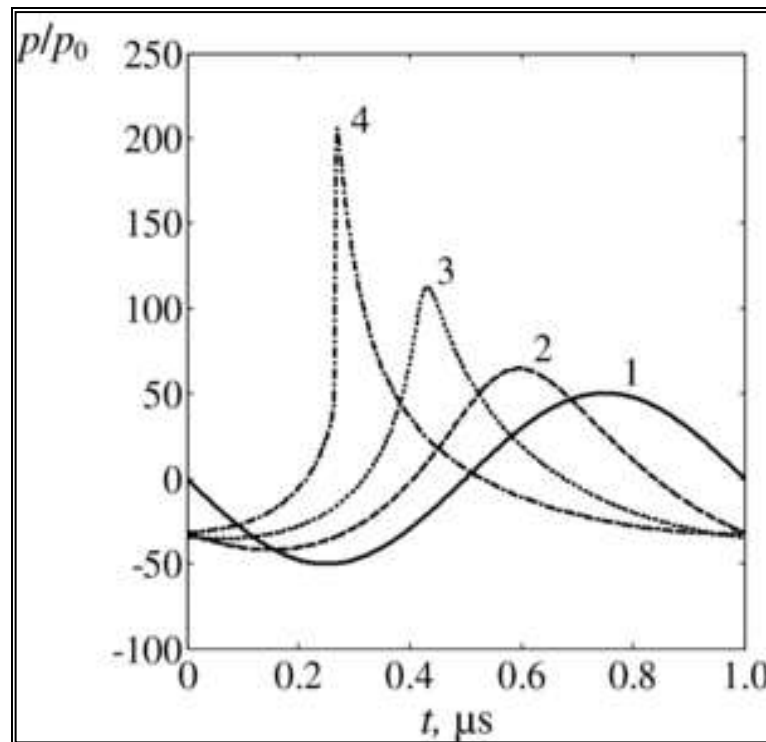
Figure 5.25. Shock wave formation

Figure 5.26 shows the ultrasound (or acoustic) pressure wave forms obtained in the water medium for varying pressures. This temporal variation of acoustic pressure was obtained at the focus from the non-linear KZK sound propagation model [70]. This figure shows that non-linearity of the medium, steepens the wave forms. Furthermore, the distorted wave forms become asymmetric with the positive peak pressures higher than the negative peaks. This can be explained by the relative phase shift between the harmonic components of the distorted wave signal caused by diffraction [89].
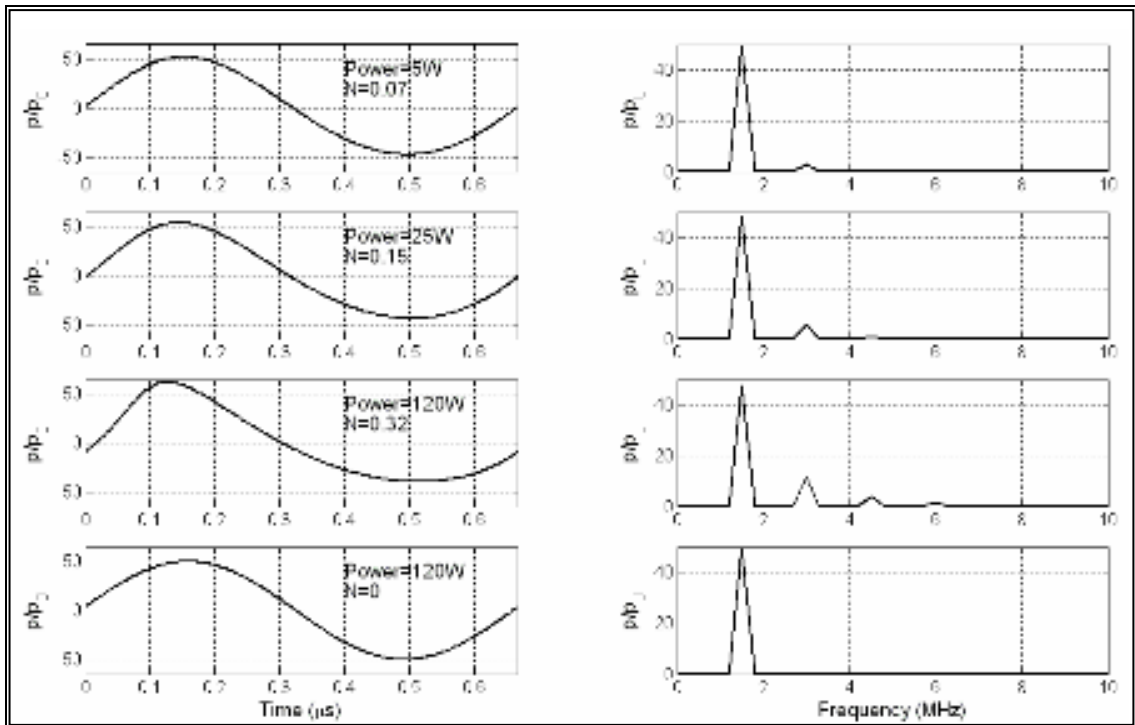
Figure 5.26. Pressure waveforms at the focus in time domain (on the left) and frequency domain (on the right)

At low and moderate powers (~25 W), higher harmonic components have a small contribution to the driving force [90]. Ignoring the effect of higher harmonics introduced an error of ~10% in the forcing term calculation. However, at high powers as seen in Figure 5.27, generation of higher harmonics is significant and this additional absorption of energy also causes an increase in the streaming velocity.

Figure 5.27 represents peak positive and peak negative pressure distributions along the **z**-axis (a) and in the focal plane (b) along the y-axis (x = 0). The distributions are normalized to the initial pressure values. The solid curves marked (1) correspond to the linear beam simulations, while the dashed curves are the results of nonlinear simulations. Again, the distributions here are normalized using the initial pressure amplitude at the elements of the array.
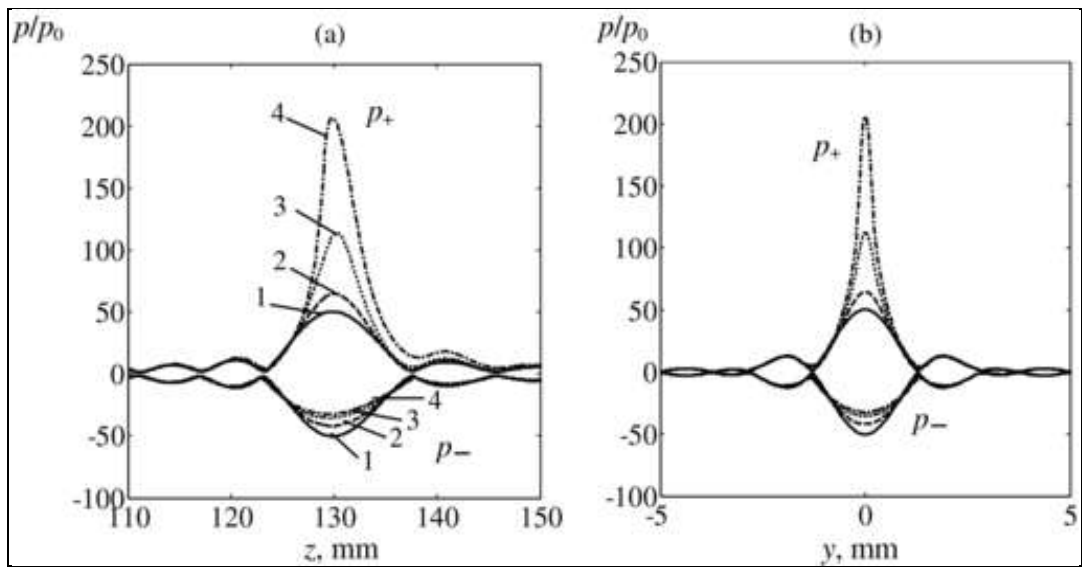
Figure 5.27. Dependency between ultrasound power and electrical power
(Peak positive and peak negative pressure distributions along the z-axis (a) and in the focal
plane (b) along the y-axis (x = 0)

5.3   TEMPERATURE DISTRIBUTION MEASUREMENTS

5.3.1   Temperature measurement results

Temperature rise inside the human body under the effect of high intensity focused fields has been investigated. First, a single PT temperature sensor was inserted inside the tissue phantom gel in order to measure inside the temperature effect.

At the same input power for HIFU transducer, phantom gel was re-oriented in three dimensions by means of a 3-D manual arm in order to measure the highest temperature. In this condition, absolute temperature was measured for the applied ultrasonic power of 40 Watts. A CW sinusoidal signal at resonance frequency (which is 1,10 MHz) was applied to HIFU transducer. When the phantom tissue is in room temperature of about 24 C, ultrasound was switched on for 30 s and switched off as it is seen in Figure 5.28. It was sharply increased to 50 ºC and slowly decreased to original temperature in 9 minutes.
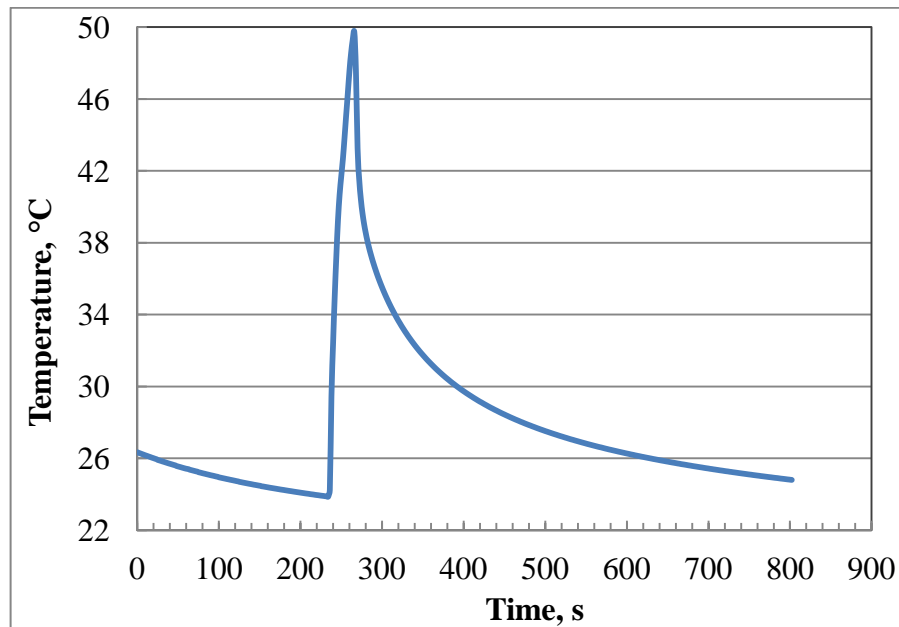
Figure 5.28. HIFU temperature measurement in the focal point induced by HIFU transducer

Temperature distribution inside the tissue phantom has been measured by using 5 thermocouples. One thermocouple was located in the center where the focal point of the HIFU transducer localized. Other 4 temperature sensors were located in 2 mm displacements. Second sensor is 2 mm away, third one is 4 mm away, fourth one is 6 mm away and last one is 8 mm away from the center. All sensors are at the same horizontal line.

It has to be mentioned that sharp peaks were not observed, since there is one second retarding between each data. When the data is taken from the central position, another data is taken after one second and vice versa. As we have total 5 sensors, it takes 5 seconds to take second date from each sensor.

In the center, temperature has reached to 48 ºC for 30 Watts of ultrasound power as it is seen in Figure 5.29. Second sensor which is 2 mm far away from the sensor, reads 11 ºC less than the temperature in the center. Temperature decreases to 23 ºC at the distance of 10 mm away from the center for the same ultrasound power.
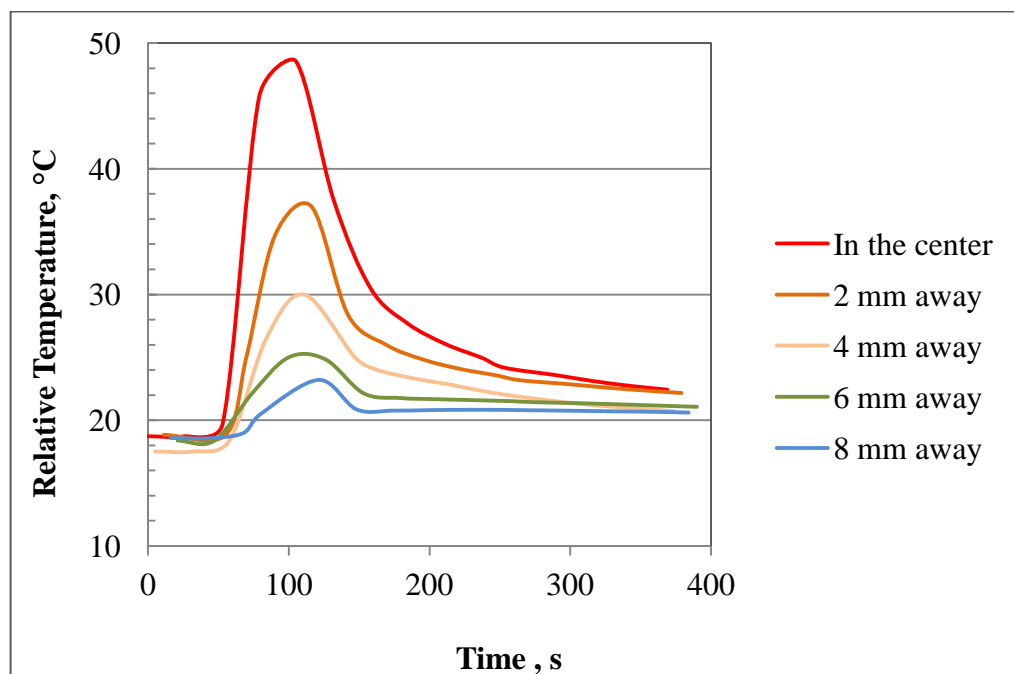
Figure 5.29. HIFU temperature disribution measurements with 5 thermocouples

Repeatability of temperature measurements were measured as 0,5 ºC. Data were taken for 20 s on and 200 s off times as it is seen in Figure 5.30. HIFU transducer were switched on for 20 s, and temperature were immediately increased to 50,4 °C for the first run and after a time to come down to original temperature, it has reached to 49,4 °C in second run, 50,0 °C and 49,4 °C for the corresponding runs.

The average temperature was determined as measured 49,7 °C with a standard deviation of 0,5 °C.
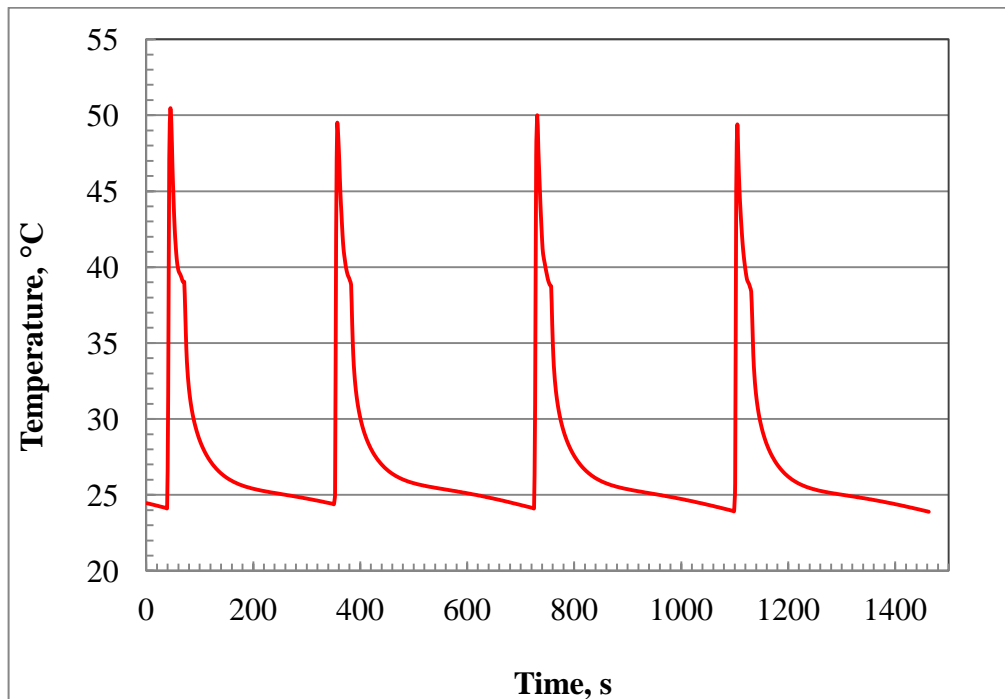
Figure 5.30. Repeatability of temperature measurements in tissue phantom under the sonication of HIFU transducer

Temperature field scanning measurements were realized under the effect of ultrasound radiation. Tissue phantom has been rotated horizontally in 20 °C's while keeping the center. Temperature data were taken with the 5 sensors at each point. Maximum temperature in the center and decrease in temperature at the points away from the center were clearly observed as it is seen in Figure 5.31. In order to compare the temperature distribution, a similar picture can be seen in Figure 5.31, taken from the literature [91].
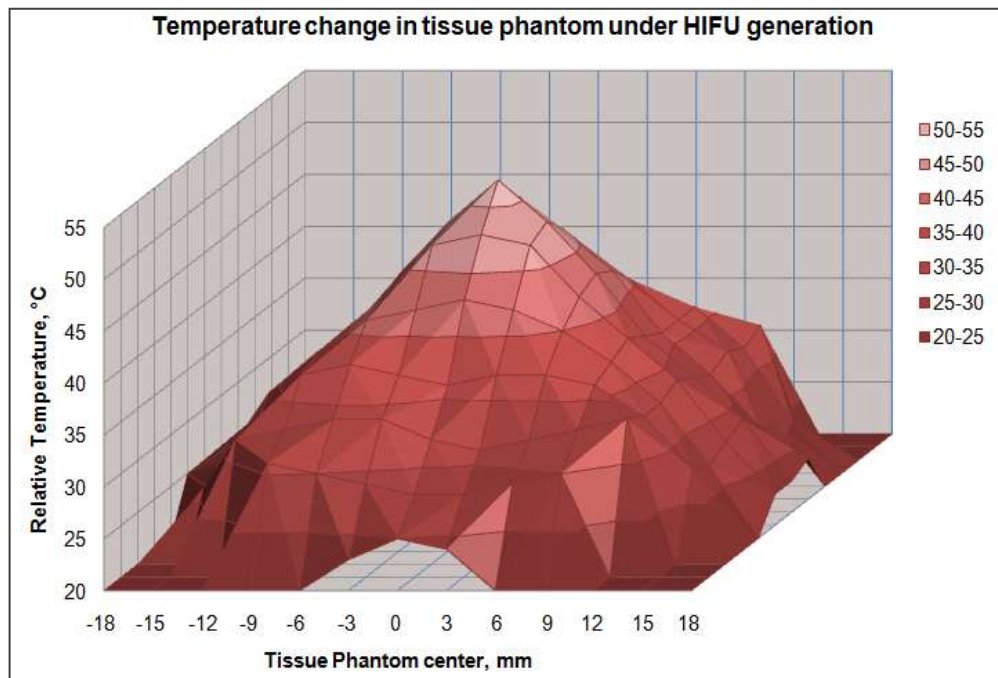
Figure 5.31. Temperature filed scanning in tissue phantom under the sonication of HIFU transducer
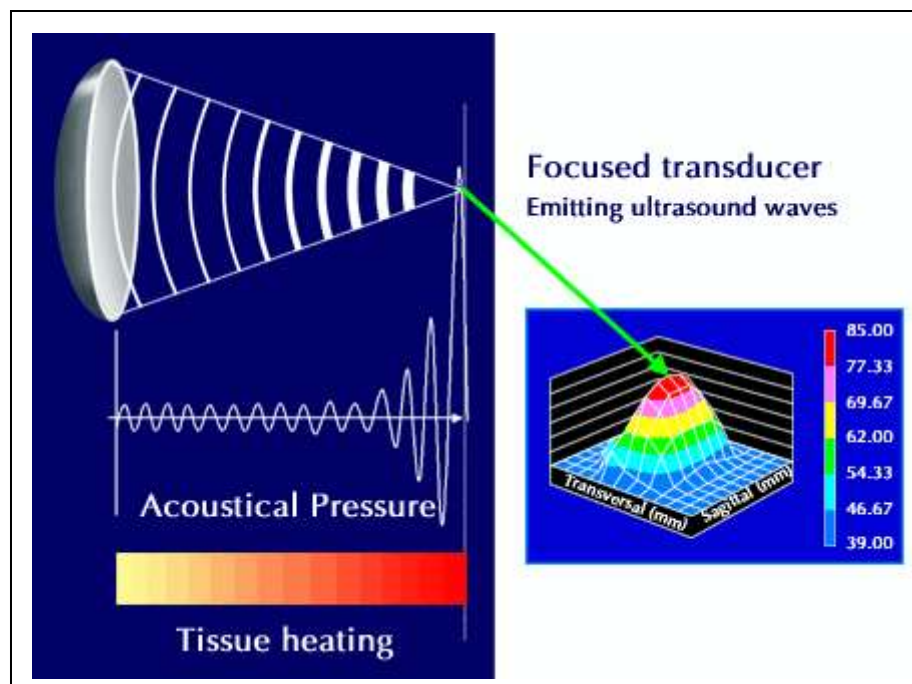
Figure 5.32. HIFU temperature measurement

5.3.2   Uncertainty in temperature measurements

Thermocouples embedded in tissue-mimicking materials are subject to mainly two types of errors that must be determined in order to obtain reliable measures of temperature rise arising from ultrasound absorption.

First type of errors is from thermocouple artifact [92-94]. Thermocouple artifacts can occur due to heat conduction along the thermocouple wire, or from differences in heat capacity or acoustic absorption between the thermocouple and the surrounding environment (water). Thermocouple artifacts can be minimized with the use of sufficiently small-size thermocouples [93].

Second type of artifact is from viscous heating at the surface of the thermocouple occurs even with thin thermocouples. A number of studies have showed that temperature rise measured using thermocouples is not the true temperature rise of the tissue material. This is because of thermocouple artifacts that bring an extra rise in temperature over the actual temperature rise of the tissue material. Thermocouple artifacts are mainly arising from viscous heating which was originally stated in the studies [95-99].

In order to determine inaccuracies due to artifacts in HIFU induced temperature measurements, some experimental investigations were performed and presented in [98]

Hysteresis:

Besides viscous heating, another source of thermocouple artifacts is the mismatch of thermal conductivity between the thermocouple junction and the surrounding tissue material. The thermocouple junction is made of metal wires like copper, constantane and chromega which have a higher conductivity than the surrounding tissue material. This causes a distortion of the temperature distribution. However, conductivity artifacts can be decreased by using small junction of the order of 30 microns in thermocouple production.

Another limitation in the use of thermocouples in temperature measurements for HIFU characterization is the error in positioning. The thermocouple junction must be well aligned with the beam at the focus. Since the size of the beam is of the order of 1 mm to 2

mm in width and 10 mm to 15 mm in length at the focus, a slight misalignment between the beam and the junction results in a significant decrease in the measured temperature.

Thermocouples can measure temperature rise only at specific locations where they are inserted. They can not measure the temperature rise over the entire ablation zone. In order to determine the size of heating region, it is necessary to determine the spatial temperature increase over a range of spatial location across the beam volume. This can be done by an array type of thermocouples inserted in the tissue.

The analog to digital conversion process, which transforms thermocouple resistance into digital values have a resolution of 0,01 ºC. Based on a rectangular distribution of the half-interval, the uncertainty component of temperature resolution is then calculated a seen in Table 5.7

Repeatability:
The more repeated determinations that are made the better the estimate will be expected. Repeatability in uncertainty can be described as a measure of the closeness of agreement between mutually independent temperature determinations obtained under repeatable environments. These is be in the conditions where mutually independent temperature determinations are obtained using the same method on a single tissue at the same measurement environment by the same operator(s) using the same equipment within a short interval of time. The quantity that needs to be obtained is the standard deviation of repeatability uncertainty.

It is apparent that all kind of temperature measurements where the thermocouple type/installation method systematic error is large, the total uncertainty is dominated on the negative side (i.e. the thermocouple reads lower than the true value). Other uncertainty sources accept the thermocouple calibration and extension cable uncertainty can be neglected. The thermocouple type/ mounting error are by far the largest source of uncertainty.

The standard uncertainty components and the resulting combined standard uncertainty of the temperature measurements, u_c, are listed in the Table 5.7. The combined uncertainty

was computed as the square root of the sum of the variances with the equation utilizing a coverage factor k=2, the expanded uncertainty, U, is expressed in Table 5.7.

Pressure and temperature field dependency is detailed in Figure 5.33. For the pressure of 2,25 MPa, temperature rise were recorded as 20 °C. The dependence between ultrasonic pressure induced by HIFU transducer and temperature rise in the tissue phantom is approximately linear.
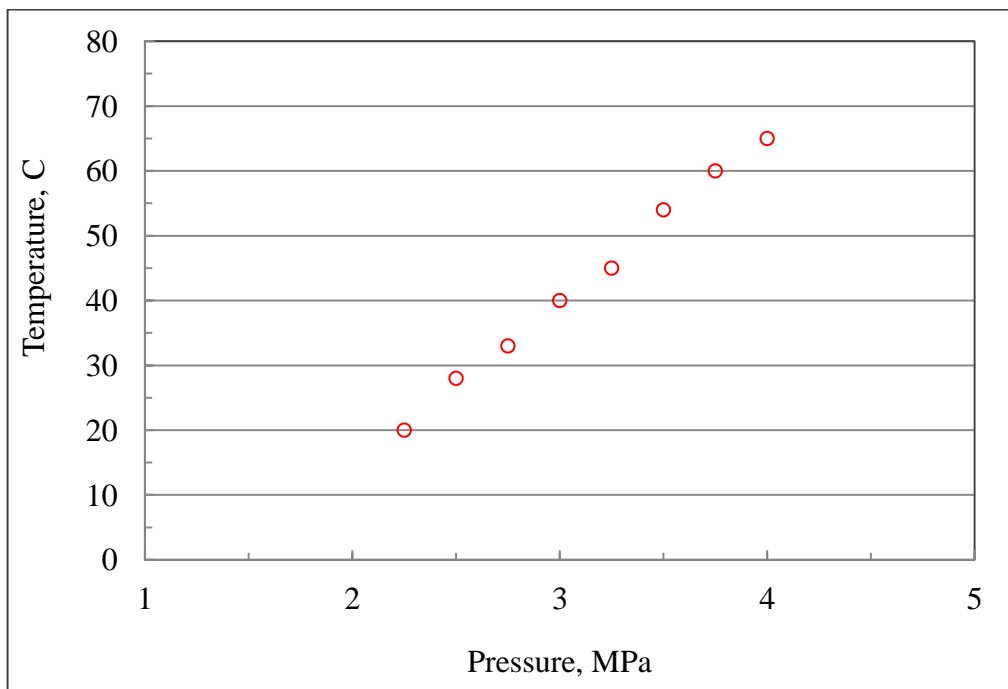
Figure 5.33. Temperature dependency for different pressure levels

Also 2-D graphs show that a good agreement between pressure field and temperature distribution measurements in Figure 5.34 and Figure 5.35.
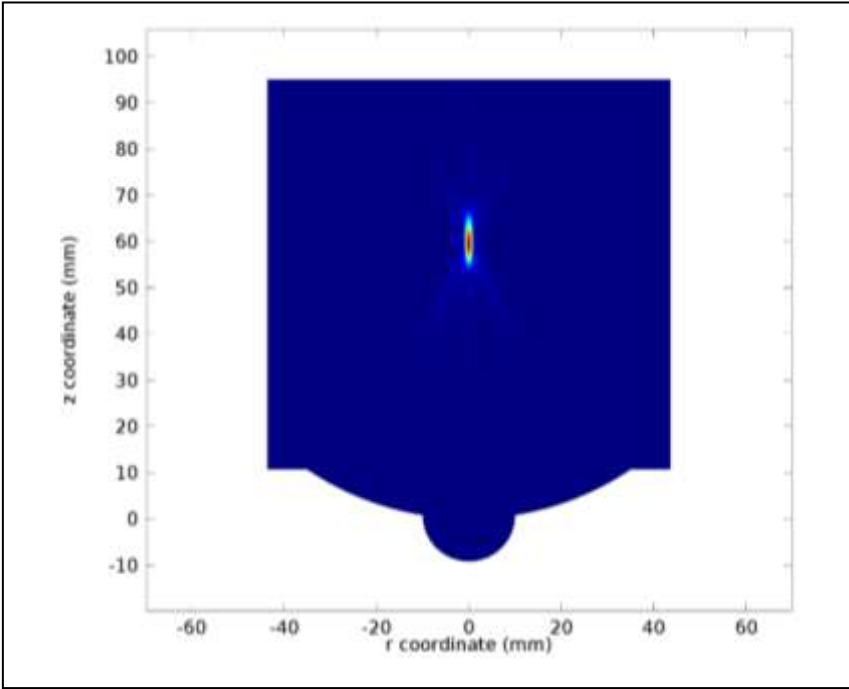
Figure 5.34. Pressure field distribution measured inside the water
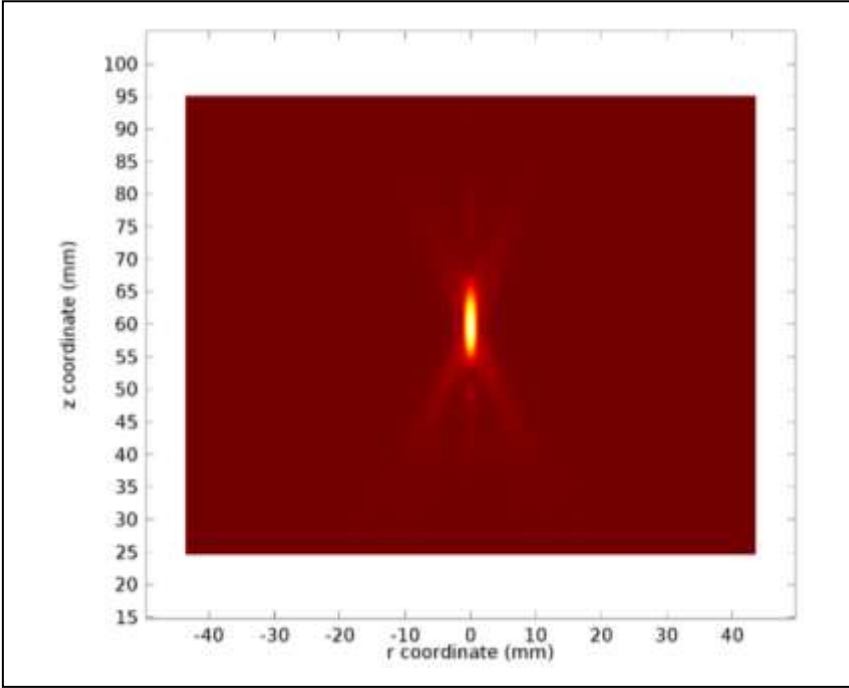
Figure 5.35. Temperature distribution in phantom tissue

Table 5.7. Uncertainty of temperature measurements

Sources of uncertainty	Error			Probability Distribution	Sensitivity Coefficients	Uncertainties	
Definition	Unit	Symbol	Value		Divisor	Value	Unit
Calibration uncertainty from certificate (k=2)	°C	u_1	0,04	Normal	2,00	0,02	°C
Calibration of analyzer (voltage)	°C	u_1	0,04	Normal	2,00	0,02	°C
Hysteresis	°C	u_2	0,02	Rectangular	1,73	0,01	°C
Environment (water) temperature	°C	u_2	0.05	Rectangular	1,73	0,03	°C
Thermocouple and ultrasound pressure field misalignment in positioning	°C	u_3	0.59	Rectangular	1,73	0,34	°C
Viscous heating	°C	u_4	0,30	Rectangular	1,73	0,17	°C
Repeatability	°C	u_7	0,02	Normal	1,00	0,02	°C

Combined uncertainty	0,39	°C
Expanded uncertainty (k=2)	0.77	°C

6. CONCLUSION

Characterization of HIFU transducers by means of electrical, acoustical and thermal methods have been resulted very useful correlations between;

- ultrasonic power - electrical power,
- ultrasonic power - ultrasonic pressure and
- ultrasonic pressure – temperature.

Theoretical model for ultrasound pressure field was realized by using a KZK nonlinear parabolic equation and experimental results were compared and an agreement was shown. Temperature rise in phantom tissue described by Pennes' bioheat transfer were analyzed and compared with the experimental measurement results.

Input electrical power in the MHz range was measured using a system established at TÜBİTAK UME Ultrasound Laboratory. Ultrasonic power output of HIFU transducers due to applied input electrical power were characterized in this study. A well known method for electrical power determination at kHz frequencies was applied for MHz frequencies by taking into account the phase between current and voltage. In order to see the differences and to compare, three different calculations were made. Moreover, the determined electrical power was compared with conventional power meters. This method (P1) shows good correlation between electrical power measurements and direct measurements of the output power of the ultrasonic transducers, which are immersed in water. The efficiency of the HIFU transducer (Precison Acoustics) was calculated as 81,9 % at resonace frequency (working frequency).

Establishment of the traceability to reference electrical standards has proven the accuracy of the method. Ultrasonic power and electrical power have similar shapes around resonance frequency as expected.

This study showed that electrical power determination by using P1 at MHz frequencies for HIFU transducers can be used with a combined uncertainty of 2,8 %, 3,3 % and 3,5 % for 60 W, 90 W and 110 W respectively.

It is clearly seen that efficiency of the HIFU transducer has the maximum at the fundamental frequency which is working frequency.

There is good agreement between the theoretical model that is based on the KZK equation and the experimental data. The near field side lobes, the main focal lobe and zero point after focal point are very well matched.

The nonlinear propagation of HIFU pressure fields in water environment has been characterized in experiments and by numerical simulation using the Khokhlov-Zabolotskaya-Kuznetsov equation. As the needle hydrophone for HIFU do not comprise an absorption body, the potential heating of the sensor is not critical. With regard to the possibility of high amplitude measurements, they are limited by the initiation of cavitations in water.

The numerical solutions were verified extensively and were shown to have a good agreement with theory and experiment. Comparisons of the measured and simulated focal plane of a diagnostic ultrasound transducer exhibited the same primary and secondary features with respect to the position and amplitude of the main lobe and side lobes for both the fundamental and harmonic components. The nonlinear propagation was also verified numerically with results from a propagating plane wave and were shown to be in good agreement.

Higher-pressure parts of the wave travel faster than lower-pressure parts, causing the distortion of the temporal waveform. In the frequency domain, such distortion generates higher harmonics of the fundamental frequency that are more readily absorbed and converted to heat. Nonlinear distortion effects accumulate as the wave propagates and are accelerated by an increase of the wave amplitude. In focused fields, nonlinear effects are the strongest within the focal zone, where the amplitudes are the highest.

In the absence of acoustic non-linearity, sound waves propagate as single frequency waves with all the energy contained in the fundamental frequency. But as the acoustic pressure is increased, the non-linearity causes generation of higher harmonics. This causes shifts in energy from the fundamental harmonic to the strongly absorbing higher frequency components that are integer multiples of fundamental frequency.

As the results of modeling were found to be in good agreement with the experimental data, in many cases numerical modeling can be employed as an effective tool, in addition to the characterization by measurements. A combination of numerical simulation and measurements up to the highest outputs experimentally accessible seems to provide the best reliability for the characterization of the acoustic output of HIFU devices.

The width and shape of the main lobe and side lobe are almost at same height. In the other lateral axis (y-axis), the sketches can be seen in Figure 5.17 for the focus at 62 mm, near field at 22 mm and 42 mm and far field at 82 mm and 102 mm for Sonic Concepts HIFU transducer. At focus, the side lobes are clearly resolved.

Side lobes are almost missing since in radial axis curves as seen in Figure 5.18. Lateral axis (z-axis) in the sketches can be seen in Figure 5.18 for the focus, near field at 22 mm and 42 mm and far field at 82 mm and 102 mm for Sonic Concepts HIFU transducer. At focus, high gain is resolved.

It also ensures that the HIFU transducer was operating in a linear way and did not generate any harmonics for low pressures.

In order to ensure safety of patients during HIFU treatment and to enhance effectiveness of the procedure proper characterization of HIFU devices, for accurate prediction of the induced thermal field distribution, is necessary. Such methods will be useful to device manufacturers as well as regulatory bodies, to better evaluate the performance of HIFU devices.

HIFU beam was focused within an array of five thermocouples for temperature mapping of inside the tissue. Direct placement of the beam on the thermocouples is avoided to prevent

thermocouple artifacts. The beam location and angular orientation which are important parameters to be assessed in the thermal field distribution characterization is determined with acceptable accuracy. On the basis of the beam location the artifact-free temperature rise can be predicted at desired locations within the tissue medium. The method is applied to refine the data obtained during the in vitro experiments using the vascularized tissue phantom, by removing inaccuracies due to beam positioning error from the data.

Temperature can easliy increase to 50 ºC's for 30 Watts of ultrasound power as it is seen in Figure 5.29. This temperature is enough to start burning the tissues [100]. Burning region is an eliptical shape region with dimensions of 5 mm and 2 mm aproximately. This means that only the tissue parts in this region will be burned and the other tissue region will remain alive since the temperature is sharply decreasing in the amount of 10 °C's in the regions few mm away from the focal region.

The in vitro experiments, which involve embedding thermocouples in a vascularized tissue material for temperature measurement, are used to assess the HIFU thermal effects. Temperature measurement results have been showed that temperature in the tissue reaches 50 °C in focal point of HIFU transducer and decreases few tens of °C's in mm displacements. Temperature field distribution characterization in a tissue phantom is a convenient tool to measure temperature rise and lesion size with acceptable accuracy. Temperature rise data measured with thin thermocouple in order to diminish the effect of viscous heating artifacts.

However, positioning errors are one of the major limitations, which impose inaccuracies in the measured data. Further, the some computational methods can be applied to assess inaccuracies due to thermocouple artifacts in the measured data.

Temperature rise due to viscous heating increases rapidly at the start of the insonation and more slowly with time. At the end of insonation (5 s) the temperature rise due to viscous heating is ~60 % of the measured temperature rise [101].

HIFU is a very attractive and new technique that is used in cancer treatment, physiotherapy and other similar treatments. Characterisation of HIFU transducers which is carried out

within the scope of this thesis will have an important achievement on the safe and efficient use of this kind of transducers. Besides acoustical power, pressure and temperature distribution measurements that are huge number of studies are going on; an electrical method applied to HIFU transducers for the first time was presented in this thesis which is original in this field.

Another innovative study in this thesis is a metrological point of view. Uncertainty budgets in measurements were studied and presented in all measurements first time in this thesis. All measurement devices are traceable to national standards.

REFERENCES

1. Miller, S., Urologist in Private Practice in Atlanta, Georgia, *MedlinePlus*, http://www.nlm.nih.gov/medlineplus/ency/article/007113.htm [retreived 27 June 2014].

2. "Therapeutic Ultrasound & Physiotherapy"*, UK Health Centre*, http://www.healthcentre.org.uk/physiotherapists/physiotherapist-therapeutic-ultrasound.html [retreived 27 June 2014].

3. Petrou, I., Guided Ultrasound For Noninvasive Skin Tightening May Be Wave of Future, *Cosmetic Surgery Times,* http://cosmeticsurgerytimes.modernmedicine.com/news/guided-ultrasound-noninvasive-skin-tightening-may-be-wave-future [retreived 27 June 2014].

4. Hynynen, K. and Clement, G., "Clinical Applications of Focused Ultrasound—The Brain"*, International Journal of Hyperthermia* 23, pp. 193–202 2007.

5. Vaezy, S., Martin, R., Kaczkowski, P., Keilman, G., Carter, S., Caps, M., and Crum, L., (1998) "Occlusion of Blood Vessels using High Intensity Focused Ultrasound", *Proceedings of the International Conference on Acoustics and 135th Meeting of Acoustical Society of America*, Proceedings of 16th ICA/135th ASA Meeting. Vol 2, pp. 1061- 1062, Washington, USA, 1998.

6. Vaezy, S., Martin, R., Yaziji, H., Kaczkowski, P., Keilman, G., Cater, S., Caps, M., Chi, E., and Crum, L., "Hemostasis of Punctured Blood Vessels Using High Intensity Focused Ultrasound"*, Ultrasound in Medicine and Biology*, vol. 24, pp. 903-910, 1998.

7. Poliachik, S., Bloch, S., Bailey, M., Kaczkowski, P., Cleveland, R., Mourad, P.D., Porter, T., Crum, L.A., Chandler, W.L. and Keilman, G.W., "Ex Vivo Studies of the Effect of High-Intensity Focused Ultrasound on Whole Human

Blood", *Journal of the Acoustical Society of America*, Volume 103, Issue 5, p. 2831, 1998.

8. Keilman, G. and Kaczkowski, P., "High-Intensity Focused Ultrasound Transducer Design For Surgical And Hemostatic Applications", *Journal of the Acoustical Society of America*, Vol 103, Issue 5, p. 2831, 1998.

9. Vaezy, S., Martin, R., Schmiedl, U., Caps, M., Taylor, S., Beach, K., Carter, S., Kaczkowski, P., Keilman, G., Helton, S., Chandler, W., Mourad, P., Rice, M., Roy, R. and Crum, L., "Liver Hemostasis Using High Intensity Focused Ultrasound", *Ultrasound in Medicine and Biology*, vol. 23, pp. 1413-1420, 1997.

10. Keilman, G.W., "New Ultrasound Hyperthermia Applicators with Improved Bandwidth and Spatial Uniformity", *No. American Hyperthermia Group (NAHG) Conference Proceeding*, Seattle, WA, March, 1989.

11. Sekins, K.M., Keilman G.W., and Anderson T.L., "Lung Cancer Hyperthermia via Ultrasound and PFC Liquids", in Hyperthermic Oncology, Vol. 1: Summary Papers, *Proceedings of 5th International Sympossium on Hyperthermic Oncology*, Kyoto, Japan, Aug. 1988, Publ. by Taylor and Francis, pp. 418-420, 1988.

12. Keilman, G.W. and Butts, H.B., "Lateral Resolution Improvement of Focused Piston Transducers by a Signal Processing Technique", *IEEE Ultrasonics Symposium Proceedings,* Chicago, IL, 1981.

13. Keilman, G.W., and Andersen J., "Active Broadband Matching of Piezoelectric Transducers", *American Institute of Ultrasound in Medicine Proceedings,* Colorado,1980.

14. IEC: Requirements for Measurement Standards For High Intensity Therapeutic Ultrasound (HITU) devices, *International Electrotechnical Commission Publication* 62649, 2010.

15. Filonenko, E. and Khokhlova, V., "Effect of Acoustic Nonlinearity on Heating of Biological Tissue By High-Intensity Focused Ultrasound", *Acoustic Physics,* 47, pp. 541–549, 2001.

16. Canney, M.S., Khokhlova, V.A., Bessonova, O.V., Bailey, M.R. and Crum, L.A., "Shock Induced Heating and Millisecond Boiling in Gels And Tissue Due To High Intensity Focused Ultrasound*", Ultrasound in Medicine and Biology,* Vol. 36, pp. 250-267, 2010.

17. Hynynen, K., "Demonstration of Enhanced Temperature Elevation Due To Nonlinear Propagation of Focused Ultrasound In Dog's Thigh In Vivo", *Ultrasound in Medicine and Biology,* 13, pp. 85–91, 1987.

18. Tjotta, J. N. and Tjotta, S., "Near Field And Far Field Of Pulsed Acoustic Radiators", *Journal of the Acoustical Society of America*, 71:824-834, 1982.

19. Khokhlova, V.A., Bessonova, O.V., Averiyanov, M.V., Soneson, J.E. and Cleveland, R.O., "Modeling of Nonlinear Shock Wave Propagation And Thermal Effects In High Intensity Focused Ultrasound Fields", *159th meeting of The Acoustical Society of America/ Noise-Con*, Baltimore, Maryland, USA, Apr. 19–23, 2010. Abstract: *Journal of the Acoustical Society of America.*, Vol. 123, p. 1827, 2010.

20. Zabolotskaya, E.A. and Khokhlov, R.V.. "Quasi-plane Waves in the Nonlinear Acoustics of Confined Beams", *Soviet Physics. Acoustics*, Vol. 15, pp. 35-40, 1969.

21. Kuznetsov, V.P., "Equations of nonlinear acoustics", *Soviet Physics. Acoustics*, Vol. 16, pp. 467-470, 1971.

22. Onda Corporation, http://www.ondacorp.com/products_hifusol_phantoms.shtml, http://www.ondacorp.com/products_hydrophones.shtml, [retreived 27 June 2014].

23. Pennes, H.H., "Analysis of Tissue and Arterial Temperatures in The Resting Human Forearm"*, Journal of Applied Physiology*, 1, pp. 93-122, 1948.

24. Bailey, M.R., Crum, L.A., Miller, N., Couret, L.N., Sapozhnikov, O.A., Pishchalnikov, Y.A., Keilman, G., McAteer, J.A., Connors, B., and Evan, A.P., "Localized Detection of Cavitation in Vivo", *Journal of the Acoustical Society of America,* Vol 109, Issue 5, p. 2481, 2001.

25. Khokhlova, V., Bailey, M., Reed, J., Cunitz, B., Kaczkowski, P., and Crum, L.*,* "Effects of Nonlinear Propagation, Cavitation, And Boiling in Lesion Formation by High Intensity Focused Ultrasound in a Gel Phantom", *Journal of the Acoustical Society of America,* 119, pp.1834–1848, 2006.

26. Focused Ultrasound Foundation, http://www.fusfoundation.org, [retreived 27 June 2014].

27. Sekins, K.M., Leeper, D.B., Hoffman, J.K., Keilman, G.W., Ziskin, M.C., Wolfson, M.R. and Shaffer, T.H.,   Feasibility of Lung Cancer Hyperthermia Using Breathable Perfluorochemical (PFC) Liquids, Part II: *Ultrasound Hyperthermia in International Journal of Hyperthermia* 2004, Vol 20; Part 3, pp. 278-299, 2004.

28. Kaczkowski, P., Keilman, G., Cunitz, B.W., Martin, R.W., Vaezy, S., and Crum, L.A., "High-Intensity Focused Ultrasound (HIFU) Array System for Image-Guided Ablative Therapy (IGAT)",   *Proceedings of SPIE*, Vol 4954: Thermal Treatment of Tissue: Energy Delivery and Assessment II, Thomas P. Ryan, Ed., pp. 209-219. 2003.

29. Kaczkowski, P.J., Vaezy S., Martin, R., Crum, L.A. and Keilman, G., "A Multi-Channel High-Intensity Focused Ultrasound (HIFU) System for Image-Guided Therapy (IGT)", *Journal of the Acoustical Society of America*, Vol. 110, Issue 5, p. 2614. 2001.

30. Vaezy, S., Martin, R., Keilman, G., Kaczkowski, P., Schmiedl, U., Chi, E., Yazaji, E., Caps, M., Poliachik, S., Carter, S., Sharar, S., Cornejo, C., and

Crum, L., "Control of Splenic Bleeding by Using High Intensity Focused Ultrasound", *J. Trauma, Injury, Infection, and Critical Care*, Vol. 47, No. 3, pp. 521-525, 1999.

31. Martin, R.W., Vaezy, S., Kaczkowski, P., Keilman, G., Carter, S., Caps, M., Beach, K., Plett, M. and Crum, L.A., "Hemostasis of Punctured Vessels Using Doppler-Guided High-Intensity Ultrasound", *Ultrasound in Medicine and Biology,* 25(6), pp. 985-90, 1999.

32. Poliachik, S.L., Chandler, W.L., Mourad, P.D., Bailey, M.R., Bloch, S., Cleveland, R.O., Kaczkowski, P., Keilman, G.W., Porter, T. and Crum, L.A., "Effect of High-Intensity Focused Ultrasound on Whole Blood With and Without Microbubble Contrast Agent", *Ultrasound in Medicine and Biology,* 25(6), pp. 991-8. 1999.

33. Crum, L., Beach, K., Carter, S., Chandler, W., Curra, F., Kaczkowski, P., Keilman, G., Khokhlova, V., Martin, R., Mourad, P., Vaezy, S., "Acoustic Hemostasis, in Nonlinear Acoustics at the Turn of the Millennium", ISNA 15, W. Lauterborn and T. Kurz, ed., *American Institute of Physics*, 2000.

34. Vaezy, S., Martin, R., Kaczkowski, P., Keilman, G., Goldman, B., Yaziji, H., Carter, S., Caps, M. and Crum, L., "Use of High-Intensity Focused Ultrasound to Control Bleeding", *Journal of Vascular Surgery*, 29(3), pp.533-42, 1999.

35. Poliachik, S., Chandler, W., Mourad, P.D., Bloch, S., Bailey, M., Cleveland, R., Crum, L.A., Kaczkowski, P., Keilman, G., and Porter T., "Ex-vivo Studies of the Effects of High-Intensity Focused Ultrasound on Whole Blood" *Proceedings of International Congress of Acoustics,* vol 2, p. 727. Seattle, 1998.

36. Martin, R., Vaezy, S., Helton, S., Caps, M., Kaczkowski, P., Keilman, G., Carter, S., Chandler, W., Mourad, P., Beach, K., and Crum, L., "Acoustic Liver Cauterization: A Potential Tool for Bloodless Surgery", Proceedings of ICA/ASA Meeting. *Proceedings of 16th International Congress of Acoustics*

/135th Acoustical Society of America Meeting. Vol 2, pp. 721- 722, Seattle,1998.

37. Lynn, J.G, Zwemer, R.L. and Chick, A.J., "The Biological Applicationof Focused Ultrasonic Waves", Science, 96, pp. 119-120, 1942.

38. Kennedy, J., Wu, F., ter Haar, G., Gleeson, F., Phillips, R., Middleton, M., and Cranston, D., "High-Intensity Focused Ultrasound For The Treatment of Liver Tumours", *Ultrasonics* 42, pp. 931–935, 2004.

39. Yagel, S. High-Intensity Focused Ultrasound: A Revolution in Non-Invasive Ultrasound Treatment, *Ultrasound in Obstetrics and Gynecology,* 23, pp. 216–217, 2004.

40. Hill, C. R., Bamber, J. C., and ter Haar, G., *Physical Principles of Medical Ultrasonics*, 2nd edition Wiley, London, 2004.

41. Harris, G., "Medical Ultrasound Exposure Measurements: Update on Devices, Methods and Problems", *Proceedings of IEEE Ultrason. Symp.* 2, pp. 1341–1352, 1999.

42. Wang, Y., Wang, W., Wang, L., Wang, J., Tang, J., "Ultrasound-Guided High-Intensity Focused Ultrasound Treatment For Abdominal Wall Endometriosis: Preliminary Results, http://dx.doi.org/10.1016/j.ejrad.2009.12.034, *European Journal of Radiology,* Vol. 79, Issue 1, pp. 56–59, 2011.

43. Sonic Concepts, Inc., http://www.sonicconcepts.com/, [retreived 27 June 2014].

44. Precision Acoustics Ltd, , http://www.pa.co.uk, [retreived 27 June 2014].

45. Cancer Research Technology, www.cancertechnology.co.uk/phased-array-high-intensity-focused-ultrasound-hifu-technology, [retreived 27 June 2014].

46. http://www.healthcare.philips.com/main/products/mri/systems/sonalleve/, [retreived 27 June 2014].

47. InSightec Ltd., http://www.insightec.com/System-Overview.html, [retreived 27 June 2014].

48. Edap TMS, http://www.edap-tms.com/products-services/ablatherm-hifu, [retreived 27 June 2014].

49. Wood, R. W. and Loomis, A. L. "The Physical and Biological Effects of High Frequency Sound Waves of Great Intensity", *Philosophical Magazine* 4 (22): 417–436, 1927.

50. IEC 61161: Ultrasonics – Power measurement – Radiation Force Balances and Performance Requirements, *International Electrotechnical Commission* Publication 61161, Ed. 2, 28, 2006.

51. Shaw, A. and ter Haar, G., Requirements for Measurement Standards in High Intensity Focused Ultrasound (HIFU) Fields, *NPL Report Dql Ac 015*, 2006.

52. Hariharan, P., Myers, M. R., Robinson, R. A., Maruvada, S. H., Sliwa, J., and Banerjee, R. K., "Characterization of High Intensity Focused Ultrasound Transducers Using Acoustic Streaming", *Journal of the Acoustical Society of America,* 123, pp. 1706–1719, 2008.

53. Hariharan, P., *Free Field Characterization of High Intensity Focused Ultrasound (HIFU) Transducers Using Acoustic Streaming*, PhD Thesis report, University of Cincinnati, Mechanical Engineering, 2008.

54. Filonenko, E, Khokhlova, V. "Effect of Acoustic Nonlinearity on Heating of Biological Tissue by High-Intensity Focused Ultrasound", *Acoustic Physics* 47, pp. 541–549, 2001.

55. Dalecki, D., Carstensen, E., Parker, K., "Absorption of Fnite Amplitude Focused Ultrasound", *Journal of the Acoustical Society of America,* 89, pp. 2435–2447, 1991.

56. Hamilton, M. and Blackstock, D., (eds). *Nonlinear Acoustics*. London: Academic Press, pp. 105–106, 1998.

57. Clarke, R., ter Haar, G., "Production of Harmonics in Vitro by High-Intensity Focused Ultrasound" *Ultrasound in Medicine and Biology*, 25, pp. 1417–1424, 1999.

58. Hynynen K., "Demonstration of Enhanced Temperature Elevation due to Nonlinear Propagation of Focused Ultrasound in Dog's Thigh in Vivo", *Ultrasound in Medicine and Biology,* 13, pp. 85–91, 1987.

59. Baker, A.C., *Finite Amplitude Propagation of Focused Ultrasound Waves in Water*, Thesis for the degree of Ph.D. of the University of Bath, School of Physics, Bath, 1989.

60. Şahin, A., *Nonlinear Pressure Fields Due to Focused Rectangular Aperatures in Water*, Thesis for the Degree of Ph.D. of the University of Bath, School of Physics, Bath, 1992.

61. Şahin, A and Baker, A.C., "Ultrasonic Pressure Fields due to Focused Rectangular Apertures", *Journal of the Acoustical Society of America*, 96(1), pp. 552-556, 1994.

62. Şahin, A., "Numerical Solution to the Nonlinear Acoustic Wave Equation", *International Journal of Applied Mathematics*. Vol. 2, No. 3, pp. 339-352, 2000.

63. Baker, A.C., Berg, A.M., Şahin, A. and Tjotta, J.N., "The Nonlinear Pressure Fields of Plane Rectangular Apertures: Experimental and Theoretical Results", *Journal of the Acoustical Society of America*, (97),pp. 3510-3517, 1995.

64. Kaya, O. A., *İki ve Üç Boyutta Doğrusal Olmayan Akustik Basınç Alanlarının Teorik İncelenmesi*, Doktora Tezi, Fen Bilimleri Enstitüsü, İnönü Üniversitesi, Malatya, 2004.

65. Kaya, O. A., Şahin, A. and Kaleci, D., "Pressure Field of Rectangular Transducers at Finite Amplitude in Three Dimensions", *Ultrasound in Medicine and Biology*, Vol. 32 (2), pp. 271-280, 2006.

66. Zanelli, C.I. and Howard S.M., "A Robust Hydrophone for HIFU Metrology", *Proceedings of 5th International Symposium on Therapeutic Ultrasound*, pp. 618–622, 2005.

67. Schafer, M.E., Gessert, J. and Moore, W., "Development of a High Intensity Focused Ultrasound (HIFU) Hydrophone System", *Ultrasonics Symposium*, 2005 IEEE Xplore, pp. 18-21, 2005.

68. Gan, W. S., "Analytical Solutions of the KdV-KZK Equation", *Non-Linear Acoustics and Vibration*, pp. 104-107, 2005.

69. Matlab - The Language of Technical Computing, http://www.mathworks.com/products/matlab

70. HIFU Simulator, www.mathworks.com/matlabcentral/fileexchange/30886-high-intensity-focused-ultrasound-simulator

71. National Instruments, NI PCI-5412,
http://sine.ni.com/nips/cds/view/p/lang/en/nid/14837

72. National Instruments, NI PCI-5105,
http://sine.ni.com/nips/cds/view/p/lang/en/nid/203360

73. Hekkenberg, R.T., Beissner, K. and Zeqiri, B., Therapy-Level Ultrasonic Power Measurement, *BCR Information, Reference Materials, Final Technical Report, SMT4-CT96*-2139, 2000.

74. Wu, F., Wang, Z., Chen, W., Zou, J., Bai, J., Zhu, H., Li, K., Xie, F., Jin, C., Su, H. and Gao, G., "Extracorporeal Focused Ultrasound Surgery for Treatment of Human Solid Carcinomas: Early Chinese Clinical Experience", *Ultrasound in Medicine and Biology, Vol.* 30, pp. 245–260, 2004.

75. Wu, F., ter Haar, G. and Chen, W.R., "High-Intensity Focused Ultrasound Ablation of Breast Cancer", *Expert Rev. Anticancer Ther.*, Vol. 7, pp. 823–831, 2007.

76. Maruvada, S., Harris, G.R., Herman, B.A. and King, R.L., "Acoustic Power Calibration of High Intensity Focused Ultrasound Transducers Using a Radiation Force Technique", *Journal of the Acoustical Society of America*, Vol. 121, pp. 1434–1439, 2007.

77. Clement, G., McDannold, N. and Hynynen, K., (eds.). Therapeutic Ultrasound: *5th International Symposium on Therapeutic Ultrasound*, Boston, MA, October 27–29, 2005. AIP Conference Proceedings. 2005.

78. Hill, C.R., Bamber, J.C. and ter Haar, G., *Physical Principles of Medical Ultrasonics*. 2nd ed. West Sussex, UK: John Wiley & Sons; 2004.

79. Ter Haar, G., "High Intensity Focused Ultrasound for The Treatment of Tumors", *Echocardiography,* Vol.18(4), pp.317-322, ISSN: 0742-2822, 2001.

80. Vaezy, S, Wyzgala, M., Keilman, G., "A Needle-Size Hydrophone and Thermocouple for High-Intensity Focused Ultrasound", *Journal of the Acoustical Society of America*, Volume 112, Issue 5, p. 2369, 2002.

81. Ren, X. L., Zhou, X. D., Yan, R. L., Liu, D., Zhang, J., He, G. B., Han, Z. H., Zheng, M. J. and Yu, M., "Sonographically Guided Extracorporeal Ablation of Uterine Fibroids with High-Intensity Focused Ultrasound: Midterm Results", *Journal of Ultrasound in Medicine,* [Letters to the Editor]. 28, pp. 95–103, 2009.

82. Huang, J., Holt, R. G., Cleveland, R. O. and Roy, R. A., "Experimental Validation of a Tractable Medical Model for Focused Ultrasound Heating in Flow-Through Tissue Phantoms", *Journal of the Acoustical Society of America,* 116, 2451, 2004.

83. Dasgupta, S., "*Improved Characterization of the High Intensity Focused Ultrasound (HIFU) Induced Thermal Field,*" PhD thesis, University of Cincinnati, Department of Mechanical and Materials Engineering, 2010.

84. Fluke Black Stack thermometer read out, http://us.flukecal.com/products/temperature-calibration/digital-thermometer-readouts/1560-black-stack-thermometer-readout

85. JCGM 100:2008, GUM 1995 with Minor Corrections Evaluation of Measurement Data — Guide to the Expression of Uncertainty In Measurement.

86. Karaböce, B., Gülmez, Y., Rajagapol, S. and Shaw, A., "Instantaneous Input Electrical Power Measurements of HITU Transducer", *Journal of Physics: Conference Series,* 279012011, doi: 10.1088/1742-6596/279/1/01201, 2011

87. Karaböce, B., Gülmez, Y., Bilgiç, E., Sadıkoğlu, E., İnce, A.T. and Skarlatos, Y., "Comparison of the Input Electrical Power Measurement Methods for HIFU Transducers", *Procdings of IEEE International Symposium on Medical Measurements and Applications (MeMeA 2014),* 11-12.06, 2014.

88. Siddiqi, A. K., *Development of Tissue-Equivalent Heat-Sensitive Gel for the Experimental Verification of Near Infrared (Nır) Laser-Mediated Cancer Detection and Therapy,* Master Thesis, Georgia Institute of Technology, 2009.

89. Parker, K.J. and Friets, E.M., "On The Measurements of Shock Waves", *IEEE IEEE Transactions on Ultrasonics, Ferroelectrics and Frequency Control,* 34 (4) pp. 454-460, 1987.

90. Hariharan, P., *Free Field Characterization of High Intensity Focused Ultrasound (HIFU) Transducers Using Acoustic Streaming*, PhD, University of Cincinnati, Engineering : Mechanical Engineering, 2008.

91. http://www.edap-tms.com/products-services/ablatherm-hifu/hifu-technology.html

92. Huang, J., Holt, R.G., Cleveland, R.O. and Roy, R.A., "Experimental Validation of a Tractable Numerical Model for Focused Ultrasound Heating in Flow-Through Tissue Phantoms", *Journal of the Acoustical Society of America,* 116, pp. 2451–2458, 2004.

93. Morris, H., Rivens, I., Shaw, A. and ter Haar, G., "Investigation of the Viscous Heating Artifact Arising From the Use of Thermocouples in a Focused Ultrasound Field", *Physics in Medicine and Biology,* 53, 4759, 2008.

94. Dickinson, R.J., "Thermal Conduction Errors in Manganine-Constantan Thermocouple", *Physics in Medicine and Biology,* 30, pp. 445–453, 1985.

95. Fry, W.J. and Fry, R.B., "Determination of Absolute Sound Levels and Acoustic Absorption Coefficients by Thermocouple Probes – Theory", *Journal of the Acoustical Society of America,* 26, pp. 294–310, 1954.

96. Parker, K.J., "Ultrasonic Attenuation and Absorption in Liver Tissue", *Ultrasound in Medicine and Biology,* 9, pp. 363–369, 1983.

97. Neill, B. O., Vo, H., Angstadt, M., Li, K.P.C., Quinn, T. and Frenkel, V., "Pulsed High Intensity Focused Ultrasound Mediated Nanoparticle Delivery: Mechanisms and Efficacy in Murine Muscle", *Ultrasound in Medicine and Biology,* 35, pp. 416–424, 2009

98. Hariharan, P., Myers, M.R. and Banerjee, R.K., "HIFU Procedures at Moderate Intensities – Effect of Large Blood Vessels", *Physics in Medicine and Biology,* 52, pp. 3493–3535, 2007.

99. King, R.L., Herman, B.A., Maruvada, S., Wear, K.A. and Harris, G.R., "Development of a HIFU Phantom", *Proceedings of 6th International Sympossium on Therapeutic Ultrasound*, Oxford, UK, 2006.

100. Cuccurullo, S., *Physical Medicine and Rehabilitation Board Review*, New York: Demos Medical Publishing, ISBN-10: 1-888799-45-5, 2004.

101. Yuldashev, P. V., Shmeleva, S. M., Ilyin, S. A., Sapozhnikov, O. A., Gavrilov, L. R. and Khokhlova, V. A., "The Role of Acoustic Nonlinearity in Tissue Heating Behind a Rib Cage Using a High-Intensity Focused Ultrasound Phased Array", *Physics in Medicine and Biology, 58,* 2537, 2013.

APPENDIX A: LABVIEW PROGRAM FOR ULTRASONIC PRESSURE FIELD SCANNING

Software programming in LabVIEW 8.1 is shown in below figures.
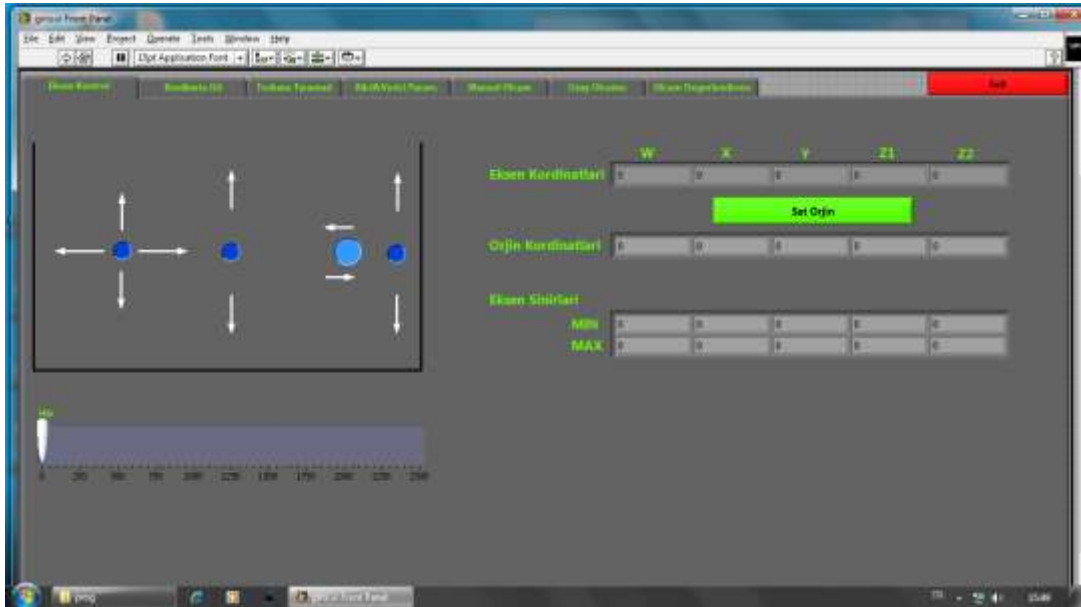
Figure 1. Main control page used in LabVIEW

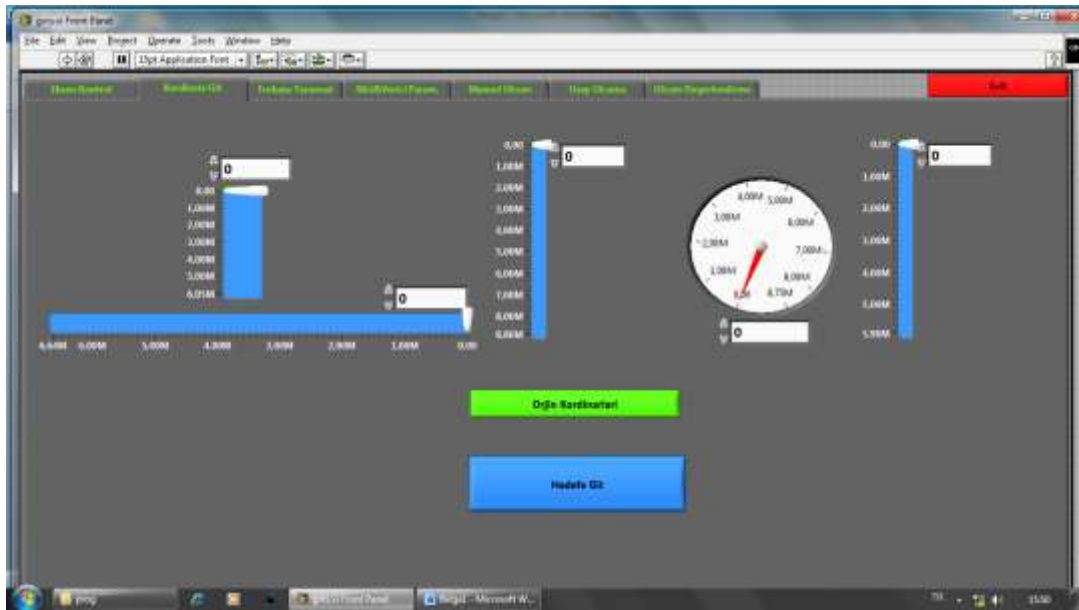Figure 2.Program start page in main cntrol page

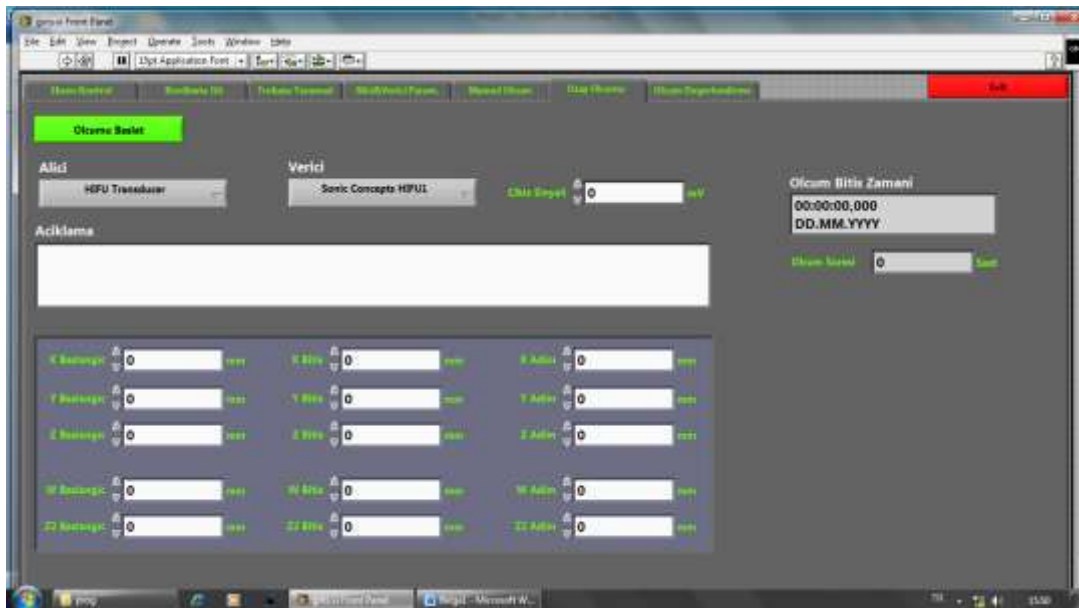Figure 3. Alignment of the transducer and hydrophone

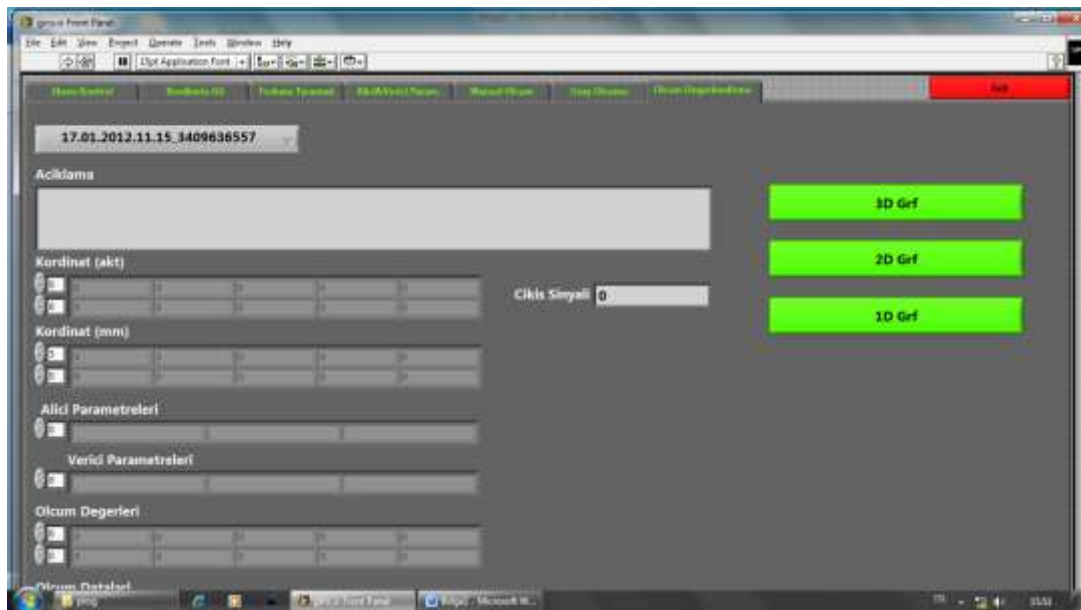Figure 4. Arrangement of the measurement parameters
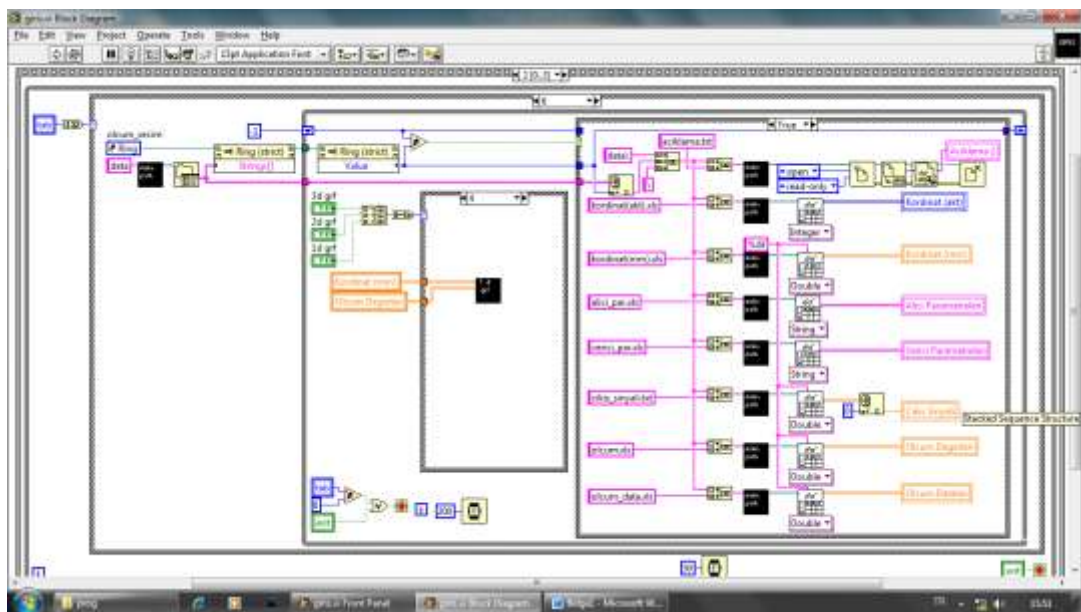
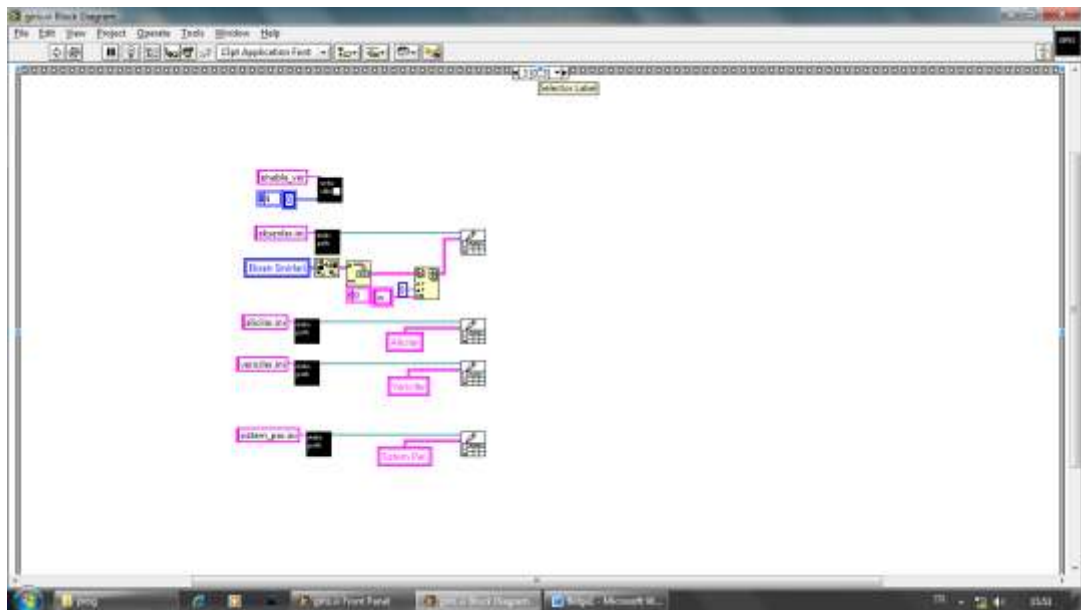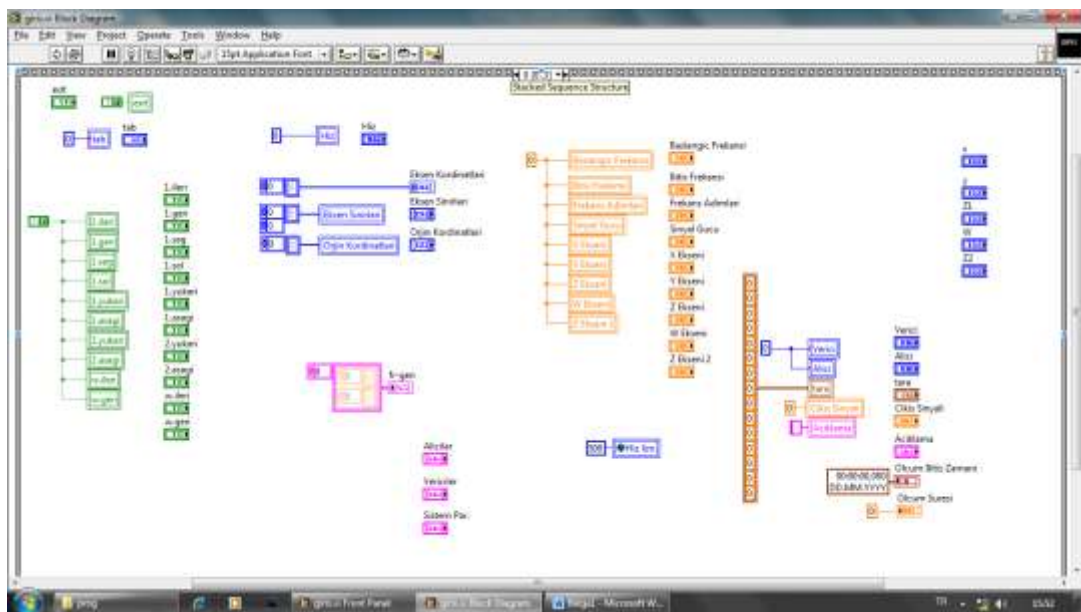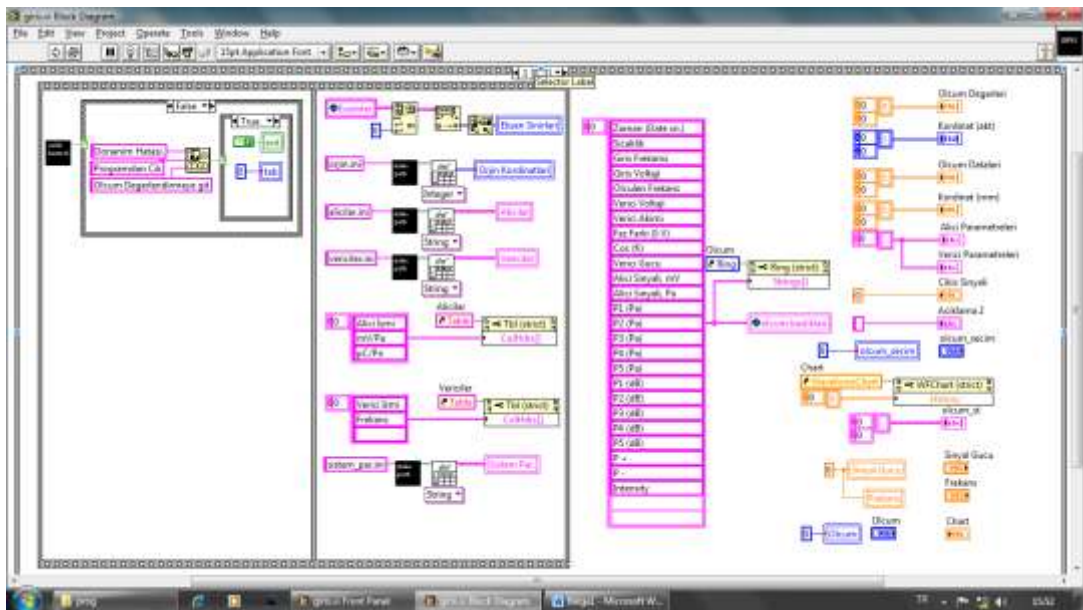Figure 5. Post processing page

Figure 6. Main diagram page

Figure 7. Diagram page 1
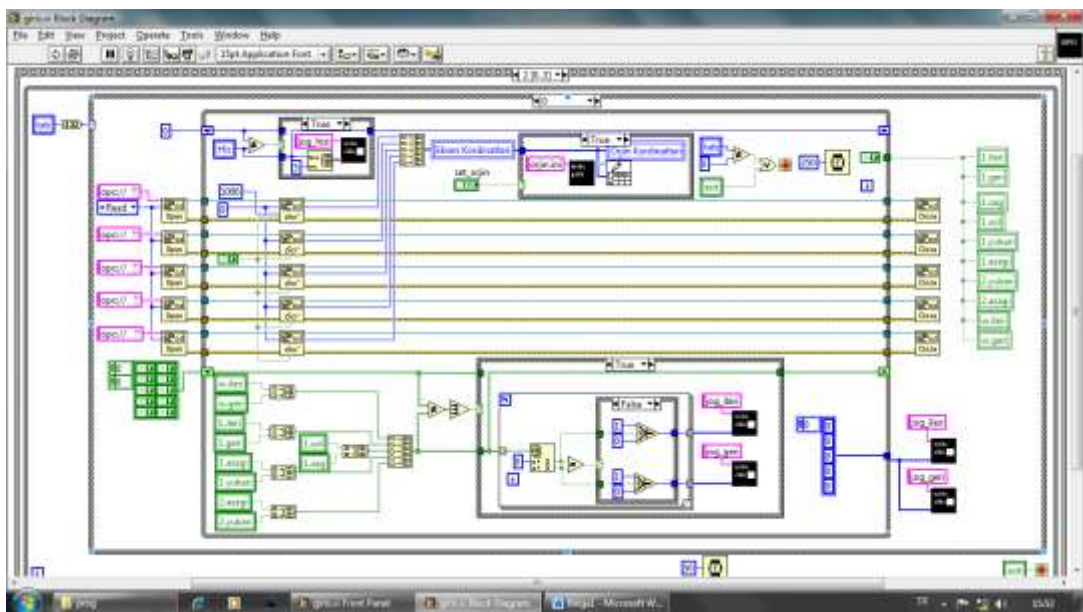

Figure 8. Diagram page 2

Figure 9. Diagram page 3
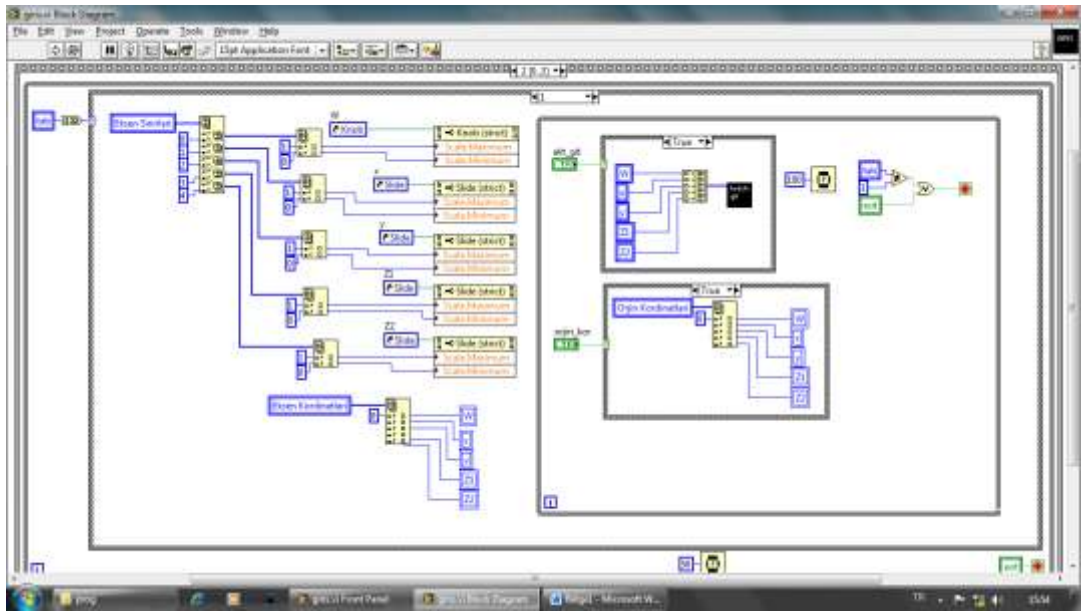

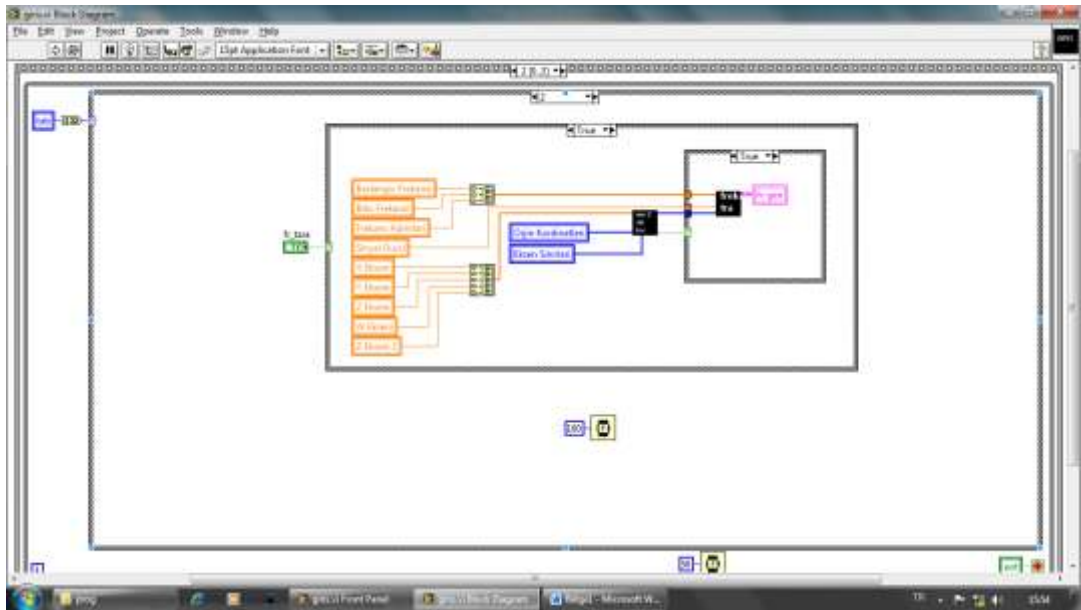Figure 10. Diagram page 4

Figure 11. Diagram page 5
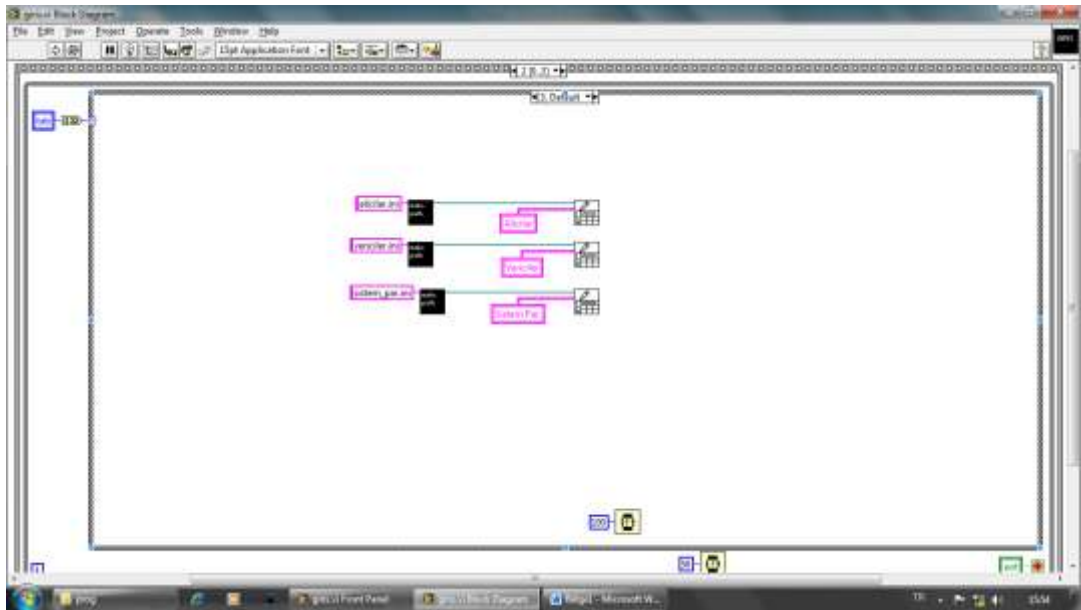

Figure 12. Diagram page 6
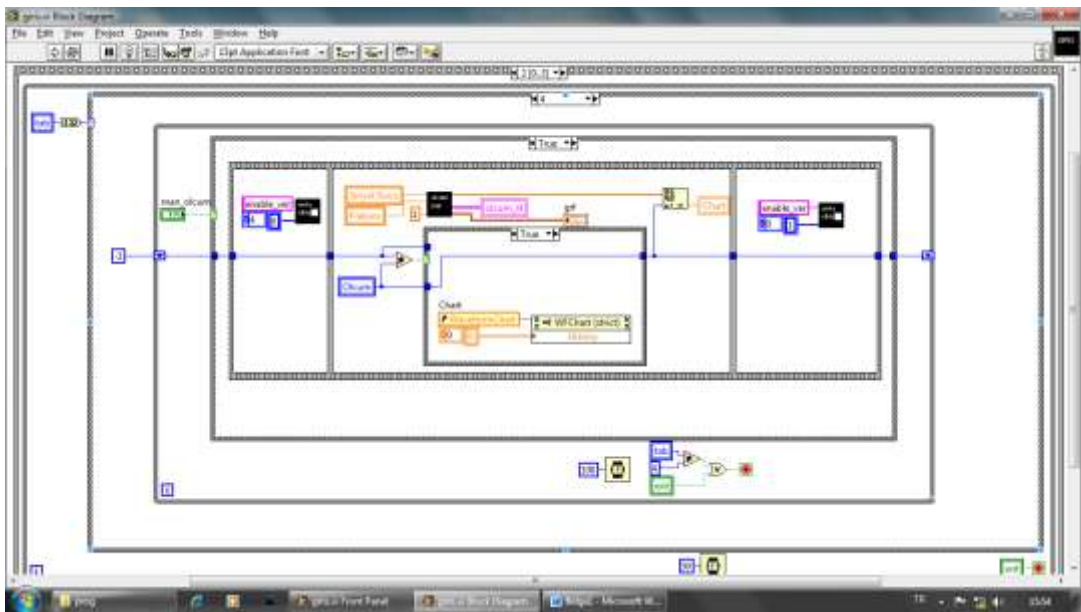
Figure 13. Diagram page 7
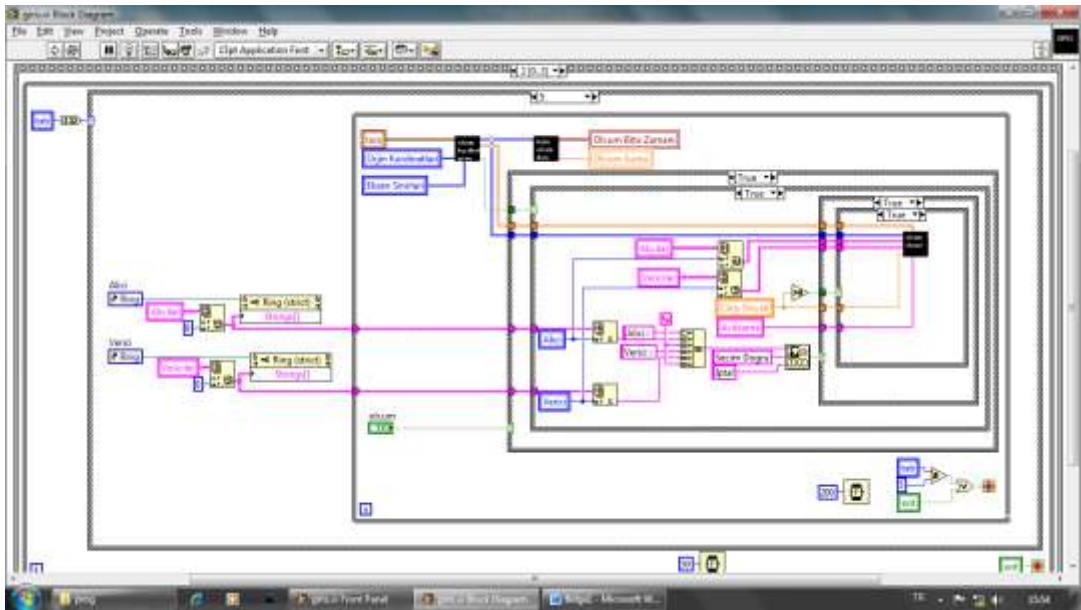

Figure 14. Diagram page 8
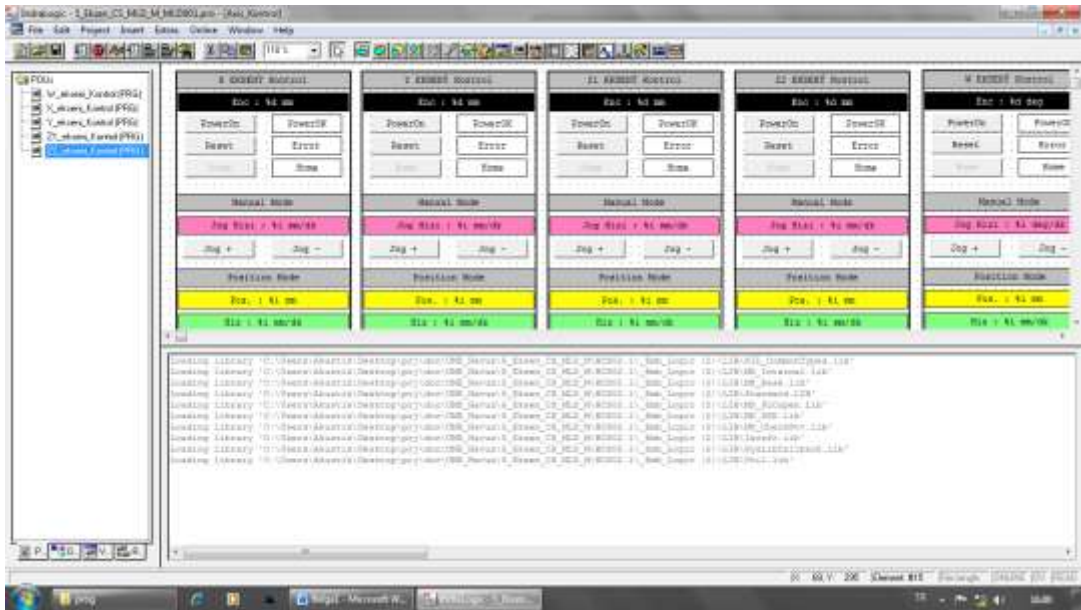
Figure 15. Diagram page 9

Figure 16. Positionning control page

APPENDIX B: MATLAB FILES FOR KZK SIMULATION

Matlab files used in KZK simulation as follows;

```matlab
%% Authored by Joshua Soneson 2007
%%%%%%%%%%%%%%%%%%%%%%%%%%%%%%%
function[p0,c1,c2,rho1,rho2,N1,N2,G1,G2,gamma1,gamma2,a,b,d,f
,R,Z,z_,K] = ...
KZK_parameters(K)
%% Input file for both axisymmetricKZK.m and
axisymmetricBHT.m
%% Consists of user-defined input parameter definitions,
including
%% material and transducer parameters, as well as the size of
the
%% computational domain; returns required computed parameters
for
%% integration of the model equations.

%%%%%%%%%%%%%%%%%%%%%%%%%%%%%%%%%%%%%%%%%%%%%%%%%%%%%%%%%%
%%%%%%
%%%% User-defined input parameters
%%%%%%%%%%%%%%%%%%%%%%%%%%%%%%%%%%
%%%%%%%%%%%%%%%%%%%%%%%%%%%%%%%%%%%%%%%%%%%%%%%%%%%%%%%%%%
%%%%%%

% material 1 parameters:
c1 = 1482;                % small-signal sound speed (m/s)
rho1 = 1000;              % mass density (kg/m^3)
alpha1 = 0.217;           % attenuation at 1MHz (dB/m)
eta1 = 2;                 % power of attenuation vs frequency
curve
beta1 = 3.5;              % nonlinear parameter
z_ = 5;                   % material transition distance (cm)

% material 2 parameters:
c2 = 1482;
rho2 = 1000;
alpha2 = 0.217;
eta2 = 1;
beta2 = 3.5;

% transducer parameters:
a = 3.5;                  % outer radius (cm)
b = 0.75;                 % inner radius (cm)
d = 8;                    % focusing depth (cm)
f = 1.1e6;                % frequency (Hz)
P = 100;                  % power (W)

% computational domain size:
R = a;                    % max radius (cm)
Z = 2*d;                  % max axial distance (cm)
K = 100;          % number of harmonics included in simulation
```

```matlab
%%%%%%%%%%%%%%%%%%%%%%%%%%%%%%%%%%%%%%%%%%%%%%%%%%%%%%%%%%
% computed equation coefficients: %%%%%%%%%%%%%%%%%%%%%%
%%%%%%%%%%%%%%%%%%%%%%%%%%%%%%%%%%%%%%%%%%%%%%%%%%%%%%%%%%

p0 = sqrt(2*rho1*c1*P/pi/((a/100)^2-(b/100)^2));    % peak
pressure at transducer face
N1 = 2*pi*p0*beta1*(d/100)*f/rho1/c1^3; % nonlinear
coefficient
N2 = 2*pi*p0*beta2*(d/100)*f/rho2/c2^3;
G1 = pi*(a/100)^2*f/c1/(d/100);      % linear pressure gain
G2 = pi*(a/100)^2*f/c2/(d/100);
gamma1 = zeros(K,1);              % attenuation coefficients
gamma2 = zeros(K,1);
h = f*[1:K]'/1e6;
alpha1 = (d/100)*alpha1/8.686;        % convert alpha from
dB/m to Np
alpha2 = (d/100)*alpha2/8.686;
if(eta1==1)
  gamma1 = alpha1*h.*(1-2*i*log(h)/pi);
elseif(eta1==2)
  gamma1 = alpha1*h.^2;
else
  gamma1 = alpha1*h.^eta1 - 2*i*(alpha1*h.^eta1-
alpha1*h)/(eta1-1)/pi;
end
if(eta2==1)
  gamma2 = alpha2*h.*(1-2*i*log(h)/pi);
elseif(eta2==2)
  gamma2 = alpha2*h.^2;
else
  gamma2 = alpha2*h.^eta2 - 2*i*(alpha2*h.^eta2-
alpha2*h)/(eta2-1)/pi;
end

% nondimensionalize grid dimensions:
R = R/a;
Z = Z/d;
```